Roles of HtrA1 in phenotypic shift of aortic vascular smooth muscle cells

(大動脈平滑筋細胞の形質転換における HtrA1 の役割)

Muthi Ikawati

Nara Institute of Science and Technology

Graduate School of Biological Sciences

Laboratory of Gene Function in Animals

(Professor Masashi Kawaichi)

August 9th, 2018

Roles of HtrA1 in phenotypic shift of aortic vascular smooth muscle cells

(大動脈平滑筋細胞の形質転換における HtrA1 の役割**)**

A Doctoral Dissertation
Submitted to Graduate School of Biological Sciences
Nara Institute of Science and Technology
in partial fulfillment of the requirements for the degree of
Doctor of Philosophy (PhD) in Biological Sciences

Muthi Ikawati

Advisory committee:

Professor Yasumasa Bessho (Member)

Professor Taro Kawai (Member)

Assoc. Professor Yasumasa Ishida (Member)

ABSTRACT

HtrA1 is a member of mammalian HtrA (high temperature requirement A) serine protease family. HtrA1 shows, at least, two activities. First, as a secreted protease, HtrA1 degrades various extracellular matrix (ECM) proteins. Second, although the mechanism is unclear, HtrA1 inhibits, in a proteolytic activity dependent manner, the signaling of transforming growth factor-β (TGF-β). Homozygous loss-of-function mutations of human *HTRA1* have been identified as the cause of a cerebral small vessel disease called CARASIL (cerebral autosomal recessive arteriopathy with subcortical infarcts and leukoencephalopathy). CARASIL features loss of vascular smooth muscle cells (VSMCs), intimal proliferation, internal elastic lamina degradation and alteration in ECM in cerebral small vessels.

HtrA1 knockout (*HtrA1$^{-/-}$*) mice have been produced. I examined whether the *HtrA1$^{-/-}$* mouse is valuable as a model for human CARASIL. *HtrA1$^{-/-}$* mice maintain a normal life span and exhibit no apparent abnormalities. No obvious defects have been observed in brain arteries even in aged (52-week-old) mice. Human CARASIL preferentially affects brain arteries of diameter between 100-1,000 μm. In mice, the aorta (500-1,000 μm) has similar size and structure with human small brain arteries affected by CARASIL. Hence, I focus on functions of HtrA1 in the aortic architecture and phenotypes of aortic VSMCs.

Compared to wild type (WT) littermates, the cross-sectional area of the aorta was increased in *HtrA1$^{-/-}$* mice of 40 weeks or older. The number of VSMCs in the aorta was increased in *HtrA1$^{-/-}$* mice of 40 weeks or younger, but decreased thereafter. Since the principal pathological site of CARASIL is reported to be VSMCs, I examined characteristics of VSMCs *in vivo* and *in vitro*. VSMCs switch from its differentiated contractile phenotype to de-differentiated synthetic phenotype in pathological conditions or in response to changes in environment. As compared to contractile cells, synthetic VSMCs are highly proliferative and migratory, produce more ECM, and show high activity of matrix metalloproteinases (MMPs).

Aortic VSMCs isolated from *HtrA1$^{-/-}$* mice rapidly proliferated and migrated, produced high MMP9 activity, and were prone to oxidative stress-induced cell death. *HtrA1$^{-/-}$* VSMCs expressed less smooth muscle α-actin, a contractile marker, and more vimentin and

osteopontin, synthetic markers, and responded to PDGF-BB more strongly than wild type VSMCs, indicating that *HtrA1*^{-/-} VSMCs were in the synthetic phenotype.

The aortic media of 40 and 52-week-old *HtrA1*^{-/-} mice showed uneven thickening. In thickened regions, elastic lamina were disrupted, and collagens were decreased.   These findings suggest that HtrA1 deficient mice show abnormalities that are related to those found in human CARASIL. Calponin, a contractile marker,in the media was decreased, whereas synthetic markers vimentin and osteopontin were increased, suggesting a synthetic shift of VSMCs *in vivo*. Although excess TGF-β signaling has been implicated in the pathogenesis of CARASIL, TGF-β signaling as represented in the level of phosphorylated Smad2 was not affected in *HtrA1*^{-/-} mouse aortas.

As conclusion, *HtrA1*^{-/-} mice may represent the very early stage of the disease.   I speculate that loss of functional HtrA1 provokes ECM abnormalities and impairs cell-ECM interaction, which induces phenotypic switching of VSMCs into synthetic phenotype and contribute to the development of arteriosclerosis. My study highlights phenotypic switching of VSMCs as a new mechanism to understand CARASIL pathogenesis. Loss of *HtrA1* therefore skews VSMCs toward the synthetic phenotype, induces MMP9 expression, and expedites cell death. We propose that the synthetic modulation is the primary event that leads to the vascular abnormalities caused by *HtrA1* deficiency.

CONTENTS

LIST OF FIGURES

LIST OF APPENDICES

ABBREVIATIONS

AMD   age-related macular degeneration

AP-1   activator protein-1

BSA   bovine serum albumin

CADASIL   cerebral autosomal dominant arteriopathy with subcortical infarcts and leukoencephalopathy

CARASIL   cerebral autosomal recessive arteriopathy with subcortical infarcts and leukoencephalopathy

CTGF   connective tissue growth factor

DAB   Diaminobenzidinine

ECM   extracellular matrix

ER   endoplasmic reticulum

ERK   extracellular signal-regulated kinase

EVG   elastica van Gieson

FBS   fetal bovine serum

HE   hematoxylin and eosin

HRP   horseradish peroxidase

IGF   insulin-like growth factor

JNK   c-Jun N-terminal kinase

LDLRP   low-density lipoprotein receptor-related protein

MAPK   mitogen-activated protein kinases

MEF   mouse embryonic fibroblast

MFS   Marfan syndrome

MMP   matrix metalloproteinase

NAC   N-acetyl cysteine

NGS   normal goat serum

PBS   phosphate-buffered saline

PCNA   proliferating cell nuclear antigen

PDGF   platelet-derived growth factor

PFA   paraformaldehyde

ROS   reactive oxygen species

SMA   smooth muscle α-actin

SVD   small vessel disease

TBS   Tris-buffered saline

TGF-β   transforming growth factor-β

TUNEL   terminal deoxynucleotidyl transferase biotin-dUTP nick end labeling

VSMC   vascular smooth muscle cell

WT   wild type

I. INTRODUCTION

1.1 HtrA

HtrA is a family of serine proteases that is highly conserved among species from bacteria to plants and human (Clausen *et al*, 2002). HtrA stands for High Temperature Requirement A, because this family was first identified in *E. coli* as proteins that give heat shock resistance to the cell (Lipinska *et al*, 1989; Lipinska *et al*, 1990). The common structural feature of HtrA family proteins is the combination of a conserved trypsin-like serine protease domain and one or two downstream PDZ (postsynaptic density of 95 kDa, discs large and zonula occludens 1) domains (Fig. 1.1) (Clausen *et al*, 2002). Besides those common domains, each family member has different structural motifs in its N-terminal region, and could have different biological functions.
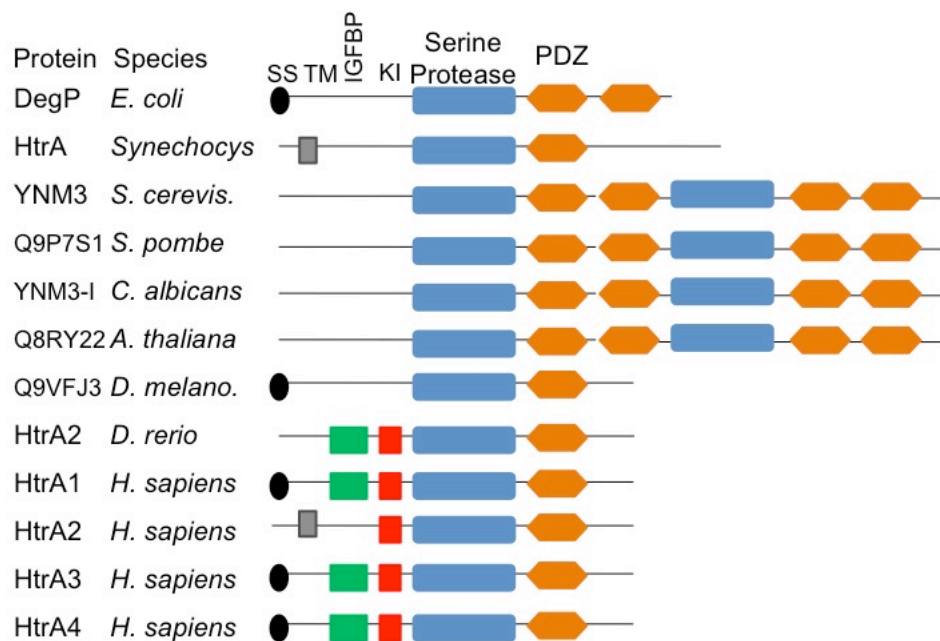
Figure 1.1. **Domain organization of HtrA family member among different species.** The relative positions of signal peptides (SS, black oval), transmembrane segments (TM, gray box), insulin-like growth factor binding-like domains (IGFBP, green box), Kazal-type protease inhibitor domains (KI, red box), trypsin-like protease (serine protease, blue box) domains, and PDZ domains (brown hexagon) are illustrated (Clausen *et al*., 2002 with modification).

1

A typical HtrA protein, *E. coli* DegP, recognizes and digests heat-denatured (Strauch and Beckwith, 1988; Skorko-Glonek *et al*, 1995) or miss-folded proteins in the periplasm with its proteolytic activity at high temperatures (Krojer *et al*, 2008). At low temperatures, DegP exhibits a chaperon activity (Spiess *et al*, 1999), which re-folds denatured proteins into their correct structures. Expression of bacterial DegP is induced by stressors such as heat (Skorko-Glonek *et al*, 1995; Rauter *et al*, 2003), ethanol treatment (Foucaud-Scheunemann and Poquet, 2003), and oxidative stress (Skorko-Glonek *et al*, 1999). DegP is therefore an authentic stress responsive factor. Studies so far done indicate that the major common function of HtrA family members is in protein quality control under various stress conditions (Clausen *et al*, 2011).

1.2 Mammalian HtrA

1.2.1 Domain organization and tissue distribution

The mammalian HtrA family consists of four members, which are divided into two groups based on their domain organization (Fig. 1.1). HtrA2 has a mitochondrial targeting sequence and a transmembrane domain in the N-terminal region. The transmembrane domain determines the position of HtrA2 on the mitochondrial membrane; the protein is anchored with the protease and PDZ domains protruding into the intermembrane space (reviewed in Clausen *et al*, 2011). HtrA1, 3, and 4 are secretory proteins and show high homology among them. They commonly share the N-terminal signal peptides for secretion followed by the insulin-like growth factor binding protein (IGFBP)-like domain and the Kazal-type protease inhibitor (KI) domain (Nie *et al*, 2003a; Clausen *et al*, 2011). The IGFBP and KI domains are thought to function in protein-to-protein interactions (Runyon *et al*, 2007).

Many studies on expression patterns have been reported for HtrA1, HtrA2, and HtrA3, but little is known about HtrA4. The relative expression level of HtrA2 is quite uniform in almost all tissues with slightly high levels found in fetal tissues. HtrA1 and HtrA3 are widely expressed in human tissues. However, expression of HtrA1 and HtrA3 shows some complementarity. HtrA1 is highly expressed in the central nervous system, whereas HtrA3 is expressed preferentially in non-neural tissues with the highest expression levels found in fetal and adult heart. Both are expressed at particularly high levels in the placenta and ovary (Nie *et al*, 2003a). In mouse placenta, HtrA3 is expressed mostly in the maternal basal decidua, but HtrA1 is expressed in the capsular decidua as well as in some fetal trophoblasts (Hasan *et al*, 2015). Expression of HtrA1 and HtrA3 in hematopoietic cells is minimal (Nie *et al*, 2003a).

1.2.2 HtrA2

HtrA2 was first reported to promote apoptosis by binding to X chromosome-linked inhibitor of apoptosis (XIAP) (Suzuki *et al*, 2001; Trencia *et al*, 2004). Upon exposure to apoptotic stress, the N-terminal region of HtrA2 is removed by proteolysis and the truncated HtrA2 is released from the mitochondria into the cytosol (reviewed in Clausen *et al*, 2011). The truncated HtrA2 enhances apoptosis by inhibiting XIAP, or in a manner dependent on HtrA2's protease activity. Later, *HtrA2* knockout mice were found to show neurodegeneration caused by malfunction of mitochondria (Martins *et al*, 2004). A polymorphism in human *HTRA2* is associated with hereditary Parkinson Disease (Strauss *et al*, 2005). The primary function of HtrA2 therefore is not the induction of apoptosis, but probably a protein quality control in the intermembrane space of the mitochondrion. Loss of HtrA2 activity leads to enhanced aging in mice (Kang *et al*, 2013).

1.2.3 HtrA1 and HtrA3

Most of HtrA1 is secreted into the extracellular compartment. HtrA1 shows two activities. First, as a secreted protease, HtrA1 degrades various extracellular matrix (ECM) proteins, such as aggrecan, biglycan, and decorin. Second, although the mechanism is unclear, HtrA1 inhibits, in a proteolytic activity dependent manner, the signaling of transforming growth factor (TGF)-β (Oka *et al*, 2004; Tsuchiya *et al*, 2005). Shiga *et al* (2011) have proposed that HtrA1 cleaves pro-TGF-β1 in the secretory pathway. HtrA1 has also been reported to cleave type II and type III TGF-β receptors (Graham *et al*, 2013). However, HtrA1 can inhibit BMP-2 signaling even when the growth factor was added to the culture medium, and HtrA1 cannot inhibit signaling from a constitutively active BMP receptor (Oka *et al*, 2004). These data suggest that TGF-β growth factors or their receptors are not the targets of HtrA1. The most plausible possibility is that HtrA1 inhibits TGF-β signaling by degrading ECM around the cells and thus preventing the effective concentration of TGF-β (Oka *et al*, 2004); biglycan and decorin are known to bind TGF-β and modulate its activity (Hildebrand *et al*, 1994). HtrA3 cleaves ECM components, including decorin and biglycan, and inhibits TGF- β signaling as effectively as HtrA1 (Tocharus *et al*, 2004). About 20% of HtrA1 remains inside the cell. Intracellular HtrA1 may represent the protein in the secretory pathway. Otherwise, it is reported that HtrA1 is in the cytoplasm and predominantly attached to microtubules (reviewed in Clausen *et al*, 2011).

1.3 HtrA1 and Human Diseases

Both increase and decrease in HtrA1 expression are implicated in a wide range of pathophysiological processes in humans. Hu *et al* (1998) observed that HtrA1 was increased several-fold in joint cartilage of human osteoarthritic patients. High levels of HtrA1 were also found in the synovial fluids obtained from rheumatoid arthritis or osteoarthritis patients

(Grau *et al*, 2006). In model mice with arthritis induced by injection of anti-collagen antibodies, HtrA1 is expressed in affected cartilage by terminally differentiated hypertrophic chondrocytes (Tsuchiya *et al*, 2005), which are usually absent in normal joint cartilage, but induced by arthritic stimuli. Probably, over-expressed HtrA1 degrades cartilage matrix and further aggravate the damage of cartilage. HtrA1 degrades fibronectin at least *in vitro*, and fibronectin-degradation products are known to induce cartilage degradation (Grau *et al*, 2006).

HtrA1 and HtrA3 are also implicated in carcinogenesis (Bowden *et al*, 2006; Zurawa-Janicka *et al*, 2012). HtrA1 is down-regulated in several types of tumors, such as melanoma (Baldi *et al*, 2002), endometrium (Bowden *et al*, 2006; Mullany *et al*, 2011), ovary (Chien *et al*, 2006), breast (Wang *et al*, 2012a), or thyroid cancers (Zurawa-Janicka *et al*, 2012). Higher expression of HtrA1 is associated with better survival of gastric adenocarcinoma patients (Catalano *et al*, 2011). Overexpression of HtrA1 inhibits cell proliferation and migration of melanoma cells, *in vitro* and *in vivo* (Baldi *et al*, 2002). These findings suggest that HtrA1 is a tumor suppressor. Several possible mechanisms have been proposed. HtrA1 increases the sensitivity of ovarian cancer cells to cytostatic agents, such as cisplatin and paclitaxel (Chien *et al*, 2006). Intracellular HtrA1 is associated with microtubules, stabilizes microtubules, and attenuates cell migration (Chien *et al*, 2009). HtrA1 digests XIAP and induce apoptosis (He *et al*, 2012). HtrA1 cleaves and activates tuberin, a product of tumor suppressor gene *TSC2* (Tuber Sclerosis Complex 2) (Campioni *et al*, 2010). HtrA1 and HtrA3 are implicated in implantation of a fertilized ovum during pregnancy and etiology of preeclampsia (Nie *et al*, 2003b; Hasan *et al*, 2015).

The cause-consequence relationship between expression levels of HtrA1 or HtrA3 and the onset of the diseases mentioned above are not very clear. However, involvement of HtrA1 in age-related macular degeneration (AMD) is of particular importance, because it is

established by un-biased methods, such as genome wide association studies. *HTRA1* is a genetic predisposing factor of AMD, a retinal degenerative disease, which is the leading cause of irreversible vision loss in aged people. Several single nucleotide polymorphisms (SNPs) in the promoter region of *HTRA1* show an extremely strong linkage to the onset of AMD (DeWan *et al*, 2006; Yang *et al*, 2006; Francis *et al*, 2008). These risk SNPs increase the expression of HtrA1 mRNA. Transgenic mice overexpressing HtrA1 in the retinal pigment epithelium (RPE) exhibit degradation of elastic fibers in the basement membrane of RPE (Bruch's membrane) and in choroidal vessel walls (Vierkotten *et al*, 2011; Jones *et al*, 2011). The transgenic mice also show polyploidal choroidal vasculopathy, which is a typical abnormality found in severe (wet) type AMD (Jones *et al*, 2011). Those transgenic mice therefore display at least a part of signs characteristic to human AMD. The major environmental factor of AMD is oxidative stress. Oxidative stress imposed by H_2O_2 treatment increases HtrA1 expression 3-4 fold in a human RPE cell line, ARPE19 (Supanji *et al*, 2013). The increased HtrA1 protects ARPE19 cells from cell death but induces cell senescence. Both environmental factors and genetic predisposition therefore increase the expression of HtrA1 and additively contribute to the onset of AMD.

1.4 CARASIL

Hara *et al* (2009) identified homozygous loss-of-function mutations of *HTRA1* as the cause of a hereditary cerebral small vessel disease (SVD) called cerebral autosomal recessive arteriopathy with subcortical infarcts and leukoencephalopathy (CARASIL). Since the first report by Maeda *et al* in 1976, this disease had been diagnosed only with Japanese patients (reviewed in Fukutake, 2011). However, identification of the causative gene expanded the recognition of this disease not only in Japan (Nishimoto *et al*, 2011) but also in other

countries, including Chinese population (Zheng *et al*, 2009; Wang *et al*, 2012b; Chen *et al*, 2013; Cai *et al*, 2015) and Caucasian population (Mendioroz *et al*, 2010; Bianchi *et al*, 2014).

1.4.1 Clinical features

CARASIL is a non-hypertensive vasculopathic subcortical encephalopathy accompanied by extra-central nervous system symptoms which appear in a young-adult ages (Maeda *et al*, 1976). The primary clinical features of CARASIL are premature baldness/alopecia (average onset at 20 years), followed by severe low back pain due to spondylosis, and early-onset dementia that is caused by non-hypertensive cerebral small vessel arteriopathy (average onset of these symptoms at 32 years). Brain imaging with MRI shows diffuse and multifocal demyelination in the cerebral white matter (reviewed in Fukutake, 2011).

1.4.2 Structure of the artery

The primary sites of CARASIL etiology are small cerebral arteries of diameter 100-1000 μm (Oide *et al*, 2008). Arteries consist of three layers: the tunica adventitia, the tunica media, and the tunica intima, from outer to inner layers (Fig. 1.2). The tunica adventitia consists of fibroblasts and connective tissues rich in collagen fibers to give a protective cover for the vessels. The tunica media is the middle layer and consists of circularly arranged vascular smooth muscle cells (VSMCs) and elastic fibers packed within ECM. The tunica media serves as the thickest layer of the arteries to counter the high blood pressure. The elastic fibers give elasticity (allow the artery to stretch and recoil), while VSMCs give contractility (allow the artery to constrict and dilate). The tunica intima is in direct contact with the blood flowing through the lumen. It consists of a single layer of endothelial cells

supported by the internal elastic membrane. The external and internal elastic membranes serve as borders between three layers.
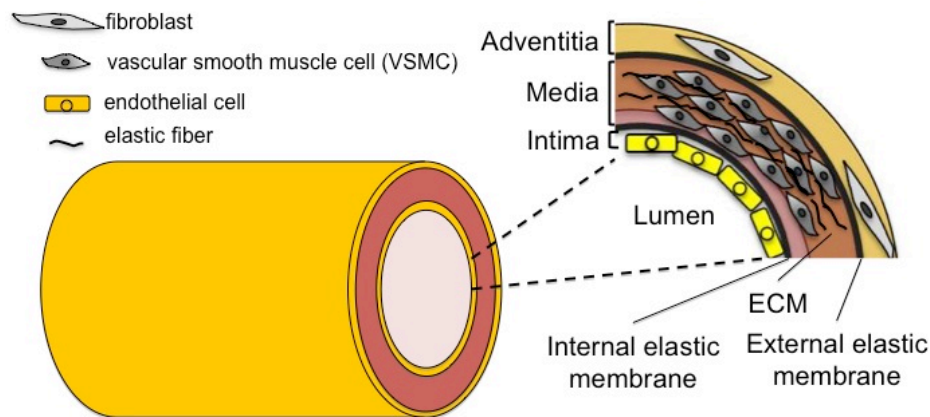
Figure 1.2. **Structure of the artery.** The artery consists of three layers: the tunica adventitia, the tunica media, and the tunica intima (from The Encyclopedia of Britannica, 2014 with modification).

1.4.3 Pathology of CARASIL

CARASIL is the second hereditary SVD characterized after cerebral autosomal dominant arteriopathy with subcortical infarcts and leukoencephalopathy (CADASIL), which is caused by *NOTCH3* gene mutations (Joutel *et al*, 1996). Different from CADASIL, which is characterized by the deposition of granular osmiophilic materials (GOM) in the media of brain arteries, CARASIL shows severe arteriosclerosis without GOM deposition (Arima *et al*, 2003). Histology of CARASIL cerebral arteries was characterized by fibrous intimal proliferation, thickening and splitting of the internal elastic lamina, massive hyaline degeneration of the media, and extensive loss of VSMCs (Arima *et al*, 2003; Hara *et al*, 2009). These damages eventually result in concentric narrowing of the lumen of small cerebral and meningeal arteries and cause insufficient blood flow, leading to multifocal or diffuse ischemic degeneration in the brain (Yokoi and Nakayama, 1985; Arima *et al*, 2003; Oide *et al*, 2008; Hara *et al*, 2009). Pathological changes in CARASIL patients are observed predominantly in brain arteries with diameter around 100-1,000 μm (Oide *et al*, 2008). Hara *et al* (2009) reported increase in fibronectin and a blood vessel proteoglycan, versican, in the

8

affected brain arteries; those two proteins are candidate substrates of HtrA1 and their production is induced by the TGF-β signaling.

On the contrary, Oide *et al* (2008) reported, based on autopsy cases, that arteriosclerotic changes were rather mild and infrequent in CARASIL. They showed medial and adventitial thinning with aneurysm formation and centrifugal enlargement of the lumen. They also showed extensive loss of VSMCs and reduction in ECM proteins such as collagens and fibronectin. VSMC loss was observed even in the arteries without intimal proliferation. From the observation of biopsy tissue samples, not of post-mortem autopsy samples used in all previous papers, Cai *et al* (2015) reported that the loss of VSMCs was also detected in leg subcutaneous arteries in CARASIL patients. Medial VSMCs is, therefore, definitely the primary site responsible for CARASIL pathophysiology. Loss of VSMCs and resulting thinning of arterial walls are likely to be the primary abnormalities in CARASIL, and strong arteriosclerotic changes may represent late-stage abnormalities secondarily caused by depletion of VSMCs in the media.

1.4.4 Genetics and molecular pathogenesis

So far, six missense mutations of *HTRA1* have been detected in exon 3, 4 and 6 (Hara *et al*, 2009; Mendioroz *et al*, 2010; Nishimoto *et al*, 2011; Wang *et al*, 2012b; Chen *et al*, 2013), which, together with exon 5, constitute the protease domain (Fig. 1.3). Two nonsense mutations have been detected in exon 4 and 6 (Hara *et al*, 2009). A two-nucleotide insertion in exon 1 was also reported which causes frameshift and generation of a stop codon 159 amino acid downstream (Cai *et al*, 2015) (see Fig. 1.3). R370X, one of the nonsense mutations, results in a quick degradation of HtrA1 mRNA by nonsense-mediated mRNA decay (Hara *et al*, 2009). The remaining missense mutations yield proteins that have very low protease activities and do not inhibit the signaling by the TGF-β family (Hara *et al*, 2009;

Mendioroz *et al*, 2010; Nishimoto *et al*, 2011; Wang *et al*, 2012). Actually, in CARASIL autopsy samples, the TGF-β1 protein levels are increased in affected arteries, and phosphorylation of a downstream signaling factor, Smad2/3, is enhanced (Hara *et al*, 2009; Cai *et al*, 2015).
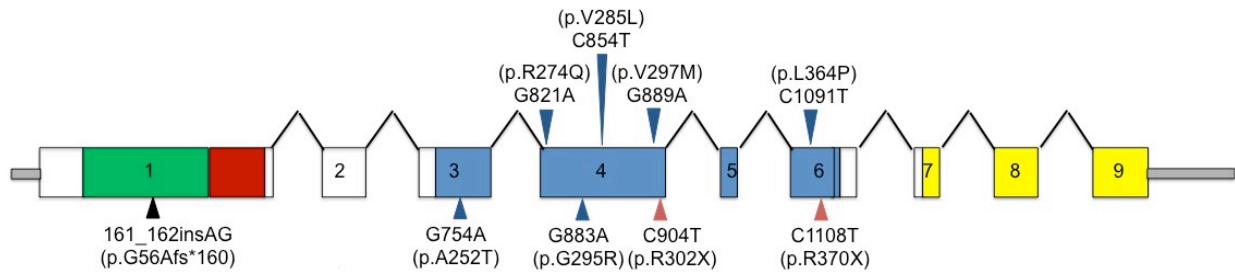
Figure 1.3.   **The distribution of mutations in *HTRA1*.** *HTRA1* consists of nine exons (squares): those encoding IGFBP domain (green), KI domain (red), serine protease domain (blue), and PDZ domain (yellow). Position of nucleotide (and corresponding amino acid) mutations are pointed by arrowhead with color according to the types of mutation: frameshift (black), missense (blue), and nonsense (red) (Hara *et al*., 2009; Mendioroz *et al*, 2010; Nishimoto *et al*, 2011; Wang *et al*, 2012; Chen *et al*, 2013; Cai *et al*, 2015).

1.4.5 Arteriopathy caused by heterozygous mutations of *HTRA1* gene

Recently, Verdura *et al* (2015) reported that heterozygous mutations of *HTRA1* gene cause a SVD that leads to stroke and cognitive impairment (dementia). SVD caused by heterozygous *HTRA1* mutations is characterized by its late onset around the age of sixty and the lack of extraneurological symptoms, alopecia and low back pain. The disease is hence almost indistinguishable from sporadic SVD caused by age and hypertension, except for family history. They identified a heterozygous mutation of R116L in *HTRA1* gene in one family. They further examined 201 probands from families with history of dominant hereditary SVD, and who had previously been screened for *NOTCH3* mutations with negative results. Heterozygous mutations of *HTRA1* gene, which were predicted pathogenic by multiple *in silico* prediction tools, were detected in 10 probands (frequency of HTRA1 mutations in dominant familiar SVD = 4.95%). Among those 11 mutations so far identified, four are missense mutations in the protease domain (Fig. 1.4). Another one is in intron 4

close to the boundary of exon 4 and predicted to interfere splicing. This abnormal splicing skips exon 5, which codes the active center serine (S328). Two other mutations are within the junctional region between the KI domain and the protease domain. This region is essential for homotrimer formation, which is indispensable for the proteolytic activity of HtrA1. All these eight mutations decreased or totally abolished the protease activity of HtrA1. They also found one missense mutation in the PDZ domain, D450H. HtrA1 with this mutation retained almost normal protease activity. Other three mutations are located in the KI domain, the protease activities of which have not been analyzed. It may be possible that the latter four mutations affect the HtrA1 function through mechanisms independent of the catalytic activity.
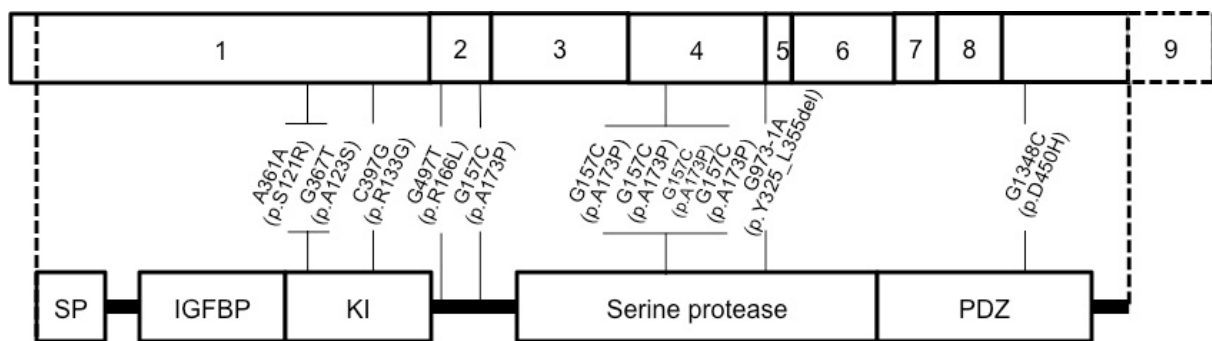
Figure 1.4. **Schematic representation of *HTRA1* gene/protein and location of mutations identified by Verdura *et al* (2015).** cDNA structure of human *HTRA1* transcript NM_002775.4 (upper) and domain organization of human HTRA1 protein NP_002766.1 (bottom). Positions of heterozygous SVD mutations and HTRA1 protein changes identified in this study are indicated. SP = signal peptide.

SVD most commonly occurs sporadically and is related to age and hypertension. Among rare cases of dominant hereditary SVD, CADASIL with *NOTCH3* mutations are most frequent. Now the mutations of *HTRA1* is the second most frequent etiology of familiar dominant SVD. These results underscore essential roles of HtrA1 in maintenance of normal arteries.

1.5 VSMC Phenotypic Modulation and Arterial Abnormalities

1.5.1 VSMC phenotypic modulation

VSMCs play a crucial role in physiology of the artery. They exhibit a wide range of phenotypic variations. There are two different cell types of VSMCs; one for contraction (contractile VSMCs) and the other for ECM synthesis (synthetic VSMCs) (Majesky *et al*, 2011). Each of these types represents one extreme end point of phenotype, and in actual blood vessels, VSMCs display a diffuse spectrum of diversity between their contractile and synthetic phenotypes. This diversity is caused by innate genetic programs during development of blood vessels and as a result of response to environmental changes. The fully-differentiated contractile VSMCs can be de-differentiated into synthetic cells and vice versa, a process often called "phenotypic switching" or "phenotypic modulation", in response to humoral factors, cell-cell interactions, mechanical forces, atherogenic stimuli, and other stress (Fig. 1.5). Each phenotype is characterized by distinct properties in morphology, cell proliferation and migration rates, and the expression of different marker proteins. Contractile
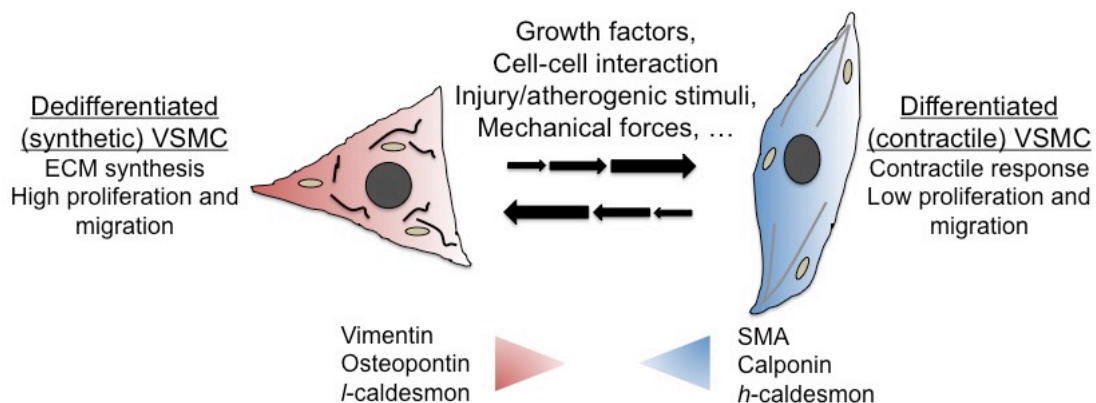
Figure 1.5. **The phenotypic modulation of VSMCs.** Many extrinsic factors or local environmental cues influence the differentiation/mature state of VSMCs and change expression levels of genes associated with a particular VSMC phenotype (Owens *et al*, 2004; Rensen *et al*, 2007 with modification).

VSMCs are elongated, spindle-shaped cells, and contain contractile filaments, whereas synthetic VSMCs are in less elongated epithelioid or rhomboid shape and contain more organelles for protein synthesis. Synthetic VSMCs exhibit higher proliferation rate and

higher migratory activity than contractile VSMCs (reviewed in Owens *et al*, 2004; Rensen *et al*, 2007).

A variety of VSMC-specific genes and proteins have been identified that can be used to distinguish phenotypic states of VSMCs. For example, the smooth muscle isoforms of contractile apparatus proteins such as smooth muscle α-actin (SMA), smooth muscle-myosin heavy chain (SM-MHC), calponin, desmin, and *h*-caldesmon are usually used to indicate contractile phenotype. On the other hand, there are a limited number of markers that are up-regulated in synthetic VSMCs. Decreases in contractile VSMC markers are usually used to characterize synthetic VSMCs (reviewed in Owens *et al*, 2004; Rensen *et al*, 2007). Vimentin (Owens, 1995), osteopontin, and *l*-caldesmon (Rensen *et al*, 2007) are among the rare proteins that are highly expressed in synthetic VSMCs (Fig. 1.5). Changes in ratios of specific splice variants (*h*-caldesmon and *l*-caldesmon) can be used to indicate the phenotypic status of VSMCs (Rensen *et al*, 2007). Because of the tremendous diversity in VSMCs phenotype, expression levels of at least two protein markers should be examined to distinguish between synthetic and contractile phenotype, in conjunction with cell morphology, proliferation rate and migration properties (Rensen *et al*, 2007).

1.5.2 VSMC phenotypic modulation as a driving force of vascular abnormalities

In normal mature arteries, contractile VSMCs are the predominant phenotype and function as the regulator of vasodilatation-vasoconstriction and blood flow. In response to injury, VSMCs switch into synthetic phenotype for tissue repair. The response to injury is multilateral and involves the production of a variety of growth factors (for example: platelet-derived growth factor (PDGF), insulin-like growth factor (IGF), TGF-β, and angiotensin II). VSMCs gain the ability to produce more ECM, and to migrate and proliferate in order to reach the injured site and fill the damage. Cells producing growth factors, which usually

work in paracrine manners, should migrate/proliferating to induce curing responses in wider area. However, if the migrating/proliferating VSMCs fail to switch back to the contractile phenotype at appropriate time, for example due to excessive cytokines, those synthetic VSMCs induce pathogenic vascular remodeling and cause intimal lesions; migratory VSMCs invade into the intima and cause protruding structures, a process called "neointima formation" or "intimal proliferation". In addition, synthetic VSMCs do not contribute vascular contraction due to reduction in contractile proteins (Louis and Zahradka, 2010). Synthetic VSMCs are therefore key elements in vascular abnormalities, including atherosclerosis, restenosis (Louis and Zahradka, 2010), and aneurysm (Mao *et al*, 2015; Crosas-Molist *et al*, 2015).

Roles of synthetic VSMCs have been studied very well in pathogenesis of atherosclerosis. Atherosclerosis is initiated by subendothelial retention of lipoproteins in localized areas of arteries. Eventually, those areas accumulate macrophages and other inflammatory cells, more lipids, and proteins derived from the blood. As a result, multiple atherosclerotic "plaques" are formed within the arteries. The "stable plaques" are rich in ECM and synthetic VSMCs, which migrate from the media. Stable plaques are covered with thick fibrous caps and usually do not cause symptoms. The "unstable plaques" are, on the other hand, poor in synthetic VSMCs. Their fibrous caps are thin and tend to rupture, and the rupture causes thrombosis. Hence, the modulation of VSMCs to synthetic phenotype is a protective mechanism in the initial steps. However, the excessive synthetic VSMC later aggravate atherosclerotic through the neointima formation (Alexander and Owens, 2012).

1.5.3 Factors and mechanisms involved in VSMC phenotypic modulation

Phenotypic modulation of VSMCs is a complex process that are affected by many factors, such as cytokines, inflammatory cell mediators, oxidized lipids, reactive oxygen

species (ROS), and physical contacts with ECM and neighboring cells. Extensive *in vitro* and *in vivo* studies have been done to reveal the mechanisms involved in VSMC phenotypic modulation. PDGF, IGF, TGF-β, and matrix metalloproteinases (MMPs) are some of the environmental factors that are proved relevant to *in vivo* observations (reviewed in Owens *et al*, 2004). There are two categories of factors that induce phenotypic modulation; one induces a directional change toward one particular phenotype, irrespective of the initial phenotype of VSMCs. The other induces different responses depending on the initial cell phenotype (reviewed by Rensen *et al*, 2007).

PDGF, a cytokine produced by activated platelets and lesion macrophages, belongs to the first category, and shifts VSMCs to synthetic phenotype irrespective of their initial phenotypic status. PDGF is a dimer composed of two chains, A and B, linked through a disulfide bond. There are two PDGF receptors: PDGFRα and PDGFRβ, the kinase activities of which are activated by PDGF-AA alone, and both PDGF-AA and BB, respectively. PDGF-BB induces rapid and potent decrease in contractile markers in cultures VSMCs and stimulates proliferation and migration through activating ERK and p38 MAPK (Hayashi *et al*, 1999). In facts, PDGF-BB is the most potent negative regulator of VSMC-selective, contractile gene expression (Owens *et al*, 2004). PDGF-BB also activates ERK MAPK and Smad3 to induce VSMC proliferation *in vitro* and *in vivo* (Mack, 2011; Suwanabol *et al*, 2012). Inhibition of PDGF receptors *in vivo* by monoclonal antibodies reduces atherosclerotic lesion and prevent neointimal proliferation in *ApoE$^{-/-}$* mice on a high fat diet, indicating that PDGF signaling stimulates VSMCs migration and proliferation (reviewed by Owens *et al*, 2004).

In contrast to PDGF, IGF-1 generally maintains the contractile phenotype of VSMCs via the inositol 1,4,5-triphosphate 3-kinase (IP3K)-Akt (PKB) signaling pathway (Hayashi *et al*, 1999). However, IGF-1 belongs to the second category, and its effects depend on the

initial phenotype of VSMCs (Hayashi *et al*, 2004). In synthetic VSMCs, IGF-1 activates ERK and p38 MAPK signaling and thus promotes cell proliferation and migration. Hayashi *et al* reported that the balance between Akt and ERK/p38 MAPK determines the phenotype of VSMCs (Hayashi *et al*, 1999; Hayashi *et al*, 2004). In atherosclerosis lesions, IGF-1 reduces apoptosis and MMP activities, and enhances cell proliferation, thus increases the VSMC population in the plaque (von der Thusen *et al*, 2011). As a consequence, IGF-1 stabilizes atherosclerotic plaques.

TGF-β also exhibits dual effects on VSMCs. TGF-β superfamily consists of TGF-βs, activins, bone morphogenetic proteins (BMPs), and growth and differentiation factors (GDFs) (reviewed by Guo and Chen, 2012). TGF-β binds to TGF-β receptor type II (TGFBRII), recruits and phosphorylates TGFBRI. The activated receptor complex phosphorylates Smad2/3 transcription factor to induce association with Smad4 and translocation into the nucleus (Massague, 2000). TGF-β can also activate a 'non-canonical' pathway which transduces signals through MAPKs and PI3K (Massague, 2012). TGF-β1 strongly induces the contractile phenotype by up-regulating contractile VSMC markers through both Smad and MAPK pathways (Tang *et al*, 2011). TGF-β induces expression of p21 and other cell cycle arrest proteins, thus inhibits cell proliferation. On the contrary, TGF-β potently stimulates ECM production by VSMCs. Overexpression of TGF-β *in vivo* enhances neointima formation, matrix deposition, and VSMC proliferation, suggesting that TGF-β signaling has an overall protective effect in the atherosclerotic plaques (reviewed by Owens *et al*, 2004).

Although cytokines are important factors for VSMC phenotypic modulation, cell-ECM and cell-cell interactions are also important in regulating this process. MMPs digest ECM, regulate the balance of ECM metabolism and control cell-ECM or cell-cell contacts. MMPs promote VSMC migration and proliferation and contribute to the development of atherosclerosis and plaque stabilization (Hameedaldeen *et al* 2014; Newby, 2006; Owens *et*

16

al, 2004). MMP2 and MMP9 are expressed at high levels and activated in VSMCs during intima proliferation in organ cultures and animal models (Newby, 2006). MMPs also regulate the availability of growth factors. For example, MMP2 and MMP9 activate TGF-β by proteolytic cleavage of latency-associated peptide (LAP) and latent TGF-β binding protein (LTBP) (Pardali and ten Dijke, 2012). On the other hands, TGF-β1 induces MMP9 expression through ROS-dependent ERK-NFκB pathways (Zhang *et al*, 2013).

1.6 Purpose of the Study

In this study, I examine whether *HtrA1*$^{-/-}$ mouse is valuable as a model for human CARASIL. I analyze arteries, including the aorta, of *HtrA1*$^{-/-}$ mice to examine whether the mice are valuable for identifying the earliest signs of this disease and whether the mice can be utilized to unveil etiology of SVDs in general. Because the primary pathologic site of CARASIL is VSMCs, I focus on the properties of VSMCs *in vivo* in the aorta. I also isolate primary cultures of VSMCs from *HtrA1*$^{-/-}$ mice and examine their phenotypic state, which categorizes VSMCs into two interchangeable types: synthetic and contractile. I treat the isolated VSMCs to test differential responsiveness to growth factors, including PDGF-BB, which induces synthetic properties irrespective of cell phenotypes, and IGF-1, which affects cells depending on the phenotypic conditions.

II. MATERIALS AND METHOD

2.1 Reagents

The following antibodies were used in this study: anti-cleaved caspase-3 (Asp175) (5A1E) rabbit monoclonal antibody (#9664, Cell Signaling Technology), anti-smooth muscle α-actin (SMA) (ab5694, Abcam), anti-calponin (ab46794, Abcam), anti-vimentin (ab45939, Abcam), anti-osteopontin (MPIIIB101, Developmental Studies Hybridoma Bank), anti-proliferating cell nuclear antigen (PCNA) (#3350R, Biovision), anti-p-ERK1/2 (Thr20/Tyr204) (#9100, Cell Signaling Technology), anti-p-Akt (Ser473) (#4060, Cell Signaling Technology), anti p-Smad2/3 (Ser423/425) (sc-11769, Santa Cruz Biotechnology), and anti-α-tubulin (t9026, Sigma). The production of anti-HtrA1 (Oka *et al*, 2004) and anti-HtrA3 (Tocharus *et al*, 2004) antibodies was described previously. Recombinant murine PDGF-BB (#315-18) and recombinant human TGF-β1 (#100-21) were purchased from Peprotech, recombinant human IGF-1 (291-G1) was from R&D System. SB203580 (BML-EI286), a selective inhibitor of p38 MAPK, was from Enzo Life Sciences. SP600125 (#10010466), a JNK inhibitor; SB431542 (#13031), an antagonist of type I TGF-β receptor; Bay11-7082 (#10010266), an NF-κB inhibitor; and U0126 (#70970), a selective inhibitor of MEK1/2, were from Cayman Chemical. N-acetyl cysteine (NAC) (A9165), a reactive oxygen species scavenger was purchased from Sigma Aldrich.

2.2 Mice

HtrA1^{-/-} mice were generated by standard homologous recombination procedures as previously described (Tsuchiya *et al*, 2005; supplement in Jones *et al*, 2011). Original 129/B6 *HtrA1*^{-/-} mice were backcrossed more than 10 times with BALB/c mice. *HtrA1*^{-/-} mice and wild type (WT) mice with BALB/c background were used unless otherwise indicated.

HtrA3^{-/-} mice were also generated by conventional homologous recombination method as previously described (Hasan *et al*, 2015). *HtrA3^{-/-}* mice were maintained as a mixed 129/B6 background. *HtrA1^{-/-};HtrA3^{-/-}* mice were obtained from mating of *HtrA1^{-/-}* and *HtrA3^{-/-}* with 129/B6 background.

Mice were bred in specific pathogen-free conditions according to the standard protocol of the animal facility of Nara Institute of Science and Technology and were sacrificed by an overdose intraperitoneal injection of sodium pentobarbital. This study was approved by the animal welfare sub-committee of Nara Institute of Science and Technology.

2.3 Histology

Mice were sacrificed by an overdose intraperitoneal injection of sodium pentobarbital. Tissues were removed and fixed overnight in 4% paraformaldehyde/phosphate-buffered saline (PBS) at 4°C then were processed for paraffin embedding [http://dx.doi.org/10.17504/protocols.io.nw5dfg6]. The upper or lower half of the descending thoracic aorta was used for histological analyses or tissue extract preparation, respectively. Serial sections (5 μm) were cut from paraffin-embedded tissues, and then stained with hematoxylin and eosin (HE), the elastica van Gieson (EVG) reagent for elastic fibers, and picrosirius red for collagens. To observe myelin, brain sections were stained with luxol fast blue and cresyl violet (Klüver-Barrera staining).

2.4 *In Situ* Hybridization

The HtrA1 probe (Oka *et al*, 2004) was prepared as described previously. *In situ* hybridization was performed as described previously (Hasan *et al*, 2015). Briefly, after deparaffinization and rehydration, 12 μm-thick paraffin sections were fixed with 4% PFA/PBS, treated with 1 μg/ml proteinase K (Takara) at 37°C for 30 min, acetylated in 0.25%

(v/v) acetic anhydride (Wako Chemicals) for 10 min, and then hybridized with the digoxigenin (DIG)-labeled probe overnight at 55°C. Following washing, the sections were blocked with a blocking solution (0.5% Block Ace (Dai Nippon Sumitomo Pharma) and 20% normal goat serum (NGS) (Sigma) in Tris-buffered saline (TBS)) for 1 h at room temperature. The sections were then incubated with alkaline phosphatase-conjugated anti-DIG antibody (Roche) diluted in the blocking solution (1:1,000) overnight at 4°C followed by washing and color developing using BCIP (5-bromo-4-chloro-3-indolyl-phosphate)/NBT (nitro blue tetrazolium).

2.5 Cell Culture

VSMCs were isolated from cultured explants of aortas from 10 week-old mice as previously described (Metz *et al*, 2012) with some modifications. The entire descending thoracic aortas were dissected and washed in Hank's balanced salt solution (HBSS, Wako). While keeping the aorta in a dish on ice, the connective tissue and adventitia were removed. After transferred into a new dish with fresh HBSS, the aorta was cut open longitudinally, and the endothelial layers were removed by gentle scrape with a sterile cotton swab. Subsequently, the aorta was cut into 4 pieces (around 4 mm^2 each), washed in Dulbecco's modified Eagle's medium/Ham's F12 (DMEM/F12) (Gibco), and transferred to a collagen-coated culture dish (35 mm) and pressed with the luminal side down on the plate. The aorta was then spread out over as large an area as possible and allowed to sit for 5 min in a 37°C, 5% CO_2 incubator in a tilting position. Fresh medium supplemented with 20% fetal bovine serum (FBS) (Sigma) and antibiotics (70 µg/ ml penicillin and 50 µg/ml streptomycin) was then slowly added until it just covered the aorta. The dish was placed in the incubator and left undisturbed for 4 days. At day 5, fresh medium was added and then changed every 3 days. Cells that migrated from the explant were harvested and expanded by culturing in 10%

FBS/DMEM/F12 (complete medium). Isolated VSMCs retained HrA1 expression comparable to that in the aorta, at least up to passage 13. VSMCs from passage 7 to 14 were used for the experiments. Three batches each of *HtrA1*^{-/-} and WT VSMCs were obtained and most of the experiments were conducted for all batches. Medial explants from 2-3 mice were used for each batch.

For treatment of cells with growth factors or inhibitors, cells were plated into 6-well plates in DMEM/F12 containing 10% FBS and grown to confluence. The cells were then serum-starved for 24 h in 0.1% or 0.5% FBS/DMEM/F12 (starvation medium). Growth factors and inhibitors were then added to the culture at the following concentrations: 20 ng/ml of PDGF-BB, 10 ng/ml IGF-1, 10 ng/ml TGF-β1, 10 μM of SB203580, 10 μM of SP600125, 10 μM of SB431542, 5 μM of NAC, 1 μM of Bay11-7082, and 10 μM of U0126.

2.6 Immunostaining

Immunohistochemistry with an anti-HtrA1 or anti-HtrA3 serum was carried using the avidin-biotin complex method as described previously (Hasan *et al*, 2015). HtrA1 and HtrA3 immunostaining of aorta sections was performed after heat-induced epitope retrieval in a pH 9 buffer solution (Immunoactive, Matsunami). Following washing in PBS, the sections were blocked with 1% bovine serum albumin (BSA) and 10% normal goat serum in 0.3 M glycine/PBS-T (PBS containing 0.25% (w/v) Triton X-100) for 30 min at room temperature. The sections were then incubated with anti-HtrA1 or anti-HtrA3 serum (1:1,000 in 1% BSA/PBS-T) overnight at 4°C. Next, the sections were incubated with biotin-conjugated anti-rabbit IgG (Jackson Immunoresearch Laboratories) in 10% NGS/T-PBS (1:200) for 1 h at room temperature, followed by incubation with streptavidin-rhodamin (1:400 in 1% BSA/PBS-T) for 1 h at room temperature. After DAPI counterstaining, the sections were mounted with an aqueous mounting medium (Fluoromount, Sigma).

The same procedures were used to detect VSMC markers. For staining of cultured VSMCs, cells were washed with cold PBS to remove the medium, and then fixed in cold methanol for 15 min. The cells were permeabilized in PBS-T for 10 min. The endogenous peroxidase activity was blocked with 0.3% H_2O_2 in methanol for 30 min at room temperature. Nonspecific sites were blocked with 1% BSA and 10% NGS in 0.3M glycine/PBS-T for 30 min at room temperature, followed by incubation in a primary antibody overnight at 4^oC. The primary antibodies were diluted in 1% BSA/T-PBS as follow: anti-SMA 1:100, anti-calponin 1:400, anti-vimentin 1:100 or 1:400 (for aorta or VSMCs, respectively), anti-osteopontin 1:50 or 1:100 (for aorta or VSMCs, respectively). After washing with PBS, samples were incubated in an appropriate biotin-conjugated IgG secondary antibody (1:200 in 10% NGS/PBS-T) for 1 h at room temperature. The bound biotin was then visualized by incubating with streptavidin-horseradish peroxidase (HRP) (1:100) and diaminobenzidinine (DAB) substrate in a DAB buffer (0.05% DAB/0.01% H_2O_2/50 mM Tris-HCl pH 7.6) at room temperature. After counterstaining with hematoxylin, the sections were dehydrated in graded ethanol, cleared in xylene, and mounted (Sotfmount, Wako). Negative controls were obtained by omitting the primary antibody.

2.7 PCNA Immunostaining and TUNEL Assay

To assess VSMC proliferation in aorta, paraffin-embedded aorta sections were immunosatined for PCNA (1:400) using the procedure as decribed in section 2.6. The sections were also subjected to a TUNEL (terminal deoxynucleotidyl transferase biotin-dUTP nick end labeling) assay using an *in situ* apoptosis detection kit (Takara) according to the manufacturer's instruction.

2.8 Western Blotting

The lower halves of the descending thoracic aortas were frozen over liquid nitrogen after removal of fat layers and the adventitia, and then thawed and minced on ice. Minced aortas from 3-4 mice were pooled and subjected to extraction. Minced aortas or harvested culture cells were homogenized in a lysis buffer (10 mM Tris-HCl pH 7.6, 1% Triton X-100, 100 mM NaCl, 2 mM EDTA, 10% v/v glycerol) containing 50 mM NaF, 20 mM $Na_4P_2O_7$, 2 mM Na_3VO_4, and 1x protease inhibitor cocktail (Nacalai Tesque) (Beaufort et al, 2014) and the lysates were centrifuged [http://dx.doi.org/10.17504/protocols.io.nxadfie]. Protein concentrations of the cleared lysates were determined using Pierce 660 nm Protein Assay Reagent (Thermo Scientific). Equal amounts of proteins or 20 μl of conditioned media (for HtrA1) were resolved on a 10% SDS-polyacrylamide gel and then electrotransferred to a PVDF membrane as previously described (Supanji et al, 2013). The membrane was blocked with TBS-T (Tris-buffered saline (20 mM Tris-HCl pH 7.6, 130 mM NaCl) containing 0.1% (w/v) Tween-20) containing 0.3% or 5% nonfat dry milk for 1 h at room temperature, and then incubated overnight at 4^oC with a diluted primary antibody. Primary antibodies used were anti-HtrA1 (1:2,000), anti-SMA (1:5,000), anti-calponin (1:50,000), anti-vimentin (1:5,000), anti-osteopontin (1:1,000), anti-p-ERK1/2 (1:1,000), anti-p-Akt (1:2,000), anti-p-Smad2/3 (1:2,000), anti-cleaved caspase-3 (1:1,000), or anti-tubulin (1:2,000). The membrane was then incubated with an appropriate HRP-conjugated secondary antibody (1:5,000; catalog number NA9310; or 1:25,000; catalog number NA9340; Amersham Bioscience). Signals from HRP on the membrane were developed by ECL Prime (Amersham Bioscience) and detected with a Luminescent Image Analyzer LAS4000 (Fujifilm). The band intensities were measured by ImageJ software and normalized with tubulin to calculate relative expression levels.

2.9 Histomorphometry

Images of at least three EVG-stained serial sections cut at 100 μm intervals from each aorta were captured for histomorphometry with a light microscope (Olympus BX50) equipped with a digital camera (Nikon DS-Fi1). Aortas from four to ten mice were used for each time point. External and internal circumferences of the media were defined and their lengths were measured using NIS Element Basic Research (Nikon). Histomorphometric parameters of the aorta were defined according to Hart *et al* (1980) and Vaja *et al* (2009) with modifications as illustrated in Fig. 2.1. Cross-sectional area representing aorta size was the area within the external circumference. Media area was calculated by subtracting the area inside the internal circumference from the cross-sectional area. Media thickness was calculated by dividing the media area by the internal circumference. Lumen diameter was determined as the internal circumference divided by π.

Cross-sectional area = external circumference area

Media area = external circumference area – internal circumference area

Media thickness = media area/ internal circumference

Lumen diameter = internal circumference/π
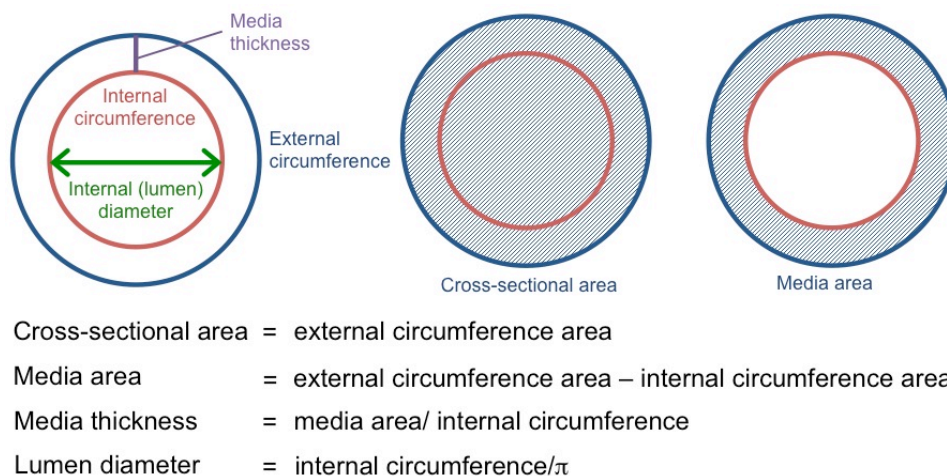
Figure 2.1. Illustration and formula for histomorphometric analysis. Shaded areas in middle and left figures represent cross-sectional and medial area, respectively.

Thickening of media was analyzed with EVG-stained sections. The aorta was categorized as having uneven thickening if its thickest area was 2.5 times or more as thick as the thinnest area. Disruption of elastic fibers was analyzed with autofluorescence of HE-stained sections that were observed with a fluorescence microscopy (Olympus BX50

24

microscope fitted with a Nikon DS-2MBWc camera). The grading of elastic fiber degradation was carried out based on the extent of elastic fiber fragmentation and branching, according to a reported method (Deckert *et al*, 2013) with the following modifications. One point was given to one incident of elastic fiber fragmentation or branching; the total points were summated to calculate "score" for each section from each aorta. Grade 1 = none (score 0-7); grade 2 = minimal (8-15); grade 3 = moderate (16-23); grade 4 = severe (>23) (adapted from Deckert *et al*, 2013). To assess the number of VSMCs, VSMC nuclei in the aortic media of HE-stained sections were manually counted.

2.10 Cell Proliferation

VSMCs (2×10^3 cells/well) were plated in 96-well plates and cultured in complete medium for 15 h. The medium was then replaced with either a medium containing a different concentration of FBS or one containing 0.5% FBS and either PDGF-BB or IGF-1. Cell numbers were assessed with a Cell Counting Kit (CKK)-8 (Dojindo Molecular Technologies) according to the manufacturer's instruction at the indicated time after medium replacement. The absorbance at 450 nm, which represents the living cell number, was normalized to the value for 0 h (time of medium replacement) to calculate fold proliferation. Data are presented as the mean of three or four measurements per condition per experiment.

2.11 Migration Assay

Wound-healing assays were performed using an Ibidi culture-insert system (supplement in Zhang *et al*, 2011). Briefly, 70 μl of cell suspension (1.4×10^4 cells) was loaded into each well of the culture-insert. After 20 h to allow the cells attached on the dish, mitomycin C solution (Nacalai Tesque) was added to 1 μg/ml to inhibit cell proliferation. Four hours later, the culture insert was gently removed using tweezers to generate a 500 μm

wide cell-free gap. The dish was then washed with PBS to remove unattached cells and filled with medium containing a different concentration of FBS, or an FBS-free medium supplemented with either PDGF-BB, IGF-1, or inhibitors. The experiments were conducted in triplicate. Images were captured at indicated time points using an inverted microscope (Nikon Diaphot 300) equipped with a digital camera (Sony α NEX-3N).

A migration assay using a modified Boyden chamber method was carried out with Transwell Permeable Support Inserts (Corning) according to the manufacturer's protocol. The insert and the receiver chambers were rehydrated with pre-warmed starvation medium containing 0.5% FBS, and then cell suspension (1×10^5 cells in 100 μl) was loaded into the insert. Five hundreds microliters of complete medium, or starvation medium containing PDGF-BB or IGF-1, were added to the receiver chamber. After 30 min to allow the cells to attach, the chambers were assembled. After 24 h, the cells that had migrated into the bottom side of the insert chamber were stained with DAPI. The number of migrated cells was counted from five fields for each insert. Three wells were used per condition per experiment.

2.12 Gelatin Zymography

MMP activities in the VSMC culture media were assayed by gelatin zymography as previously described (supplement in Hasan *et al*, 2015). The culture medium was centrifuged to remove cell debris. The volume of the cleared culture supernatant applied to the zymography gel was adjusted according to the tubulin content in the cell lysate recovered from the same culture, to compensate the difference in cell numbers in each culture. The culture supernatant was mixed with zymograph sample buffer (62 mM Tris-HCl pH 6.8, 2% SDS, 10% glycerol and 0.01% bromophenol blue) and loaded into a well of an 8% SDS-polyacrylamide gel containing 1% gelatin. After electrophoresis and washing the gel in 2.5% (w/v) Triton X-100, 50 mM Tris-HCl pH 7.5, three times each for 20 min, the gel was

incubated in a gel development buffer (10 mM CaCl$_2$, 150 mM NaCl, 50 mM Tris-HCl pH 7.5, 0.02% NaN$_3$) for 48 h at 37°C. Next, the gel was stained with 0.125% Coomassie Brilliant Blue R-250 for 1 h at room temperature and destained in methanol:acetic acid:water (1:2:17). The destained gel was scanned with a CanoScan LiDE 200 (Canon), and intensities of white bands indicating gelatinolytic activities were measured by ImageJ software (NIH).

2.13 qRT-PCR

Total RNA from VCMCs was extracted using Sepasol-RNA I Super G (Nacalai Tesque) according to the manufacturer's instructions. After contaminating genomic DNA was degraded with gDNA Eraser, 1 μg of total RNA was reverse transcribed using the PrimeScript RT reagent kit with gDNA Eraser (Takara). cDNA samples were amplified in triplicate using the SYBR qPCR mix (Toyobo) with the LightCycler 96 PCR System (Roche Applied Science). The following conditions were used: denaturation at 95°C for 1 min; 45 cycles of PCR at 95°C for 10 s, 55°C for 30 s, 72°C for 20 s; and final steps at 95°C for 15 s, 60°C for 30 s, and 95°C for 15 s for dissociation curve analysis. A dissocation curve for each PCR product was determined following the LightCycler's instructions to ensure specific amplification of the target gene. The data were analyzed by the ΔΔtC method, using GAPDH as the internal control. The primers used are listed as follow: 5'-CAAGTTCCCCGGCGATGTC-3' and 5'-TTCTGGTCAAGGTCACCTGT-3' for mouse *mmp2*, 5'-GCGTCGTGATCCCCACTTAC-3'and 5'-CAGGCCGAATAGGAGCGTC-3' for mouse *mmp9*, 5'-AACATCATCCCTCATCCAC-3′and 5'-CCCTGTTGCTGTAGCCGTAT-3′ for mouse *gapdh*.

2.14 Cell Viability and Apoptosis Assay

VSMCs (2x10^3 cells/well) were plated in 96-well plates and cultured in complete

medium for 24 h, and then serum-starved for 24 h in DMEM/F12 containing 0.1% FBS. The cells were treated with 0.1 mM or 0.3 mM H_2O_2 in the latter medium for 24 h and the cell number was examined using Cell Count Reagent SF (Nacalai Tesque). For the apoptosis assay, VSMCs were grown to confluence on cover glass in 6-well plates. VSMCs were serum-starved as above and then treated with 0.1 or 0.3 mM H_2O_2 for 6 h in the starvation medium. Cells were triply stained with an Apoptotic/Necrotic/Healthy Cells Detection Kit (PromoKine) according to the manufacturer's instruction, or immunostained with anti-cleaved caspase-3 rabbit monoclonal antibody (1:400). The cells were cultured in 6 cm dishes, and similarly treated with 0.3 mM H_2O_2 in medium containing 0.1% FBS. Cell lysates were then prepared at several time points to assay cleaved caspase-3 by Western blot using the same antibody (1:1,000).

2.15 Statistical Analysis

Data are presented as mean ± standard deviation (SD) or mean ± standard error (SE) as indicated in the figure legends, and were analyzed for significance using Student's *t*-Test. Data for grading of elastic fiber degradation were analyzed for significance using the nonparametric Mann-Whitney U-Test. Values of $p < 0.05$ were considered significant. Raw data on which statistical calculations were carried out are presented as Appendix

III. RESULTS

3.1 Brain Arteries of *HtrA1*^{-/-} Mice are Normal

The Riken Mouse Clinic, a systematic and comprehensive phenotyping platform in Japan (http://www.brc.riken.jp/lab/jmc/mouse_clinic/en/m-strain_en.html), detected no abnormality in *HtrA1*$^{-/-}$ mice in various tests, including behavioral neurological assessments, except for a slight decrease in body mass index. *HtrA1*$^{-/-}$ mice are fertile, and develop and grow normally. *HtrA1*$^{-/-}$ mice do not show neurological abnormalities and hair-loss, which are related to symptoms of human CARASIL. Preliminary behavioral studies showed no significant difference between wild type (WT) and *HtrA1*$^{-/-}$ mice at an adult stage (7 week-old) in the open field test that measured exploratory behavior and general activity. The modified SHIRPA test that covered morphology and behavioral aspects also revealed no significant difference in overall appearance between WT and *HtrA1*$^{-/-}$ mice at 8 weeks of age. Aged *HtrA1*$^{-/-}$ mice sometimes displayed minor vertebral deformation reminiscent of spondylotic changes found in CARASIL patients. The body mass index of *HtrA1*$^{-/-}$ mice was significantly reduced due to an increase in body length and a decrease in body weight (C. Oka, *unpublished data*).

Histological abnormalities found in cerebral small arteries of CARASIL patients feature loss of vascular smooth muscle cells (VSMCs), elastic fiber degradation, and neointima formation (Arima *et al*, 2003; Oide *et al*, 2008; Hara *et al*, 2009). I first analyzed if the brain arteries of *HtrA1*$^{-/-}$ mice showed these signs. HtrA1 was expressed in the brain arteries of adult mice as confirmed by *in situ* hybridization and immunostaining (Fig. 3.1A, B). However, *HtrA1*$^{-/-}$ mice showed no clear defect in brain arteries, including the middle cerebral artery with diameter around 50-100 μm, even in old (52-week-old) mice (Fig. 3.2). HE staining or immunostaining for smooth muscle α-actin (SMA) showed no apparent loss of
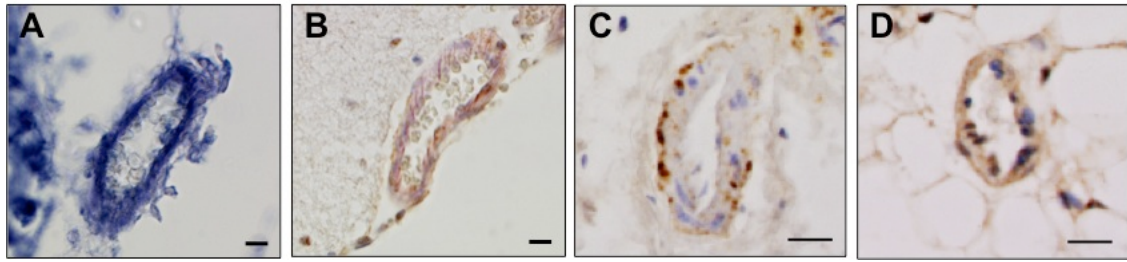
Figure 3.1 **HtrA1 and HtrA3 expression in small arteries.** Coronal sections of midbrains from an adult mouse were analyzed by *in situ* hybridization with the antisense probe for HtrA1 **(A)**, or stained with anti-HtrA1 antibody **(B)**. Arteries near knee joints (popliteal arteries) from an adult mouse were stained with anti-HtrA1 **(C)** or anti-HtrA3 **(D)** antibody. Bars = 50 μm.

VSMCs in $HtrA1^{-/-}$ mouse brain arteries (Fig. 3.2E and G). The intima of $HtrA1^{-/-}$ mouse brain arteries appeared normal and the internal elastic lamina remained intact (Fig. 3.2F). Klüver-Barrera staining, which stains myelin blue, did not reveal signs of leukoencephalopathy in the $HtrA1^{-/-}$ mouse brain (Fig. 3.2H).
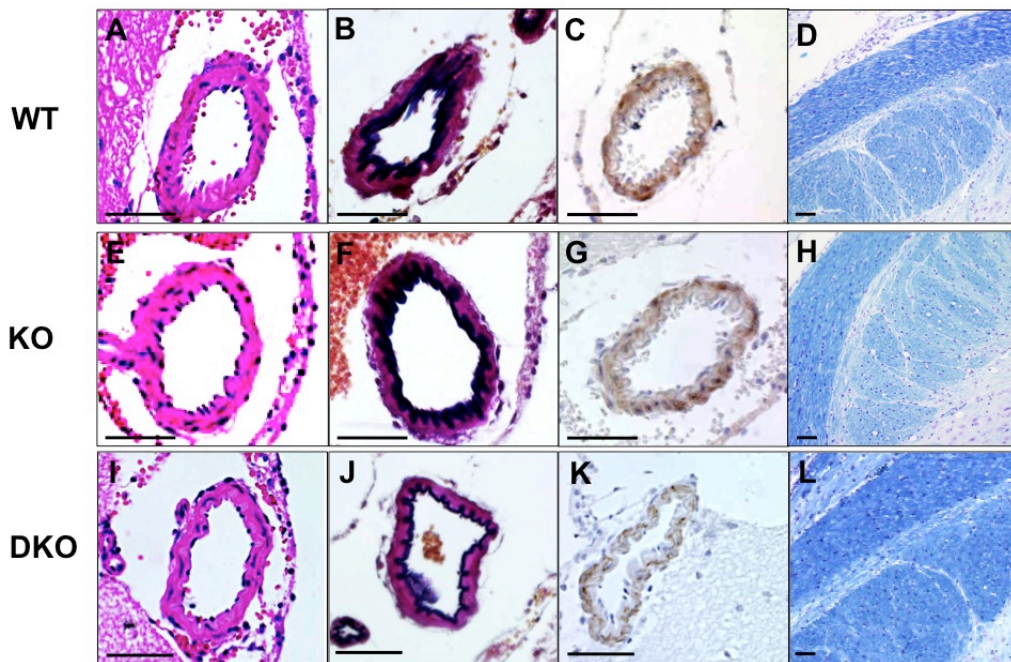
Figure 3.2 **Histology of brain arteries of wild type, $HtrA1^{-/-}$, and $HtrA1^{-/-};HtrA3^{-/-}$ mice.** Coronal sections of midbrains from 52-week-old wild type (WT), $HtrA1^{-/-}$ (KO), and $HtrA1^{-/-};HtrA3^{-/-}$ (double knockout, DKO) mice from 129/B6 background were stained with hematoxylin and eosin **(A, E, I)**, elastica van Gieson for elastic fibers **(B, F, J)**, anti-smooth muscle α-actin antibody, a VSMC marker **(C, G, K)**, and luxol fast blue and cresyl violet for myelin **(D, H)**. No obvious defects were observed in $HtrA1^{-/-}$ and $HtrA1^{-/-};HtrA3^{-/-}$ brain arteries. Bars = 50 μm.

Similar to HtrA1, HtrA3 was also expressed in arteries (Fig. 3.1.D). I expected that *HtrA1^{-/-};HtrA3^{-/-}* double knockout mice would show more apparent artery abnormalities compared to *HtrA1^{-/-}* mice. Nonetheless, *HtrA1^{-/-};HtrA3^{-/-}* mice showed neither reduction in VSMCs, neointima formation, or elastic fiber degradation (Fig. 3.2I-K).
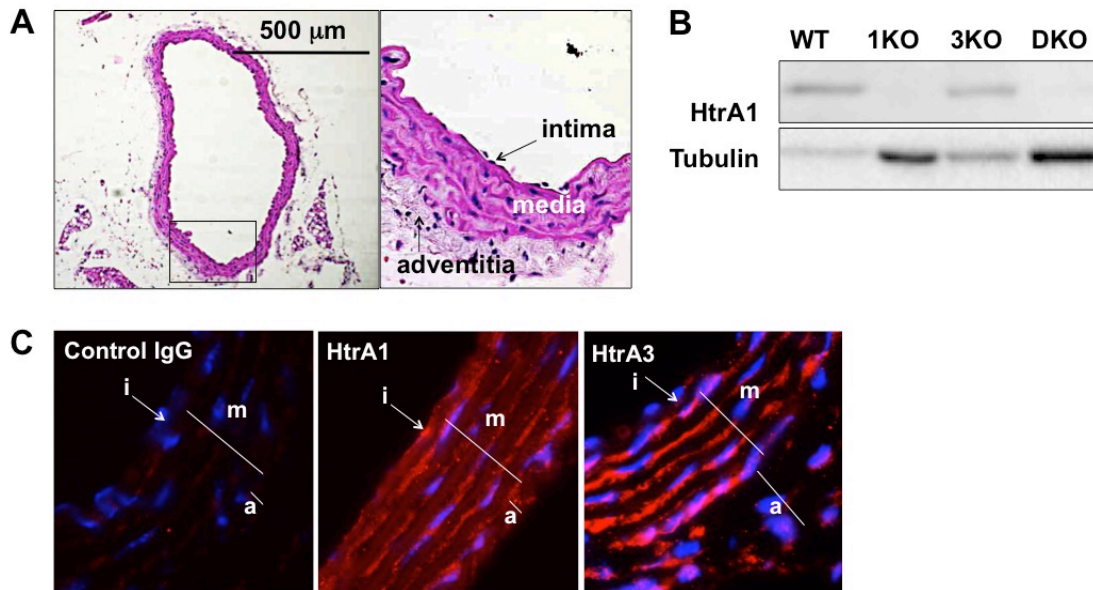
Figure 3.3 **Size, structure and HtrA1 expression in mouse aorta.** **(A)** Hematoxylin and eosin staining of the aorta from 16-week-old mice. The aorta is around 500-1,000 μm in diameter (left) and consists of three distinguishable layers (right). Right panel shows higher magnification (6x) of the aorta in the left panel (box). **(B)** Western blot analysis of HtrA1 in the aorta of wild type (WT), *HtrA1^{-/-}* (1KO), *HtrA3^{-/-}* (3KO), and *HtrA1^{-/-};HtrA3^{-/-}* (DKO) mice. 129/B6 mice at 52 weeks of age were used. **(C)** HtrA1 or HtrA3 staining of aorta from 8-week-old ICR mice. Aortas were immunostained with anti-HtrA1 (middle) or anti-HtrA3 (right) antibody and counterstained with DAPI (blue). HtrA1 and HtrA3 were expressed in VSMCs in the media. Staining without primary antibody was uses as control (left). i=intima; m=media; a=adventitia.

3.2 Mouse Aorta has Similar Size and Structure with Human Brain Arteries and Expresses HtrA1

Brain arteries of 100-1,000 μm in diameter are preferentially damaged in human CARASIL (Oide *et al*, 2008). Mouse brain arteries are smaller than this size, whereas mouse aorta is 500-1,000 μm in diameter and has structures similar to human small brain arteries (Fig. 3.3A). Similar to human brain arteries, mouse aorta consists of the tunica adventitia, the

tunica media, and the tunica intima, from outer to inner layers. The media is the largest

portion, which consists of VSMCs packed between layers of elastic fibers and the

extracellular matrix (ECM). Moreover, mouse HtrA1 is expressed not only in small brain

arteries but also in the aortic media (Fig. 3.3B, C). I therefore assumed that the aorta of the

$HtrA1^{-/-}$ mouse should exhibit detectable abnormalities.

3.3 Altered Structure of $HtrA1^{-/-}$ Mouse Aortas

Morphometric analysis of the aorta showed that the cross-sectional area, medial

thickness, and lumen diameter were greater, though not always significantly, in $HtrA1^{-/-}$ mice

than in WT mice (Fig 3.4A-C) at most time points during 16 to 60 weeks of age. In

particular, $HtrA1^{-/-}$ mice of 40 and 52 weeks old displayed significantly increased cross-

sectional area, which represents aorta size and correlates inversely with contractility of the

vessel (Fig 3.4A).

Loss of VSMCs is the earliest and most distinct event in CARASIL brain arteries

(Arima et al, 2003; Oide et al, 2008; Hara et al, 2009; Cai et al, 2015). The number of

VSMCs in $HtrA1^{-/-}$ aortas, however, was increased at 16 weeks of age, and significantly

higher than that in WT aortas at 24 and 40 weeks of age (Fig. 3.4D). The aortic VMSC

number usually decreases as the mouse ages (Zhu et al, 2001). The decrease in VSMC

number was faster in $HtrA1^{-/-}$ mice than in WT mice after 40 weeks. Consequently, the

VSMC numbers in $HtrA1^{-/-}$ mice became similar to those of WT mice at 52 weeks, and then

became significantly lower than those of WT mice at 60 weeks. .
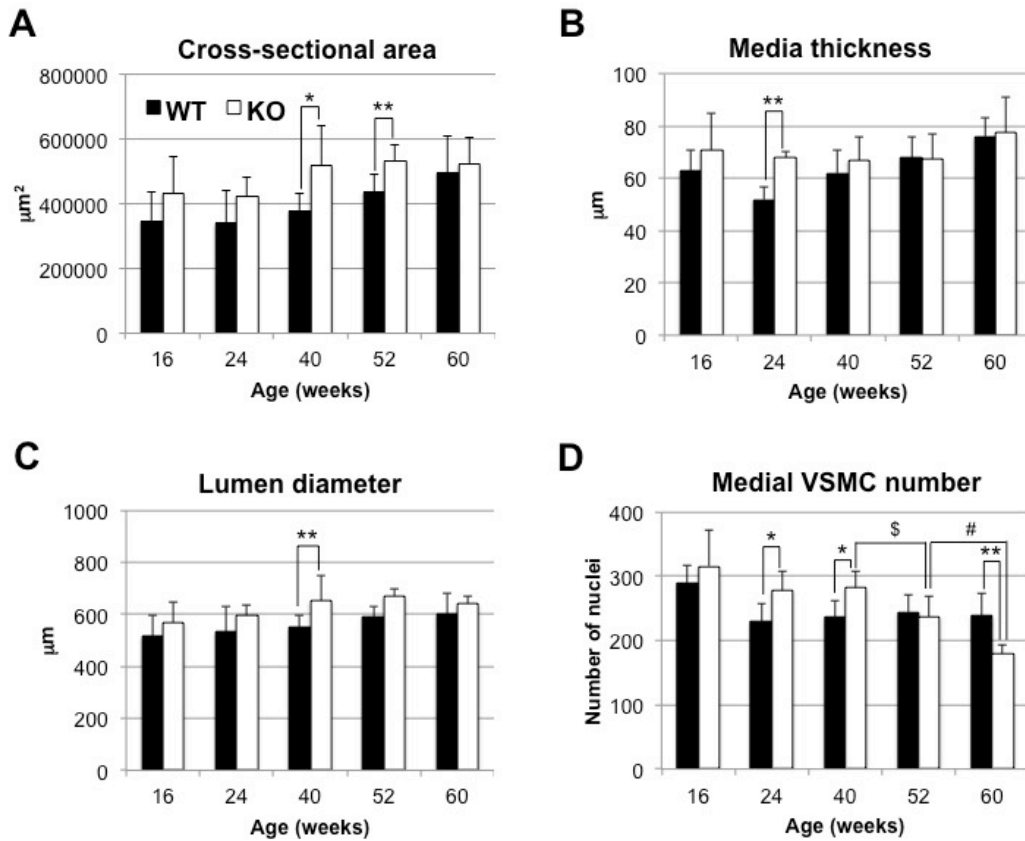
Figure 3.4   Histomorphometric parameters of aortas isolated from *HtrA1*$^{-/-}$ mice.   Cross sections from the upper half of the descending aorta were stained with elastic van Gieson (EVG), hematoxylin and eosin (HE), or picrosirius red.   The EVG-stained sections were analyzed for **A**, cross-sectional area; **B**, media thickness; **C**, lumen diameter; the HE-stained sections were analyzed for **D**, medial VSMC number.   Bars represent means ± SD (four to 10 mice were used for each group and 3-8 aorta sections per mouse were analyzed.   The details are described in Appendix 1).   Statistical significance was determined by Student's *t*-Test.   Asterisks show significance between wild type (WT; black bars) and *HtrA1*$^{-/-}$ (KO; white bars) mice at the same age (*, p <0.05; **, p <0.01). $ or # show significance (p <0.05) of the difference in medial VSMC numbers between 40- and 52-week-old, or 52- and 60-week-old, *HtrA1*$^{-/-}$ mice, respectively.

Throughout this study, I used *HtrA1*$^{-/-}$ mice of BALB/c genetic background.   I examined aortas of *HtrA1*$^{-/-}$;*HtrA3*$^{-/-}$ mice, which had 129/B6 genetic background, using *HtrA1*$^{-/-}$ and *HtrA3*$^{-/-}$ mice with the same 129/B6 genetic background as control.   At 52 weeks of age, the media thickness of all types of knockout mice was similar to WT (Fig. 3.5A). However, medial VSMC numbers in *HtrA1*$^{-/-}$, *HtrA3*$^{-/-}$, and *HtrA1*$^{-/-}$;*HtrA3*$^{-/-}$ mouse aortas were significantly decreased as compared to WT littermate (Fig. 3.5B).   There was no

33

difference in VSMC numbers among $HtrA1^{-/-}$, $HtrA3^{-/-}$, and $HtrA1^{-/-};HtrA3^{-/-}$ mouse aorta. Hence, I focus my study on $HtrA1^{-/-}$ mice.
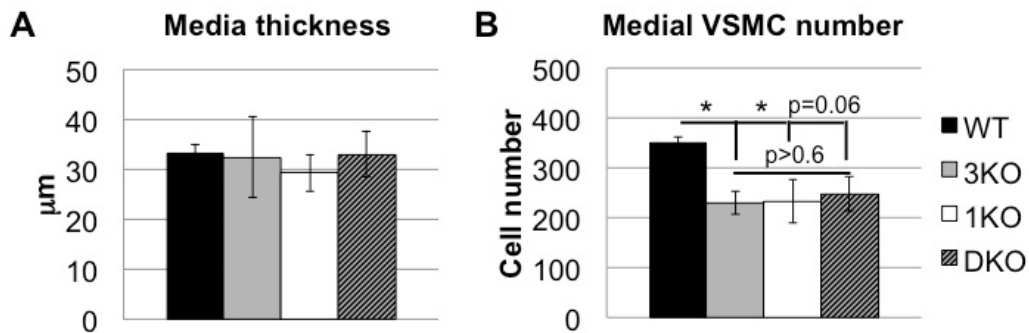
Figure 3.5 **Morphometric parameters of aortas isolated from 52-week-old 129/B6 mice.** Cross sections from the upper half of the descending aorta were stained with elastic van Gieson (EVG), hematoxylin and eosin (HE), or picrosirius red. The EVG-stained sections were analyzed for **A**, media thickness and the HE-stained sections were analyzed for **B**, medial VSMC number. Bars represent means ± SD (two to 6 mice were used for each group and 6-10 aorta sections per mouse were analyzed). Statistical significance was determined by Student's *t*-Test. Asterisks show significance in medial VSMC numbers (p <0.05) between wild type (WT; black bars) and $HtrA3^{-/-}$ (3KO). The VSMC medial number was decreased, though not significantly, in $HtrA1^{-/-};HtrA3^{-/-}$ (DKO) aortas compared to WT aortas.

Increase in cell numbers can be caused by an increase in proliferation or a decrease in apoptosis, or both. Staining with PCNA, a marker for proliferation, showed that cell proliferation was increased, though not significantly, in $HtrA1^{-/-}$ aortas at 40 weeks of age (Fig. 3.6A), whereas an apoptosis assay by terminal TUNEL staining revealed that WT and $HtrA1^{-/-}$ aortas showed comparable percentages of TUNEL-positive cells at 52 weeks of age (Fig. 3.6B).
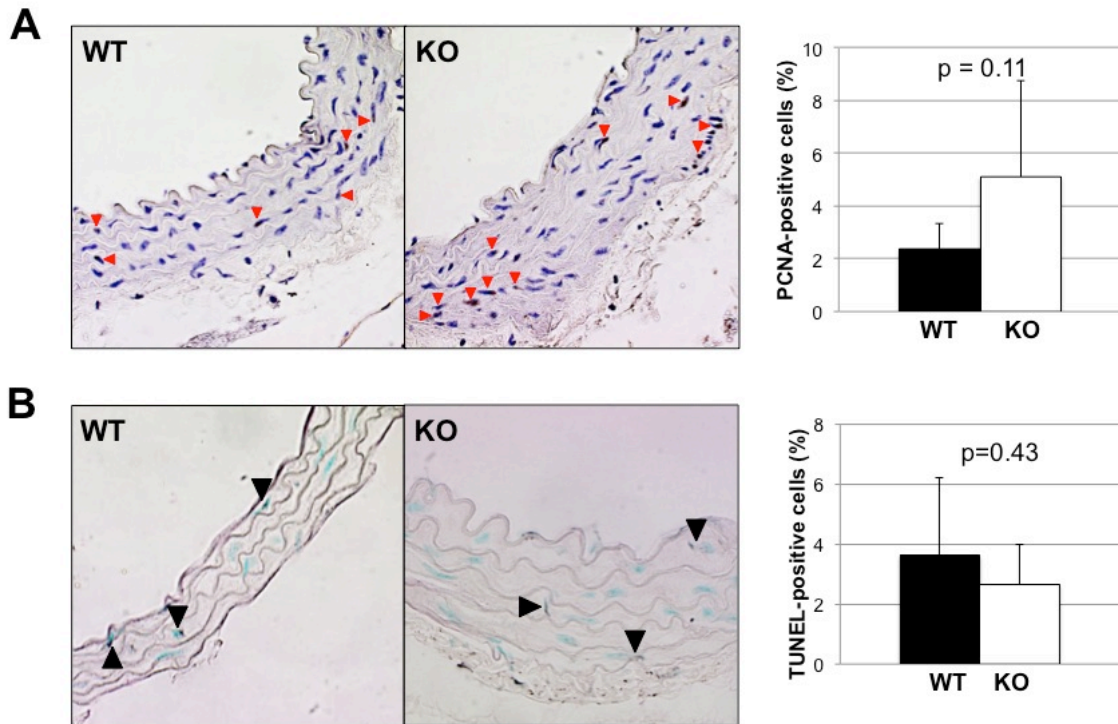
Figure 3.6 **PCNA immunostaining and TUNEL staining of the *HtrA1⁻ᐟ⁻* mouse aorta. (A)** Cross-sectioned aortas from 40-week-old wild type (WT) and *HtrA1⁻ᐟ⁻* (KO) mice were stained with anti-PCNA antibody and counterstained with hematoxylin. Red arrowheads indicate PCNA-positive cells, and percentages of PCNA-positive cells are shown in the graph on the right. Bars represent means ± SD (WT, n=6; KO, n=5). **(B)** Cross-sectioned aorta tissues from 52-week-old mice were stained with TUNEL and counterstained with methyl green. Arrowheads indicate TUNEL-positive cells, and percentages of TUNEL-positive cells are shown in the graph on the right. Bars represent means ± SD (n=6). p values were calculated by Student's *t*-Test.

3.4 Loss of HtrA1 Shifts Isolated VSMCs to Synthetic Phenotype

The increase and then decrease in the number of VSMCs in the *HtrA1⁻ᐟ⁻* mouse aorta during aging prompted me to further analyze the properties of VSMCs. I established primary culture VSMCs from aortas of 10-week-old WT and *HtrA1⁻ᐟ⁻* mice. VSMCs were isolated as cells that migrated out of minced pieces of the aortic media on the culture dishes. Cells that migrated from the medial pieces of *HtrA1⁻ᐟ⁻* mouse aortas spread faster than cells from those of WT mouse aortas (Fig. 3.7A) suggesting that *HtrA1⁻ᐟ⁻* VSMCs in vivo had shifted to the synthetic phenotype.

The identity of VMSCs was determined by the positive immunoreactivity to smooth muscle specific marker, SMA. Majority of cells isolated from both WT and $HtrA1^{-/-}$ mouse aortas expressed SMA (>90%) at least until passage 6 (Fig. 3.7B). Cells from passage 7-14 were used for experiments.
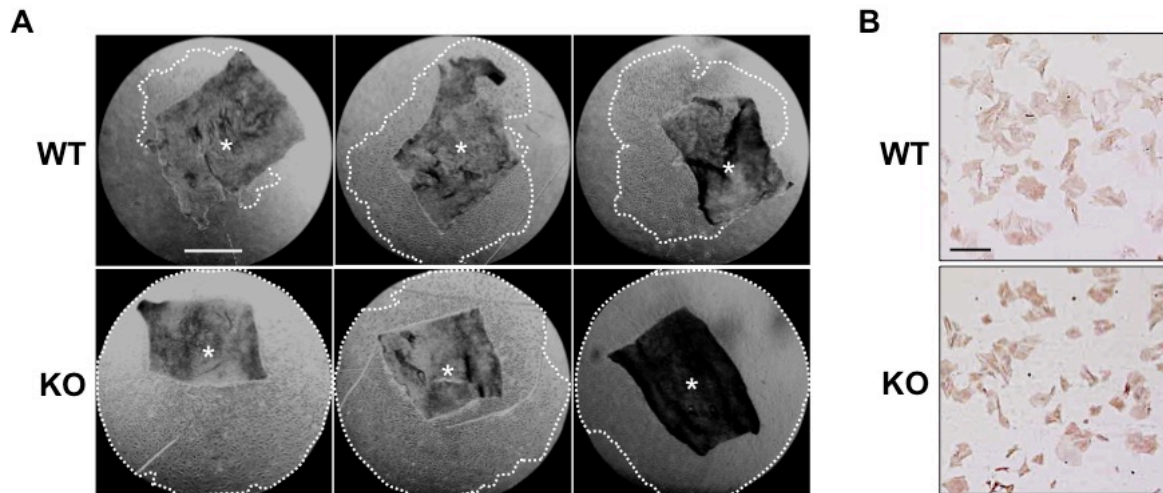
Figure 3.7   Medial explants of wild type and $HtrA1^{-/-}$ mouse aortas.   (A) The aortic media isolated from 10-week-old wild type (WT) and $HtrA1^{-/-}$ (KO) mice were cut into pieces and placed in culture dishes. Cells that had migrated from the medial explants at day 14 are depicted. Dotted lines mark the forefront of migrated cells. Asterisks mark the medial explant. Scale bar=1 mm. **(B)** Expression of a smooth muscle-specific marker, smooth muscle α-actin (SMA), in isolated WT and $HtrA1^{-/-}$ VSMCs at passage 6. Cells (1×10^4/well) were plated in a 6-well plate, cultured for 72 h, and immunostained for SMA (brown). Scale bar=100 μm.

To confirm the synthetic modulation, I next evaluated marker protein expression in VSMCs using SMA and calponin as contractile markers and vimentin and osteopontin as synthetic markers. $HtrA1^{-/-}$ VSMCs expressed less SMA but more vimentin and osteopontin than WT VSMCs (Figure 3.8). Although calponin is a contractile marker, it was expressed at high levels in $HtrA1^{-/-}$ VSMCs. Since the expression patterns of three out of four markers agreed with characteristics of synthetic VSMCs, I postulated that $HtrA1^{-/-}$ VSMCs were in the synthetic phenotype.
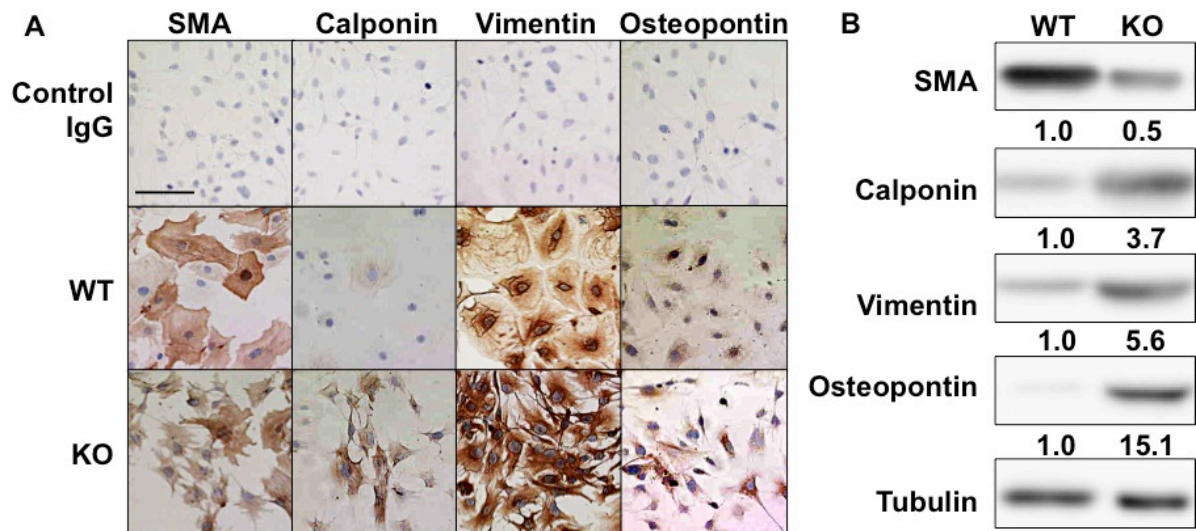
Figure 3.8   **Expression of contractile and synthetic markers in wild type and *HtrA1⁻/⁻* VSMCs.** **(A)** Immunostaining of VSMCs. Cells at passage 13 were immunostained for the indicated VSMC markers (brown) and counterstained with hematoxylin to visualize nuclei (blue). Staining without primary antibody served as control (top panels). Scale bar=100 μm. **(B)** Western blot analysis of VSMC markers. Cell lysates from passage 8 VSMCs were separated by SDS-PAGE and Western blot analysis was performed for the indicated VSMC markers. The expression levels were normalized with tubulin, and relative expression levels were calculated and are shown below the panels.

3.5 *HtrA1⁻/⁻* VSMCs Proliferate and Migrate Faster than Wild Type VSMCs

Rapid proliferation and fast migration are major characteristics of synthetic VSMCs. *HtrA1⁻/⁻* VSMCs proliferated faster than WT VSMCs in all media containing different concentrations (0, 5, and 10%) of FBS (Fig 3.9). Furthermore, *HtrA1⁻/⁻* VSMCs migrated faster than WT VSMCs in wound-healing assays under the different FBS concentrations (Fig 3.10A). The modified Boyden chamber assay in medium containing 10% FBS also showed that three times or more *HtrA1⁻/⁻* VSMCs migrated to the bottom side of the chamber than WT VSMCs (Fig 3.10B). The expression patterns of the VSMC markers together with the rapid cell proliferation and robust migration indicated that *HtrA1⁻/⁻* VSMCs are highly synthetic.
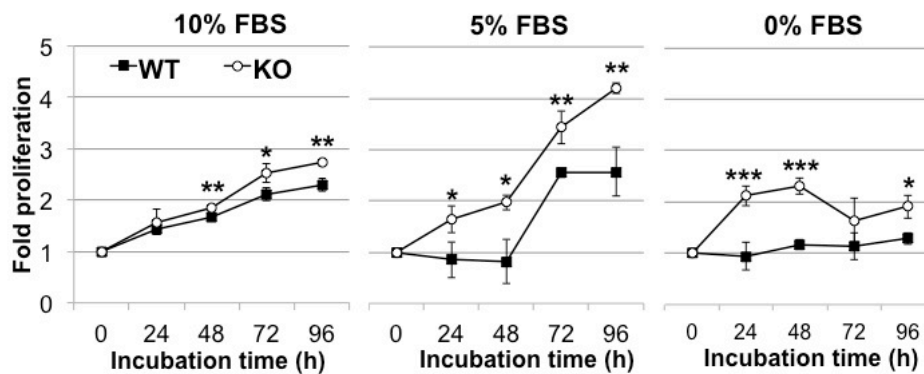
Figure 3.9 **Rapid proliferation of *HtrA1^-/-* VSMCs.** *HtrA1^-/-* (KO) and wild type (WT) VSMCs were cultured in medium containing 10%, 5%, or 0% FBS as indicated. Cell proliferation was assayed at the indicated time points (0 h was set at 15 h after plating). Points in the graph represent means ± SD (n = 3-4). The experiments were carried out independently for three different batches of WT and *HtrA1^-/-* VSMCs at the matching passage. The data shown are a representative result from cells at passage 7. Statistical significance was determined by Student's *t*-Test. *; p <0.5. **; p < 0.01. ***, p <0.001.
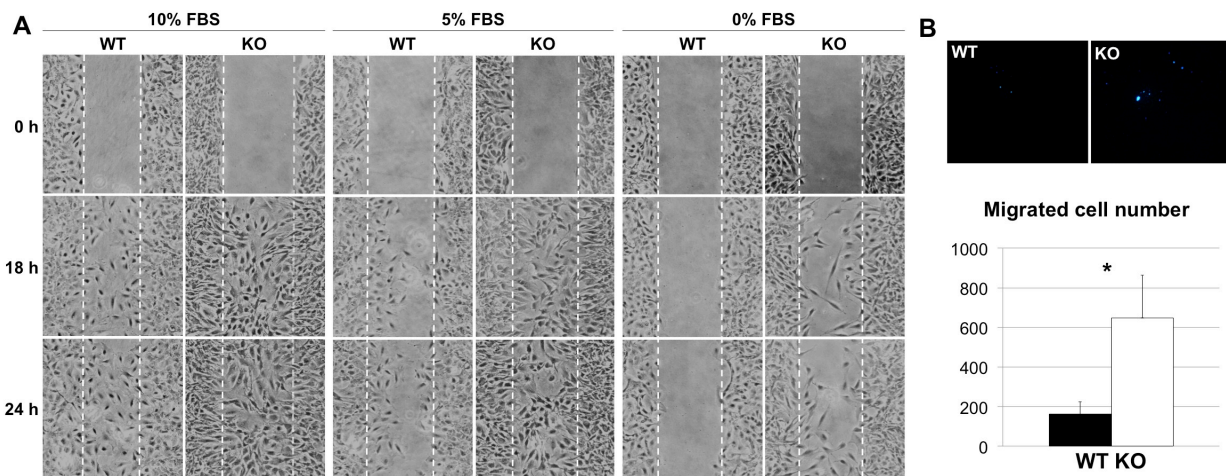
Figure 3.10 **Rapid migration of *HtrA1^-/-* VSMCs.** **(A)** Cell migration was analyzed by the wound-healing assay. *HtrA1^-/-* (KO) and wild type (WT) VSMCs were cultured in medium containing 10%, 5%, or 0% FBS as indicated. Photographs were taken at the indicated time points. White dotted lines indicate boundaries of the initial wounded area. The experiment was repeated three times and representative results are shown. Cells at passage 13 were used. **(B)** Cell migration was analyzed by a modified Boyden chamber assay. Cells were cultured in the chamber in medium containing 10% FBS for 24 h. The number of cells that migrated through the membrane was counted after DAPI staining. The bars are means ± SD (n=3). The experiment was repeated twice and representative results are shown. Cells at passage 12 were used. Statistical significance was determined by Student's *t*-Test. *; p <0.5.

3.6 High MMP9 Activity in the Culture Media of *HtrA1⁻/⁻* mouse VSMCs

MMPs play important roles in promoting cell migration because they degrade ECM, thereby regulate cytokine availability, cell-to-matrix interaction, and cell-to-cell interaction (reviewed in Newby, 2006). MMP9 activities in the culture media of all three batches of the *HtrA1⁻/⁻* VSMCs were more than 10 times higher than those of corresponding WT VSMC (Fig. 3.11A). On the other hand, MMP2 activities were similar between *HtrA1⁻/⁻* VSMCs and WT VSMCs (Fig. 3.11A). Consistent with the gelatin zymography, I observed higher MMP9 mRNA levels in *HtrA1⁻/⁻* VSMCs than in WT cells, but similar levels of MMP2 mRNA in these cells (Fig 3.11B). The increase in MMP9 activity of *HtrA1⁻/⁻* VSMCs is hence caused mostly by an increase in transcription.
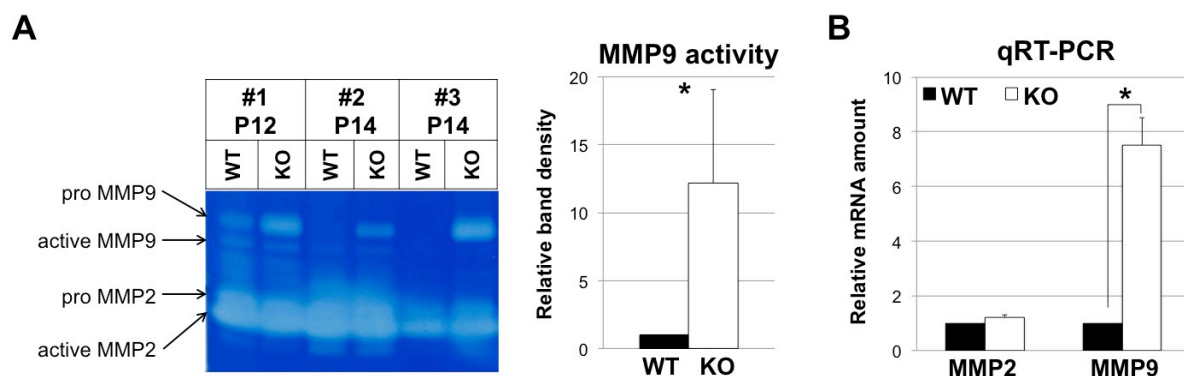
Figure 3.11 Production of MMPs by isolated *HtrA1⁻/⁻* mouse VSMCs. (A) Increased MMP9 activity in the culture media of *HtrA1⁻/⁻* VSMCs. Wild type (WT) and *HtrA1⁻/⁻* (KO) VSMCs were cultured in medium containing 0.5% FBS. After 24 h, the culture medium was recovered. The cells were also harvested, and cell lysates were analyzed by Western blot for tubulin content. The media, whose volumes were normalized by tubulin, were loaded onto a zymography gel. Three different batches of WT and *HtrA1⁻/⁻* VSMCs at the matching passage (passage 12, P12 or 14, P14) were analyzed. The zymogram was analyzed by densitometer and the results are presented in the bar graph on the right. MMP9 activity of WT VSMCs was set to 1, and the relative MMP9 activity of *HtrA1⁻/⁻* is shown as mean ± SD. **(B)** MMP mRNA expression in WT and *HtrA1⁻/⁻* VSMCs. RNA was extracted from cells that were harvested as described in A. MMP2 and MMP9 mRNA were measured by quantitative RT-PCR and normalized with GAPDH. The relative expression levels in *HtrA1⁻/⁻* VSMCs were calculated using the levels of MMP2 and MMP9 mRNA in WT VSMCs as 1. Value represents mean ± SD (n=3), Statistical significance was determined by Student's *t*-Test. *; p <0.5.

3.7 Signal Transduction Pathway that Induces MMP9 Activity of *HtrA1*$^{-/-}$ VSMCs

MMP9 is induced through various signal transduction pathways. I next tried to identify the signal transduction pathway that induced MMP9 activity of *HtrA1*$^{-/-}$ VSMCs. TGF-β is known to induce MMP9 in VSMCs (Zhang *et al*, 2013). VSMCs were treated with TGF-β1, various inhibitors of signal transduction, or a reactive oxygen species (ROS) scavenger. TGF-β1 induced secreted MMP9 activity 3-fold in WT VSMCs, but only 1.2-fold in *HtrA1*$^{-/-}$ VSMCs (Fig. 3.12). An inhibitor of TGF-βR1 (SB431542) did not decrease the MMP activity of *HtrA1*$^{-/-}$ VSMCs. These data indicated that TGF-β signaling was not activated in *HtrA1*$^{-/-}$ VSMCs, at least at the receptor level. NF-κB and AP-1 are the main transcription factors for MMP9 expression in VSMCs (Yabluchanskiy *et al*, 2013). An inhibitor (Bay11-7082) of NF-κB did not affect the MMP9 activity of either WT or *HtrA1*$^{-/-}$ VSMCs. Among the MAP kinase inhibitors examined, only an inhibitor (SP600125) of JNK, which is upstream of AP-1, suppressed the MMP9 activity of *HtrA1*$^{-/-}$ VSMCs, but not that of WT VSMCs, indicating that the JNK pathway was activated in *HtrA1*$^{-/-}$ VSMCs (Fig. 3.12). JNK also serves as a signal transducer of oxidative stress (Li *et al*, 2007). A ROS scavenger. N-acetylcycsteine (NAC), however, did not affect MMP9 activity in either WT or *HtrA1*$^{-/-}$ VSMCs. Besides, inhibitors of p38 MAP kinase (SB203580) and MEK1/2 (U0126), two kinases that are downstream transducers of ROS signaling, did not suppress the MMP9 activity of *HtrA1*$^{-/-}$ VSMCs. These data suggested that the MMP9 activity was elevated by stress other than oxidative stress. The increased migration of *HtrA1*$^{-/-}$ VSMCs was specifically inhibited by the JNK inhibitor (SP600125), but not by the inhibitors of TFG-ßR1, MEK1/2, p38, or NF- κB (Fig. 3.13). This result supports the view that the increased migration of *HtrA1*$^{-/-}$ VSMCs is mainly due to the production of MMP9 induced through the JNK pathway.
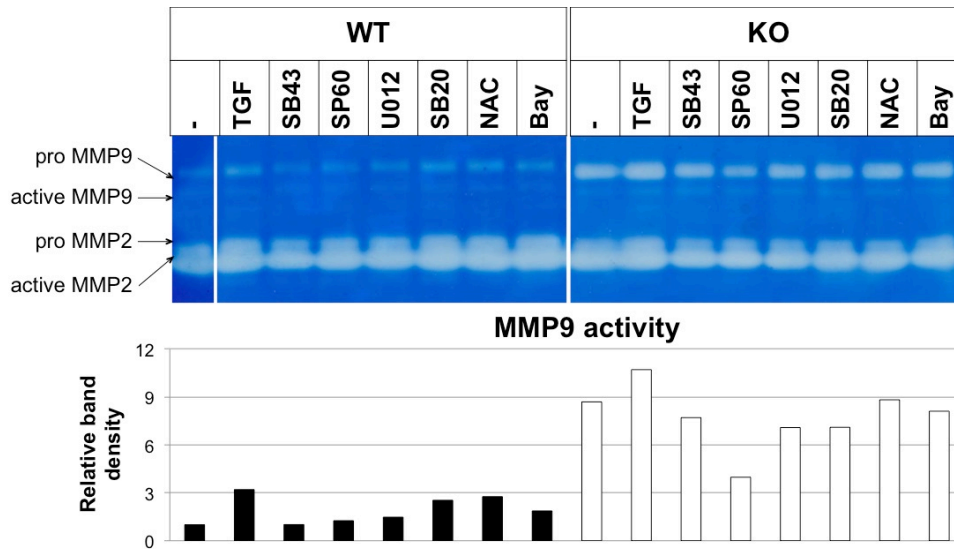
Figure 3.12 **Effects of TGF-β1, a radical scavenger, or signaling inhibitors on MMP9 activity of wild type and *HtrA1-/-* VSMCs.** VSMCs were cultured in medium containing 0.1% FBS and treated for 24 h with various reagents as indicated. The culture supernatants were recovered and applied to zymography gels as described in Fig. 3.11. The same samples (culture supernatants of untreated wild type (WT) and *HtrA1-/-* (KO) VSMCs) were applied to both gels and used as standards to compare activities on the separate gels. The uncropped zymograph pictures are shown in Appendix 7. MMP9 activity in the culture supernatants of untreated WT was set to 1 (leftmost lane) and relative activities for treated WT and *HtrA1-/-* VMSCs were calculated an are presented in the bar graph in the lower panel. Cells at passage 14 were used. TGF=TGF-β1. SB43=SB431542, a TGF-βR1 antagonist. SP60=SP600125, a JNK inhibitor. U012=U0126, a MEK1/2 (ERK1/2 upstream) inhibitor. SB20=SB203580, a p38 MAPK inhibitor. NAC=N-acetylcysteine, a ROS scavenger. Bay=Bay11-7082, an NF-κB inhibitor. Black bars represent WT VSMCs; white bars represent *HtrA1-/-* VSMCs.
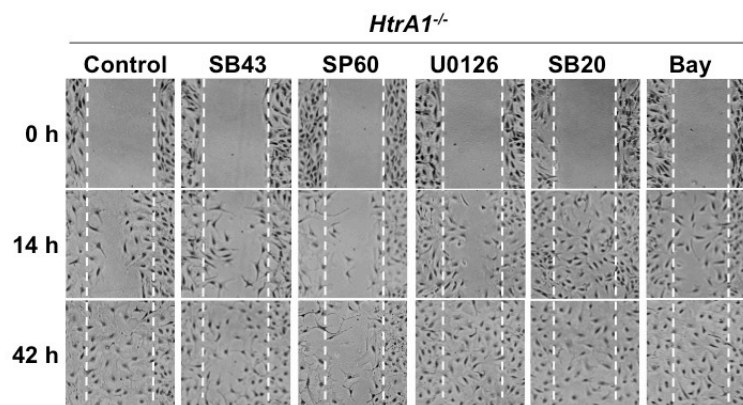
Figure 3.13 **Effects of signaling inhibitors on *HtrA1-/-* VSMC migration.** Cell migration was analyzed by the wound-healing assay. Cells were cultured in medium containing 0.5% FBS without (Control) or with inhibitors as indicated. Photographs were taken at the indicated time points. White dotted lines indicate boundaries of the initial wound area. The experiment was repeated three times and representative results are shown. SB43=SB431542, a TGF-βR1 antagonist. SP60=SP600125, a JNK inhibitor. U012, a MEK1/2 (upstream of ERK1/2) inhibitor. SB20=SB203580, a p38 MAPK inhibitor. Bay=Bay11-7082, a selective NF-κB inhibitor.

41

3.8 Effects of PDGF-BB or IGF-1 on Proliferation, Migration, and MMP9 Activity

Growth factors affect the phenotypic modulation of VSMCs. In general, PDGF-BB induces the synthetic phenotype and IGF-1 maintains the contractile phenotype (Hayashi *et al*, 1999). I then examined effects of PDGF-BB or IGF-1 on the proliferation, migration, and MMP activities of VSMCs. PDGF-BB induced proliferation of both WT and, more strongly, *HtrA1*^{-/-} VSMCs (Fig. 3.14). IGF-1 also stimulated proliferation of both *HtrA1*^{-/-} and WT VSMCs, although its effect was weaker than that of PDGF-BB. PDGF-BB induced migration of WT VSMCs only slightly, but stimulated that of *HtrA1*^{-/-} VSMCs strongly (Fig. 3.15A, right panels). Similar results were obtained with the modified Boyden chamber assay (Fig. 3.15B). The number of *HtrA1*^{-/-} VSMCs that migrated through the membrane in the absence of growth factors was about three times higher than that of WT VSMCs. The PDGF-BB treatment increased the migration of *HtrA1*^{-/-} VSMCs 10-fold, but the migration of WT VSMCs only 2.5-fold. In contrast to the 2.5-fold stimulation of *HtrA1*^{-/-} VSMC migration by IGF-1, it did not induce migration of WT VSMCs.
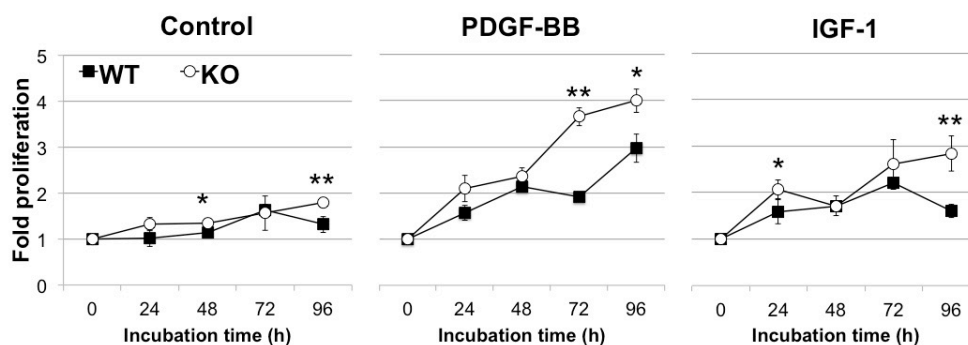
Figure 3.14   Effects of PDGF-BB or IGF-1 on proliferation of wild type and *HtrA1*^{-/-} VSMCs.
Wild type (WT) and *HtrA1*^{-/-} (KO) VSMCs were cultured in medium containing 0.5% FBS with or without 20 ng/ml PDGF-BB or 10 ng/ml IGF-1, as indicated. Cell proliferation was assayed at the indicated time points (0 h was set at 15 h after plating). Points represent means ± SD (n=3-4). The experiments were carried out independently for three different batches of WT and *HtrA1*^{-/-} VSMCs at the matching passage. The data shown are a representative result from cells at passage 7. Statistical significance was determined by Student's *t*-test. *; p <0.05. **; p < 0.01.
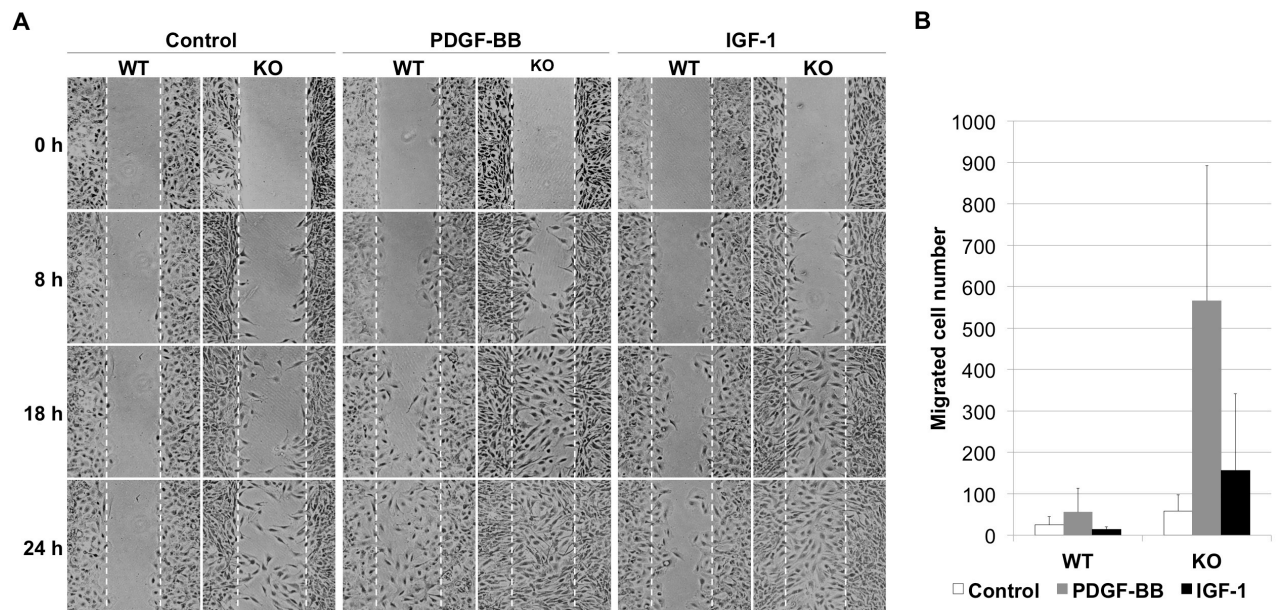
Figure 3.15   Effects of PDGF-BB or IGF-1 on migration of wild type and *HtrA1*^{-/-} VSMCs. (A) Cell migration was analyzed by the wound-healing assay. Wild type (WT) and *HtrA1*^{-/-} (KO) VSMCs were cultured in medium containing 0.5% FBS with or without 20 ng/ml PDGF-BB or 10 ng/ml IGF-1, as indicated. Photographs were taken at the indicated time points after wounding. Dotted white lines indicate the borders of the initial wounded area. The experiment was repeated three times and representative results are shown. Cells at passage 13 were used. **(B)** Cell migration was analyzed by the modified Boyden chamber assay. Cells were cultured in the assay chamber in medium containing 0.5% FBS with or without 20 ng/ml PDGF-BB or 10 ng/ml IGF-1, as indicated, for 24 h. The number of cells that migrated to the bottom side of the chamber was counted after DAPI staining. Data shown are means ± SD (n=3). The experiment was repeated twice and representative results are shown. Cells at passage 9 were used.

Overall, these results indicate a unique property of *HtrA1*^{-/-} VSMCs; PDGF-BB, which induces the synthetic phenotype irrespective of the phenotypic state of VSMCs, strongly stimulates proliferation and migration in *HtrA1*^{-/-} VSMCs. In addition, proliferation and migration of *HtrA1*^{-/-} VSMCs were also induced by IGF-1, which usually maintains contractile phenotype but induces cell proliferation and migration of synthetic VSMCs (Hayashi *et al,* 2004). On the contrary, proliferation of WT VSMCs was induced only weakly by PDGF-BB and IGF-1, and the increase in migration was only observed with PDGF-BB.

I next examined the effects of PDGF-BB or IGF-1 on MMP activities. In agreement with the migration assays, treatment with PDGF-BB highly induced MMP9 activity in the culture media of WT and *HtrA1*^{-/-} VSMCs, whereas IGF-1 only moderately induced MMP9

activity of both WT and *HtrA1*$^{-/-}$ VSMCs (Fig. 3.16). MMP2 activity was not affected by PDGF-BB or IGF-1.
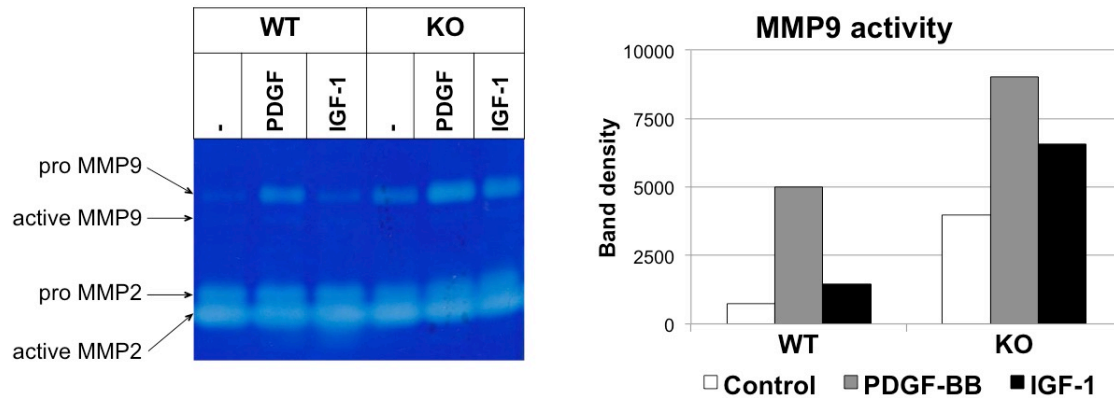
Figure 3.16   Effects of PDGF-BB or IGF-1 on MMP9 activity of VSMCs. Wild type (WT) and *HtrA1*$^{-/-}$ (KO) VSMCs were cultured for 72 h in medium containing 0.5% FBS without (- or Control) or with 20 ng/ml PDGF-BB (PDGF) or 10 ng/ml IGF-1, as indicated. The supernatants were recovered and applied to the zymography gel in volumes adjusted for the tubulin content in the cell lysates. Bands of MMP9 were analyzed by densitometer and are presented in the graph in the right panel. The experiment was repeated twice and representative results are shown. Cells at passage 12 were used.

3.9 Effects of PDGF-BB and IGF-1 on HtrA1 Expression in VSMCs

HtrA1 expression was examined in the supernatants and cell lysates of WT VSMCs treated with PDGF-BB or IGF-1. After 72 h of treatment with PDGF-BB or IGF-1, HtrA1 was decreased in the supernatants but increased in the cell lysates (Fig 3.17A). The proportion of HtrA1 remaining inside the cell however was increased by both PDGF-BB and IGF-1 treatment (Fig. 3.17B). The total HtrA1 expression was reduced by both growth factors (Fig. 3.17C). PDGF-BB and IGF-1 seem to inhibit the secretion of HtrA1, however significance of this finding is not clear now. The levels of HtrA1 mRNA after treatment with these growth factors are required to be investigated.
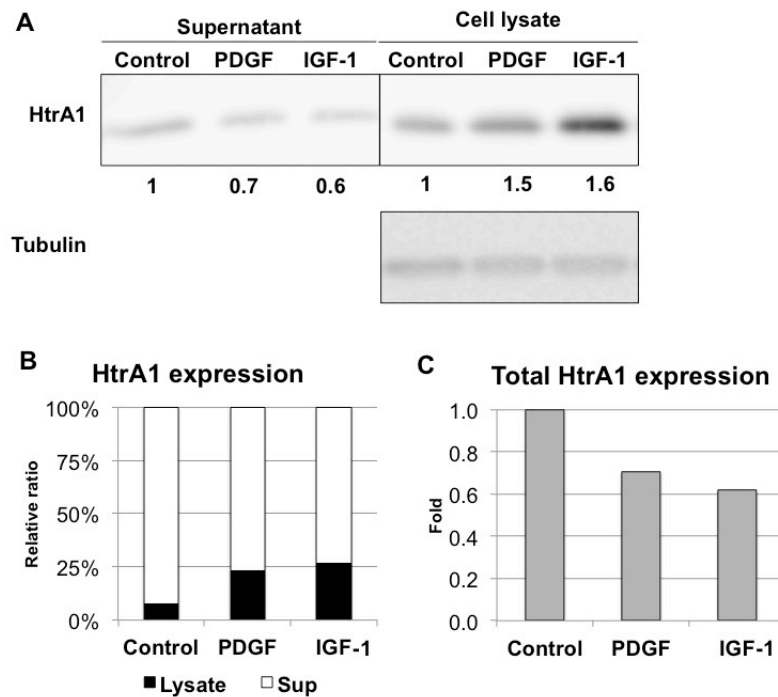
Figure 3.17 HtrA1 expression in VSMCs after PDGF-BB or IGF-1 treatment. Wild type VSMCs were cultured in medium containing 0.5% FBS with or without (Control) 20 ng/ml PDGF-BB (PDGF) or 10 ng/ml IGF-1 for 72 h, as indicated. **(A)** Culture supernatants and cell lysates were separated by SDS-PAGE and Western blot analysis for HtrA1 was performed. Band density was analyzed by densitometry. The expression levels were normalized with tubulin, and relative expression levels were calculated and are shown below the panel. PDGF-BB and IGF-1 affected the secretion of HtrA1 in VSMC. **(B)** Ratios of HtrA1 expression in supernatants and cell lysates were calculated and are shown. **(C)** Ratios of total HtrA1 were calculated and are shown. Cells at passage 8 were used.

3.10 Loss of HtrA1 Induces VSMC Death under Oxidative Stress

Loss of VSMCs is the main characteristics of human CARASIL arteries (Hara *et al*, 2009). Our group has reported that HtrA1 deficiency made mouse embryonic fibroblast cells prone to oxidation-induced cell death (Supanji *et al*, 2013), and I therefore examined the effect of H_2O_2 on cell death of VSMCs. As anticipated, low concentrations (0.1 and 0.3 mM) of H_2O_2 caused acute cytotoxicity in *HtrA1*$^{-/-}$ VSMCs but not in WT VSMCs (Fig. 3.18A). At 0.3 mM, H_2O_2 induces significantly higher incidence of apoptosis and necrosis in *HtrA1*$^{-/-}$ VSMCs than in WT VSMCs, and the cells died mainly through apoptosis (Fig 3.18B). After treatment with 0.1 or 0.3 mM H_2O_2, more *HtrA1*$^{-/-}$ VSMCs than WT VSMCs became cleaved caspase-3-positive (Fig 3.18C). Western blot analyses at various time points after H_2O_2

45
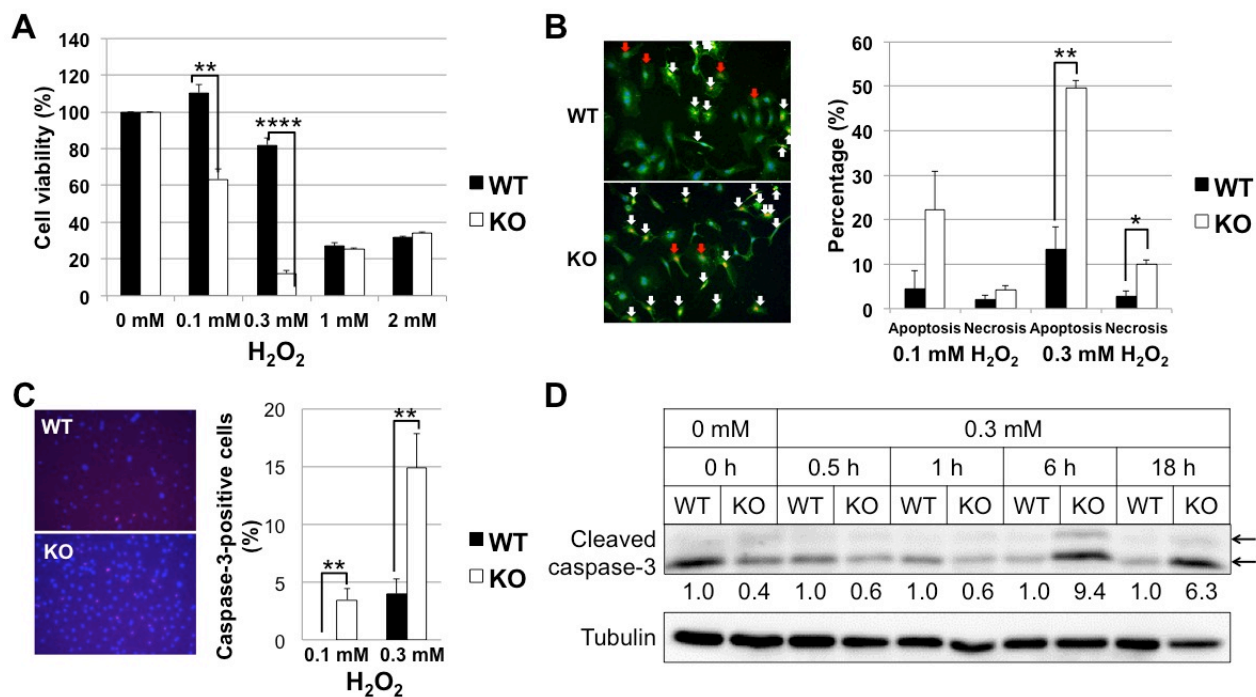
Figure 3.18 **Effects of oxidative stress on wild type and *HtrA1*^{-/-} VSMCs.** Wild type (WT) and *HtrA1*^{-/-} (KO) VSMCs at passage 10 were starved in medium containing 0.1% FBS for 24 h. **(A)** Effect of H_2O_2 on cell viability of WT and *HtrA1*^{-/-} mouse VSMCs. Cells were treated with the indicated concentrations of H_2O_2 for 24 h in medium containing 0.1% FBS. Cell viability was examined using Cell Count Reagent SF (Nacalai Tesque). **(B)** Effect of H_2O_2 on cell death of WT and *HtrA1*^{-/-} mouse VSMCs. Cells were treated with 0.1 or 0.3 mM H_2O_2 for 6 h in medium containing 0.1% FBS. Cells were triply stained with Apoptotic/Necrotic/Healthy Cells Detection Kit (PromoKine) as follows: Hoechst 33342 (blue) indicating the entire cell population, FITC-Annexin V (green) indicating apoptotic cells and Ethidium homodimer III (red) indicating necrotic cells. Representative images of merged data are shown in the left panel. Apoptotic (white arrows) and necrotic (red arrows) cells were counted, and their percentages of the total cell number were calculated and are presented in the bar graph in the right panel. **(C)** Effect of H_2O_2 on apoptosis of WT and *HtrA1*^{-/-} mouse VSMCs. Cells were treated with 0.1 or 0.3 mM H_2O_2 for 6 h in medium containing 0.1% FBS. Cells were then immunostained with anti-cleaved caspase-3 antibody. Representative images of WT and *HtrA1*^{-/-} VSMCs treated with 0.3 mM H_2O_2 are shown in the left panel. Caspase-3-positive cells were counted, and their percentages of the total cell number were calculated and are presented in the bar graph in the right panel. **(D)** Effect of H_2O_2 on the expression of cleaved caspase-3 on WT and *HtrA1*^{-/-} mouse VSMCs. WT and *HtrA1*^{-/-} VSMCs were treated with 0.3 mM H_2O_2 in medium containing 0.1% FBS. Cell lysates were prepared at the time points indicated, separated by SDS-PAGE, and analyzed by Western blot for cleaved caspase-3. Band density was analyzed by densitometry. The expression levels were normalized with tubulin, and relative expression levels were calculated and are shown below the upper panel. The anti cleaved caspase-3 antibody detected the large fragments (17/19 kDa, indicated by arrows). Band densities of both were analyzed by densitometry, and summated. Bars in A, B, and C represent means ± SE (n=3). Statistical significance was determined by Student's *t*-test. *; p <0.05. **; p <0.01. ****; p < 0.0001.

treatment showed that the expression of cleaved caspase-3 was higher in *HtrA1*^{-/-} VSMCs than in WT VSMCs after 6 h (Fig 3.18D). These data suggested that *HtrA1*^{-/-} VSMCs died more easily than WT VSMCs upon oxidative stress, and the cell death was mainly caused by apoptosis.

3.11 Phenotypic Shift of Aortic VSMCs *In Vivo*

VSMCs have a wide range of phenotypic variations and unique plasticity characteristics, in which their contractile phenotype can be shifted into synthetic phenotype as a response to change in environment (reviewed in Owens *et al*, 2004 and Rensen *et al*, 2007). The failure of synthetic VSMCs to switch back to the contractile phenotype induces pathogenic vascular remodeling. Each phenotype has its own characteristics in terms of protein expression, rate of proliferation, and robustness in migration. I next examined the expression of synthetic and contractile marker proteins to evaluate the phenotype characteristics of VSMCs in vivo.

Aortas from 5-day-old *HtrA1*^{-/-} mice expressed SMA, calponin, and vimentin at similar levels to those from WT mice, indicating that the differentiation and maturation of VSMCs were not affected in *HtrA1*^{-/-} mice (Fig. 3.19B, leftmost panel). *HtrA1*^{-/-} mouse aortas expressed more calponin than WT mouse aortas at 16 and 24 weeks of age, but both expressed comparable levels of SMA, osteopontin, and vimentin (Fig. 3.19A, B). Calponin levels in *HtrA1*^{-/-} mouse aortas decreased to about half of those in WT mouse aortas at 40 and 52 weeks of age, and aortas of *HtrA1*^{-/-} mice expressed osteopontin more strongly than WT mouse aortas (Fig. 3.19A, B). The expression profile of these marker proteins at 40 and 52 weeks agrees with the notion that aortic VSMCs are in the synthetic phenotype.
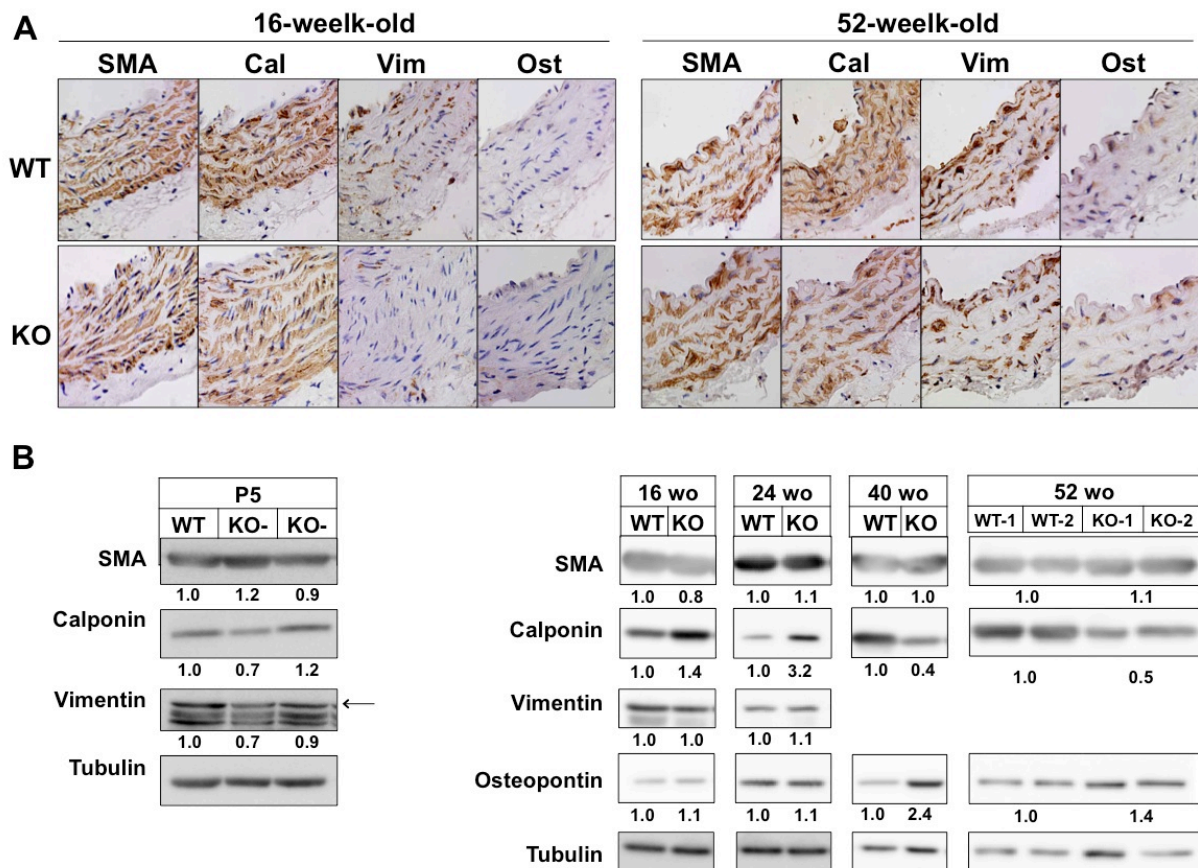
Figure 3.19   **Expression of VSMC contractile and synthetic markers in aortas of wild type and *HtrA1*⁻/⁻ mice.** **(A)** Cross sections of the upper half the descending aortas from 16 (left) and 52-week-old (right) wild type (WT) and *HtrA1*⁻/⁻ (KO) mice were stained with anti-smooth muscle α-actin (SMA), anti-calponin (Cal), anti-vimentin (Vim), or anti-osteopontin (Ost). Representative images are shown. **(B)** The entire descending thoracic aortas from three or four mice of 5 days old (P5) or 16, 24, 40, or 52-weeks old (wo) were combined and tissue extracts were prepared. The extracts were separated by SDS-PAGE and Western blot analysis was performed with VSMC markers, as indicated. Expression levels were normalized with tubulin, and relative expression levels were calculated and are shown below each panel. Two different batches of aortic extract from P5 *HtrA1*⁻/⁻ mice (KO-1 and KO-2), 52-wo wild type mice (WT-1 and WT-2), and *HtrA1*⁻/⁻ mice (KO-1 and KO-2) were analyzed. The arrow in the P5 blots shows the vimentin band; bands below the arrow are nonspecific proteins.

3.12 ERK1/2 and Akt Signaling in *HtrA1*⁻/⁻ Mouse Aortas

ERK1/2 sends signal to induce synthetic phenotype in VSMCs, while Akt usually sends signals to maintain contractile phenotype (Hayashi *et al*, 1999; Hayashi *et al*, 2004). To clarify the phenotypic status of VSMCs more precisely in *HtrA1*⁻/⁻ mouse aortas, ERK1/2 and Akt signaling were analyzed in aortas of WT and *HtrA1*⁻/⁻ mice by Western blot (Fig.

3.20). ERK1/2 signaling activity was suppressed in *HtrA1*^{-/-} mouse aortas at 16 and 40 weeks

of age. On the other hand, Akt was highly phosphorylated at 16-week-old mouse aortas. This

indicates that the aorta of young *HtrA1*^{-/-}mice receives more contractile signals than synthetic

signals. At 52 weeks of age, WT aortas showed decrease in phosphorylation of ERK1/2, and

phosphorylation levels were almost comparable for WT and *HtrA1*^{-/-} mouse aortas. Activity

of Akt signaling was decreased in *HtrA1*^{-/-} aortas at 40-week-old. Later at 52-week-old,

levels of p-Akt was comparably low both in WT and *HtrA1*^{-/-} aortas.
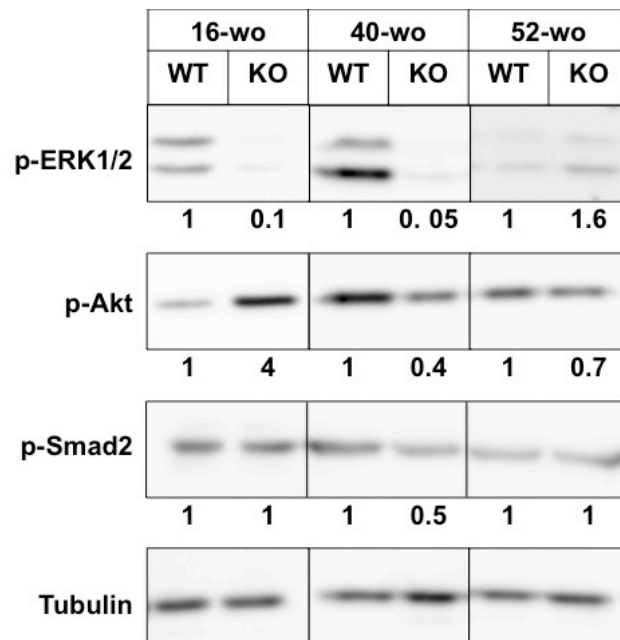
Figure 3.20 Phosphorylation of ERK1/2, Akt, and Smad2 in aortas of wild type and *HtrA1*^{-/-} mice. The entire descending thoracic aortas from three or four wild type (WT) and *HtrA1*^{-/-} (KO) mice of 16, 40, or 52-week-old (wo) were combined and tissue extracts were prepared. The extracts were separated by SDS-PAGE and Western blot analysis was performed for p-ERK1/2, p-Akt, or p-Smad2, as indicated. Expression levels were normalized with tubulin, and relative expression levels were calculated and are shown below each panel.

The onset of CARASIL has been associated with modified TGF-β signaling (Hara *et*

al, 2009). The *HtrA1*^{-/-} mouse aortas, however, did not show either an increase or a decrease

in the level of phosphorylated Smad2 (Fig. 3.20). Together with the data for isolated VSMCs

(Fig 3.12 and Fig. 3.13), this result suggests that the TGF-β signaling pathway does not contribute to the early etiology of CARASIL.

3.13 Histological Abnormalities of *HtrA1*$^{-/-}$ Mouse Aortas

Elastic fiber degradation is a main histological finding in CARASIL arteries. The increased MMP9 activity of *HtrA1*$^{-/-}$ VSMCs may disrupt the elastic fibers and other components in the aorta. The aortas of *HtrA1*$^{-/-}$ mice exhibited uneven thickening of the media (Fig. 3.21) more frequently and more severely than in WT mice. I defined the uneven thickening of the media as the thickest part of the aorta being 2.5 times or more as thick as the thinnest part. Uneven medial thickening was observed in 20 of 31 aorta sections from five 40-week-old *HtrA1*$^{-/-}$ mice (64%), but only in 10 out of 35 aorta sections from six age-matched WT mice (26%) (Fig. 3.21A). Uneven medial thickening was also observed in 17 of 24 aorta sections from eight 52-week-old *HtrA1*$^{-/-}$ mice (71%), but only in 5 out of 30 aorta sections from ten age-matched WT mice (17%) in 52-week-old mice (Fig. 3.21B). The ratio of the thickest to the thinnest aortic media was significantly higher in 52-week-old *HtrA1*$^{-/-}$ mice than in WT mice (Fig. 3.21D).
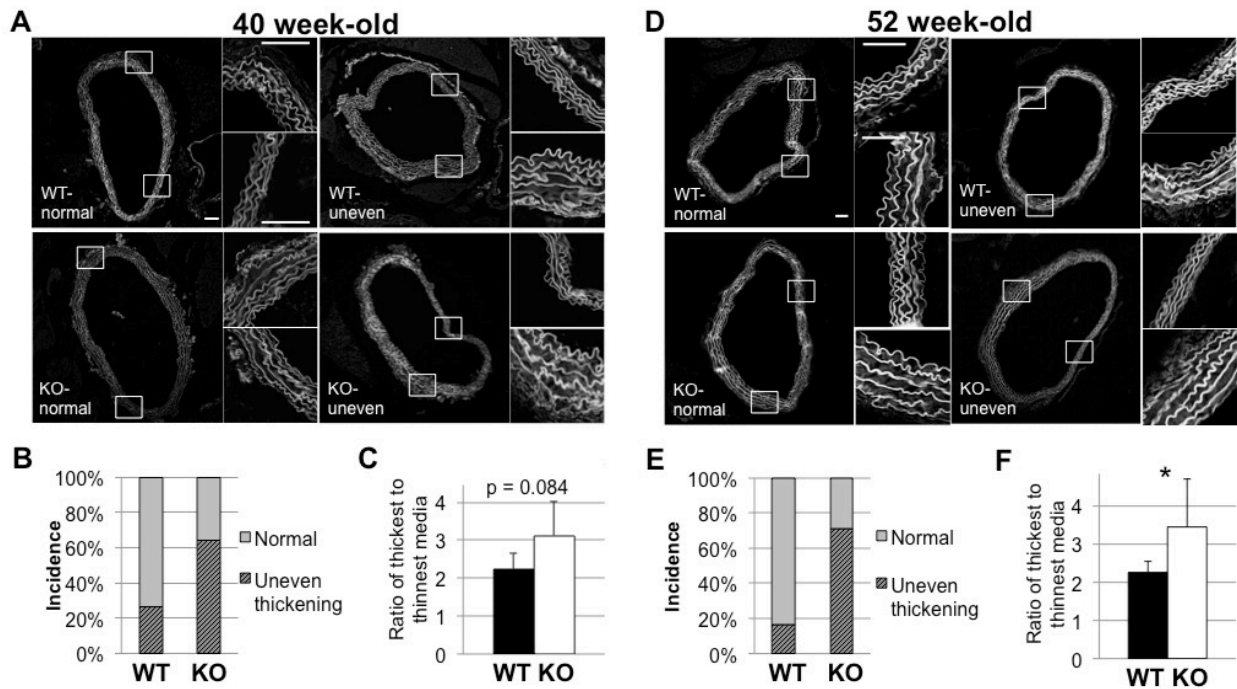
Figure 3.21   Uneven thickening of aortic media of wild type and *HtrA1*^{-/-} mice at 40 and 52 weeks of age. Cross sections from the upper half of the descending aorta were stained with hematoxylin and eosin, and autofluorescence images were obtained with a fluorescence microscope to visualize elastin structures. Uneven medial thickening was defined as the thickest part of the aorta being 2.5 times or more as thick as the thinnest part. Representative images of normal aorta or aorta with uneven thickening in 40-week-old **(A)** and 52-week-old **(D)** of wild type (WT) and *HtrA1*^{-/-} (KO) mice are shown. Two small images on the right side of each large image show magnified (4x) views of the boxed areas and represent the thickest and the thinnest areas. Bars=100 μm. Three up to eight adjacent sections were analyzed for each aorta, and the incidence of uneven thickening **(B, E)** and the ratio of thickest-to-thinnest **(C, F)** were calculated. Bars in C represent means ± SD (WT, n=6; *HtrA1*^{-/-}, n=5). Bars in F represent means ± SD (WT, n=10; *HtrA1*^{-/-}, n=8). The details are described in Appendix 11. Statistical significance was determined by Student's *t*-Test. *; p <0.05.

I then examined one section per aorta that represents the most uneven thickening of the media. The aortas of *HtrA1*^{-/-} mice exhibited splitting or degradation of elastic fibers (Fig. 3.22). The elastic fibers of the *HtrA1*^{-/-} mouse aorta were fragmented and the interval between elastic fibers was increased. I used a modification of a reported grading system (Deckert *et al*, 2013) to estimate elastin degradation semi-quantitatively (Appendix 13). The *HtrA1*^{-/-} mouse aortas at 52 weeks of age showed significantly more severe degradation than the WT mouse aortas at the same age (Fig. 3.22).
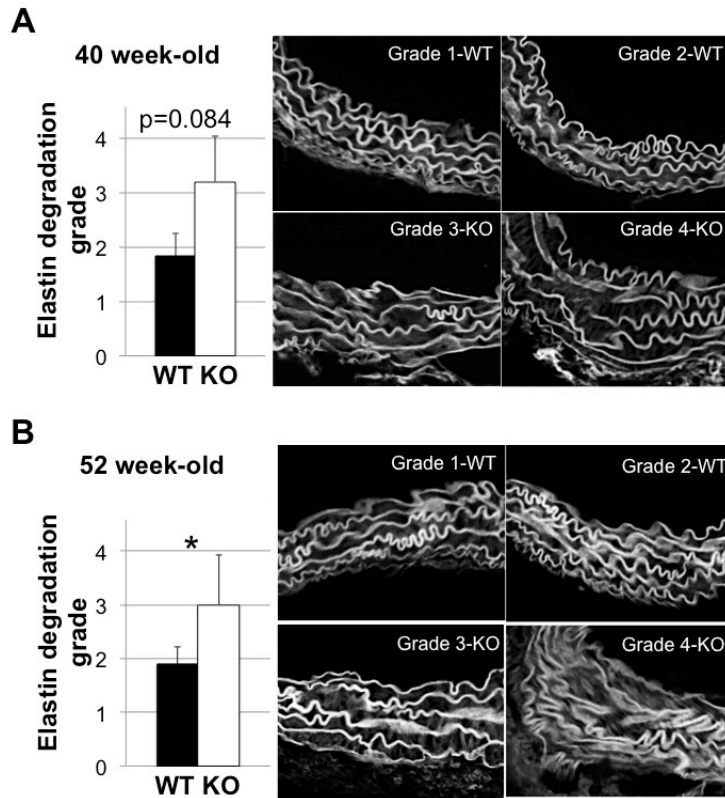
Figure 3.22 Elastic fiber degradation in the aortic media of 40 and 52-week-old *HtrA1*^{-/-} mice. Cross sections from the upper half of the descending aorta were stained with hematoxylin and eosin (HE). Grading of elastic fiber degradation was carried out based on a reported method (Deckert *et al*, 2013); the details are described in the Materials and Method. Representative images of the wild type (WT) and *HtrA1*^{-/-} (KO) aortas at 40 **(A)** and 52 **(B)** weeks of age are shown at right panels according to the grading key came from actual WT and *HtrA1*^{-/-} aorta sections. Pictures depicting typical images of the WT and *HtrA1*^{-/-} aortas are shown in Appendix 12. Grade 1-2 were representative images from WT mice and Grade 3-4 were from *HtrA1*^{-/-} mice. Grade 1=none; Grade 2=minimal; Grade 3=moderate; Grade 4=severe (adapted from Deckert *et al*, 2013). Bars in A represent means ± SD (WT, n=6; *HtrA1*^{-/-}, n=5). Bars in B represent means ± SD (WT, n=10; *HtrA1*^{-/-}, n=8). The details are described in Appendix 13. Statistical significance was determined by nonparametric U-Test (Mann-Whitney). *; $p < 0.05$.

Although the actual cause is not yet clear, thickening of the media was caused by expansion of intervals between elastic fibers, either by increase in the size of VSMCs or in the amounts of ECM. To address this point, I observed histological stained-sections of the aortas from 52-week-old mice. Fibrillar collagens are specifically decreased in the media of CARASIL arteries (Hara *et al*, 2009). Collagens were also decreased in the aged *HtrA1*^{-/-} mouse aorta (Fig. 3.23). Picrosirius red staining showed that collagen content was low in the entire area of the aortic media of *HtrA1*^{-/-} mice at 52 weeks of age. The adventitia of both

HtrA1⁻/⁻ and WT aortas, however, stained equally strongly (Fig 3.23C, G). The lowest collagen staining coincided with the thickened areas of *HtrA1⁻/⁻* aortas (Fig 3.23G, boxed area, and H).
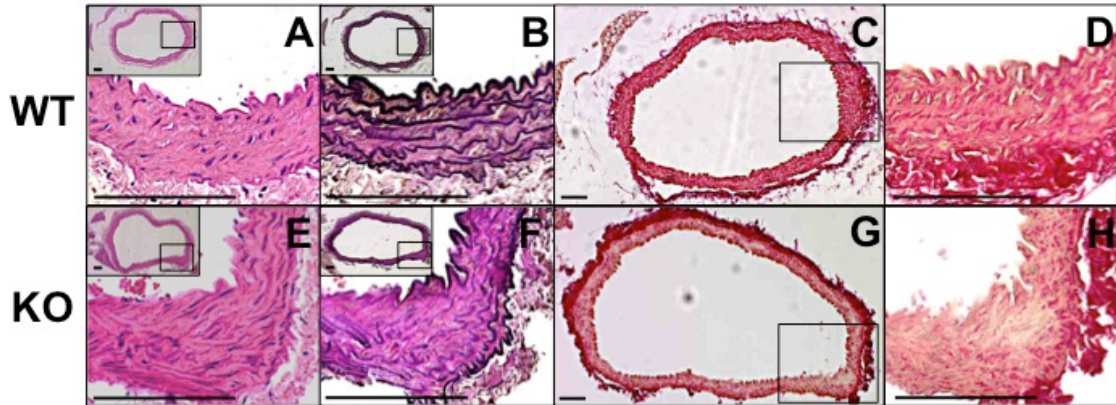
Figure 3.23   Elastic fiber degradation and decrease in collagens in 52-week-old *HtrA1⁻/⁻* mouse aortas. Cross sections from the upper half of the descending aorta from wild type (ET) and *HtrA1⁻/⁻* (KO) mouse aortas were stained with hematoxylin and eosin **(A, E)**, elastica van Gieson **(B, F)** for elastic fibers, or picrosirius red.**(C, G)** for collagens. Insets in A, B, D, E, F, and H depict the entire cross sections, with boxed areas that are magnified in the main images. D and H show higher magnifications of the boxed areas of C andg G, respectively. Bars=100 μm.

Protruding structures, probably an initial event of neointima formation, were observed in four cases among eight 52-week-old *HtrA1⁻/⁻* mouse artas (50%), but none in age-matched WT mice (Fig. 3.24E). The protruding structures consist of cells that were positive to SMA staining (Fig. 3.24D), suggesting that the origin of these cells was VSMCs from the media. However, the elastic fiber between the media and the protrusion was intact (Fig. 3.924B). Irregular small fragments of elastic fibers were detected in the structures. Despite the decrease of collagen content in *HtrA1⁻/⁻* aortas (Fig. 3.23G, H), the protrusion exhibited higher collagen content compared to the media (Fig. 3.24C). The protrusion might be an independent event; the protruded area did not coincide with the thickened or thinned areas, or with the areas of VSMC loss.
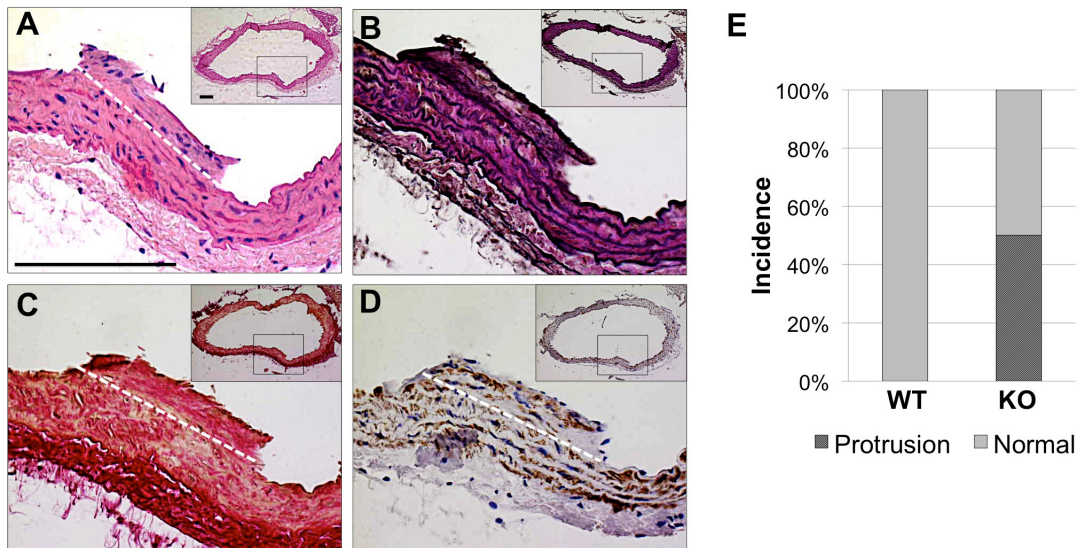
Figure 3.24 **Protrusion in aortas of 52-week-old *HtrA1*^{-/-} mouse.** Cross sections from the upper half of the descending aortas were stained with hematoxylin and eosin (HE), elastica van Gieson (EVG) for elastic fibers, picrosirius red. for collagens, or immunostained with anti-smooth muscle α actin (SMA) antibody. Representative images of protrusion structures in *HtrA1*^{-/-} aortas are shown: **A**, HE; **B**, EVG; **C**, picrosirius red; **D**, anti-SMA. Insets depict the entire cross sections, with boxed areas that are magnified in the main images. White dashed-lines represent border between the media and the protrusion in A, C, and D. Bars=100 μm. **(E)** Incidence of protrusion structure was calculated in wild type (WT) and *HtrA1*^{-/-} (KO) mouse aortas.

Taken together, all these data show that the aorta of the *HtrA1*^{-/-} mouse recapitulates major abnormalities found in human CARASIL arteries: loss of VSMCs, elastic fiber disruption, and collagen depletion.

IV. DISCUSSION

4.1 Histological Abnormalities in the Aorta of *HtrA1*^{-/-} Mouse and Human CARASIL

In this study I examined whether $HtrA1^{-/-}$ mouse is valuable as a model of human CARASIL. I demonstrated that brain arteries of $HtrA1^{-/-}$ mice or even $HtrA1^{-/-};HtrA3^{-/-}$ mice are normal. This study has revealed that the thoracic aorta of aged homozygous $HtrA1^{-/-}$ mice shows pathological changes characteristic of those in the brain arteries of CARASIL patients (Oide *et al*, 2008); among those changes is the loss of VSMCs (Fig. 3.4D). The pathological changes in our mice are prominent in the aorta, which has a structure and diameter similar to the human small brain arteries preferentially affected in CARASIL. CARASIL patients frequently show mild sclerotic changes in the coronary arteries, and arteries of other visceral organs and subcutaneous tissues (Yokoi and Nakayama, 1985; Arima *et al*, 2003; Oide *et al*, 2008; Cai *et al*, 2015). These findings suggest that CARASIL is a systemic vascular disorder, and the size, and hence the structure, of the artery may contribute to the pathological changes.

Human CARASIL in its full-blown form is characterized by severe arteriosclerosis accompanied with fibrous intimal proliferation, splitting of the internal elastic lamina, extensive hyaline degeneration of the media, and extensive loss of VSMCs (Arima *et al*, 2003; Hara *et al*, 2009). However, Oide *et al* (2008) proposed that loss of ECM, loss of medial VSMCs, and the thinning of the adventitia and the media are the initial histological abnormalities of CARASIL. The number of aortic VSMCs increased in young $HtrA1^{-/-}$ mice (Fig. 3.4D), but decreased rapidly after 40 weeks and became significantly lower than that in WT aortas at 60 weeks. The initial increase of VSMCs may be caused by synthetic modulation.

CARASIL patients show severe vascular abnormalities in their twenties. In contrast, the *in vivo* phenotype is weak even in aged $HtrA1^{-/-}$ mice. One possible explanation for this

discrepancy is a difference in the functional contribution of secretory HtrA family members in mouse and human vessels. HtrA1 may play the main role in human brain vessels, but not in mouse vessels, and HtrA3 or HtrA4 may compensate for the loss of HtrA1 in mouse vessels. Heterozygous mutations of *HTRA1* cause late onset SVD in humans (Verdura *et al*, 2015). The *in vivo* phenotype of *HtrA1*^{-/-} mice might thus mimic the abnormalities caused by heterozygous *HTRA1* mutations. Another possibility is the difference in ageing processes in human and mouse vessels. Lipid metabolism is different (Xu, 2004; Jawien *et al*, 2004; Wong *et al*, 2009) and the telomeres are longer in mouse cells than human cells (Wong *et al*, 2009; McKee *et al*, 2003). Analysis of double knockout mice for *HtrA1* and *ApoE*, *Lrp1*, or *Terc* may give the answer to this possibility.

4.2 Modulation of Aortic VSMC Phenotype in *HtrA1*^{-/-} Mice

In this study, I present evidence indicating that the VSMCs of *HtrA1*^{-/-} mouse aortas show more synthetic phenotype than WT VSMCs. The significant increase in VSMCs number found in the media of 24-40-week-old *HtrA1*^{-/-} mice is the first sign that indicates the synthetic phenotype of VSMCs (Fig. 3.4D). Primary cultures of aortic VSMCs established from *HtrA1*^{-/-} mice are highly synthetic and proliferate more quickly, migrate faster, and produce higher MMP9 activity than WT mouse VSMCs (Fig 3.7A, Figs. 3.9-3.11). Responses of isolated VSMCs to PDGF-BB and IGF-1 support our conclusion that *HtrA1*^{-/-} VSMCs are skewed towards the synthetic phenotype (Figs. 3.14-3.16). The fast migration of *HtrA1*^{-/-} VSMCs may be ascribed to the high activity of MMP9, because both are inhibited by a JNK inhibitor (Figs. 3.12, 3.13). The high activity of MMP9 may also explain the elastic fiber degradation in the aorta (Fig. 3.22). MMP9 plays critical roles in pathological processes of cardiovascular diseases that involve tissue remodeling, inflammation, or fibrosis (Yabluchanskiy *et al*, 2013). The increased MMP9 activity of *HtrA1*^{-/-} mouse VSMCs should

hence contribute heavily to the onset of aortic abnormalities. Examination of the MMP9 activity in human CARASIL arteries should give a good insight into the etiology of this disease.

This study highlights the synthetic modulation of VSMCs as the earliest key event caused by HtrA1 deficiency. The mechanisms that underlie the synthetic modulation of $HtrA1^{-/-}$ VSMCs are unclear. One possible mechanism could be damage to elastic fibers, collagens, or other ECM molecules. Oide *et al* (2008) proposed that ECM abnormalities, in particular loss of collagens such as type I, III, IV, and VI, is the cause of VSMC degeneration. CARASIL is a systemic disorder of the ECM; vertebral disc herniation and spondylosis deformans are major diagnostic signs of CARASIL, and patients frequently show limb arthropathy and keratotic skin changes. Changes in the vascular ECM are a major factor that induces synthetic modulation of VSMCs (Owens, 1995; Rensen *et al*, 2007). Abnormalities of ECM impair cell-ECM interaction and cell-elastic fiber anchoring, possibly resulting in alteration of VMSC phenotypes.

Bunton *et al* (2001) analyzed Marfan syndrome (MFS) model mice carrying genetically disrupted *fibrillin 1* gene, an essential gene for the formation of cell-elastic fiber connecting filaments, and proposed that loss of connection between VSMCs and elastic fibers initiated the synthetic modulation of VSMCs. This modulation contributes to early elastolysis due to overproduction of MMP9, a known mediator of elastolysis, and leads to eventual collapse of the vessel structure in this disease (Bunton *et al*, 2001). In VSMCs, MMP9 is positively regulated mainly by NF-κB and AP-1 transcription factors (Yabluchanskiy *et al,* 2013), including c-Jun, c-Fos, and ATFs (reviewed in Shaulian and Karin, 2001). The enhanced activities of MMP9 in $HtrA1^{-/-}$ mouse VSMCs are inhibited specifically by an inhibitor of JNK (c-Jun N-terminal kinase), a direct upstream regulator of c-Jun (Figs. 3.12, 3.13). The JNK cascade represents a stress-activated signaling pathway, and different forms

of stress have been shown to mediate JNK activation via various cellular pathways. It was also reported that JNK activates MMP9 transcription via FoxO4 in response of oxidative stress (Li *et al*, 2007). Mouse embryonic fibroblast (MEF) isolated from homozygous $HtrA1^{-/-}$ mice respond to oxidative stress with higher JNK activation than cells from heterozygous $HtrA1^{-/+}$ mice (Supanji *et al*, 2013). The enhanced activity of MMP9 thus suggests accumulated stress in $HtrA1^{-/-}$ mouse VSMCs.

MMP9 plays important roles in pathological processes of cardiovascular diseases that involve remodeling of tissues, inflammation, and fibrosis (Yabluchanskiy *et al,* 2013). A polymorphism of human *MMP9* gene which increases transcription of MMP9 is correlated with severity of coronary atherosclerosis. MMP9 activity is increased when vascular tissues undergo compensatory remodeling in hypertensive patients at early stages. In atherosclerotic plaques, MMP9 plays conflicting roles; it induces VSMC migration into the plaque and contributes to form "stable" plaques, but it also triggers rupture of the plaque, which leads to thrombosis (reviewed in Yabluchanskiy *et al,* 2013). The increase in MMP9 activity in $HtrA1^{-/-}$ mouse VMSCs may contribute heavily to the onset of CARASIL.

4.3 Signaling in $HtrA1^{-/-}$ Mouse Aortas

In contracts to the *in vitro* findings with isolated VSMCs, phosphorylation of ERK1/2 and Akt *in vivo* in the aorta behaves unexpectedly (Fig. 3.20). The aorta of 16-week-old $HtrA1^{-/-}$ mouse exhibits little phosphorylation of ERK1/2 and high phosphorylation of Akt. These unexpected patterns are gradually resolved as the mouse ages, and at 52 weeks of age, $HtrA1^{-/-}$ and WT mouse aortas show the same levels of p-ERK1/2 and p-Akt. At 16 weeks of age, $HtrA1^{-/-}$ mouse aorta already shows tendency of increases in the media thickness and the medial VSMC number, although not statistically significant (Fig. 3.4). At 24 or 40 weeks of age, VSMCs in the $HtrA1^{-/-}$ mouse aorta are definitely in synthetic phenotype as judged from

the significant increase in cell numbers. Since VSMCs were isolated from 10-week-old mice, and the isolated cells respond to PDGF-BB and IGF-1 as expected from the properties of the growth factors and characteristic of the cells (Figs. 3.14-3.16), it is unlikely that the VSMCs themselves behave abnormally, rather the environment of the cells in the aorta may be abnormal. This unexpected pattern therefore may indicate a compensatory reaction of the body against synthetic modulation of VSMCs. The aorta or surrounding tissues send contractile signals to VSMCs to shift them back to contractile cells, resulting in low p-ERK1/2 and high p-Akt before 40-week-old. This is consistent with the data showing that, at the early stages, higher levels of calponin are detected (Fig. 3.19B), probably as the result of this compensatory mechanism. After 40 weeks of age, mice get older and possibly lose their compensatory capacity, thus p-ERK1/2 and p-Akt levels return to their normal levels, and loss of VSMCs and other signs related to CARASIL may begin to appear.

HtrA1 is known to inhibit TGF-β signaling (Oka *et al*, 2004; Tsuchiya *et al*, 2005). Increased TGF-β signaling has been reported as an etiologic factor of CARASIL (Hara *et al*, 2009). They reported an increase in the TGF-β1 protein in the tunica media of CARASIL arteries. Their group also reported that phosphorylation of Smad2, a downstream signaling protein of TGF-β1, is increased in endothelial cells of CARASIL arteries (Shiga *et al*, 2011). The increase in TGF-β1 is also detected in the subcutaneous tissue or cultured fibroblasts from CARASIL patients (Cai *et al*, 2015). In contrast, Beaufort *et al* (2014) reported down-regulation of TGF-β signaling in CARASIL. They showed that p-Smad2/3 and connective tissue growth factor (CTGF), which is induced by TGF-β, are decreased in HtrA1-deficient mouse brain and embryonic fibroblasts as well as in skin fibroblasts of a CARASIL patient. Nonetheless, I did not detect significant changes in the level of p-Smad2 in the aorta of *HtrA1*^{-/-} mice by Western blot (Fig. 3.20). Although I cannot exclude the possibility that the activation of TGF-β is very localized, my data suggests that the increase in the TGF-β

signaling is not a primary event, but probably a late-stage event induced by extensive degradation of the ECM, which absorbs TGF-β, or by secondary inflammatory reactions. All those data indicate that our $HtrA1^{-/-}$ mice represent the very initial stage of the disease, while the findings on CARASIL so far reported may depict advanced or secondary signs appeared in the later stages of the disease.

4.4 Function of HtrA1 and Onset of Vasculopathy

It is not clear what triggers the loss of VSMCs in the $HtrA1^{-/-}$ mouse aorta at 52 weeks of age and older. One possibility is the enhanced migration of synthetic $HtrA1^{-/-}$ VSMCs, which dislocates the VSMCs. More likely, however, the long-lasting synthetic state and stress accumulated therein might induce cell death. In support of this, we showed that primary cultures of $HtrA1^{-/-}$ VSMCs are prone to cell death caused by oxidative stress (Fig. 3.18). $HtrA1^{-/-}$ VSMCs died mostly through apoptosis (Fig. 3.18B-D). Other types of stress, such as oxidized low-density lipoprotein treatment and endoplasmic reticulum (ER) stress induced by tunicamyicin or thapsigargin treatment, also promoted cell death of $HtrA1^{-/-}$ VSMCs more strongly than that of WT VSMCs (C. Oka *et al*, unpublished data).

Apoptosis of VSMCs contributes substantially to the pathogenesis of cardiovascular diseases such as atherosclerosis, MFS, and CADASIL. These diseases are associated with medial cystic degeneration, which is characterized by medial atrophy, VSMC loss, elastin fragmentation, increased glycosaminoglycans, and speckled calcification. Lines of evidence suggest that VSMC apoptosis is a primary and early event in these diseases, and it can alone trigger all of these secondary damages (Bennet *et al*, 2016). In atherosclerosis, VSMCs become highly mobile due to synthetic modulation and translocate to the intima, where apoptosis of VSMCs is activated by macrophages through death ligand-death receptor interaction (Boyle *et al*, 2002). Reduced extracellular deposition and altered quality of ECM

proteins may play a role in VSMC apoptosis in MFS. Up-regulated MMP2 and caspases exteriorized from apoptotic VSMCs may contribute to the degradation of ECM proteins and subsequent VSMC apoptosis in MFS (Nataatmadja *et al*, 2003; Emrich *et al*, 2015). Although TGF-β is known to heavily contribute to the pathogenesis of MFS, blockade of TGF-β signaling by losartan is not effective in preventing apoptosis of MFS VSMCs (Granata *et al*, 2017). Rather, the p38 MAP kinase pathway appears to regulate apoptosis of MFS VSMCs. Loss of VSMCs through apoptosis is also prominent in the small arteries of the brain of CADASIL patients (Gray *et al*, 2007). Mutated Notch3 extracellular domain peptides are aggregated and deposited on the surface of VSMCs. This abnormal deposition is toxic to cells and induces oxidative stress, ER stress, or mitochondrial dysfunction and subsequently triggers apoptosis of VSMCs (Formichi *et al*, 2009; Ihalainen *et al*, 2006). Apoptosis caused by altered interaction with the ECM, by activated MAP kinase pathways, or by various stress conditions may account for the decrease in aortic VSMCs in aged $HtrA1^{-/-}$ mice.

Zhang *et al* reported that activation of the JNK pathway promoted VSMC apoptosis (Zhang *et al*, 2013). I showed activation of the JNK pathway in $HtrA1^{-/-}$ VSMCs (Figs. 3.12, 3.13). I could not detect a significant increase in TUNEL-positive VSMCs in 52-week-old $HtrA1^{-/-}$ mouse aortas (Fig. 3.6B). Detection of apoptosis *in vivo* is usually difficult, however, particularly when the cell loss is a slow process (Bennet *et al*, 2016).

Our previous study revealed that the PDZ domain of mouse HtrA1 binds to denatured C-terminal ends of C-propeptides of fibrous collagens (type I, II, and III), and this binding stimulates the protease activity of HtrA1 (Murwantoko *et al*, 2004). We proposed that mammalian HtrA1 functions in a protein quality control system for collagens and other ECM proteins in the secretion processes inside or in the vicinity of cells. Oxidative stress induces HtrA1 expression in ARPE-19 human cell lines and MEF cells, and protects cells from

oxidation-induced cell death but enhances cell senescence (Supanji *et al*, 2013). Although the precise functions of mammalian secretory HtrA proteases are largely unknown, these findings suggest that mammalian HtrA1 is a stress response factor. In fact, HtrA proteases in a wide range of organisms are induced by various type of stress, recognize and degrade stress-denatured proteins with their protease activity, or refold them with the chaperon activity within a varieties of cellular compartments; such as bacterial Deg proteases in the periplasm, plant Deg proteases in chloroplasts, and mammalian HtrA2 in mitochondria (reviewed in Clausen *et al*, 2011). Deficiency of HtrA1 may disturb the secretory processes of collagens and other ECM proteins, causing stressful conditions inside the cell and leading to modulation of VSMC phenotypes. Impairment of the secretion of ECM proteins may also compromise cell-ECM interaction of VSMCs, further enhancing the phenotypic changes. Synthetic VSMCs produce high MMP9 activity that degrades the ECM, resulting in a vicious cycle that may lead to VSMC death and eventually to the onset of CARASIL.

Interestingly, HtrA1 levels are increased in the aorta of mice in which the low-density lipprotein receptor-relate dprotein 1 (*lrp1*) gene is deleted in smooth muscle cells (*smLRP1*^{-/-} mice) (Muratoglu *et al*, 2013). Low-density lipoprotein receptor-related protein 1 (LRP1) is a large endocytic and signaling receptor abundant in VSMCs. LRP1 binds and internalize HtrA1 and CTGF, thereby negatively regulate extracellular concentrations of these proteins. The *smLRP1*^{-/-} mice have extensive aortic dilatation accompanied by elastic fiber degradation and medial thickening. Aortic VSMCs of *smLRP1*^{-/-} mice show a highly synthetic phenotype, and this modulation is independent from the PDGF signaling. Heterozygous mutations of *HTRA1* were recently reported in a late-onset familial SVD group (Verdura *et al*, 2015). These reports and my current work suggest that optimal proteolytic activity of HtrA1 is essential to maintain VSMCs in the contractile phenotype. Both excessive proteolytic activity of HtrA1 and the absence of the protein quality control by HtrA1 result in impairment of

ECM-cell interaction, and as a consequence induce synthetic modulation of VSMCs and excessive remodeling of the vasculature. Since the *HtrA1*$^{-/-}$ mouse recapitulates the early events of the major vascular pathology of human CARASIL, it may be a valuable tool to reveal the molecular mechanisms underlying the vascular abnormality of this disease

4.4 Proposed Mechanism of HtrA1 in CARASIL Pathogenesis

Based on the data presented in this thesis, I would like to propose a model of CARASIL etiology (Fig. 4.1). Absence of HtrA1 impairs the protein quality control mechanism for collagens or other ECM proteins, thus produces denatured or unfolded collagens or other ECM proteins. As a consequence, the cellular secretory systems may become stuck, or expression and secretion of collagens or other ECM proteins may be suppressed. These conditions themselves can cause a cellular stress response in VSMCs, and induce phenotypic modulation to synthetic VSMCs due to accumulated stress. Synthetic VSMCs produce MMP9 activity that causes elastic fibers disruption and degradation of denatured collagens. Loss of normally matured type I, III, and VI collagens or other ECM proteins results in (1) accumulated stress inside the cells which eventually causes loss of VSMCs and arteriosclerotic reaction, and (2) impairment of cell-ECM interaction that induces phenotypic switching of VSMCs into further synthetic phenotype, which may aggravate already chaotic conditions. Synthetic VSMCs proliferate, migrate robustly, and invade into the intima to form intimal protrusion, an initial event of neointima formation. CARASIL is a slow onset disease; symptoms appear a couple of decades after birth, even though the patients have the deficiency of HtrA1 from the beginning of their lives. The pathological processes described above may require long time to reach a threshold for devastating malfunction to become overt. To confirm the stress condition in VSMCs as well as the morphological changes toward synthetic VSMCs, ultrastructure analysis would give more precise insights.

Bloating of ER, Golgi apparatus, or exosomes are expected on electron microscope. Electron microscopy also should give information on the structures and abundance of elastic fibers, collagens, and other ECM, as well as the conditions of connecting fibers, which indicates cell-elastic fiber interactions.
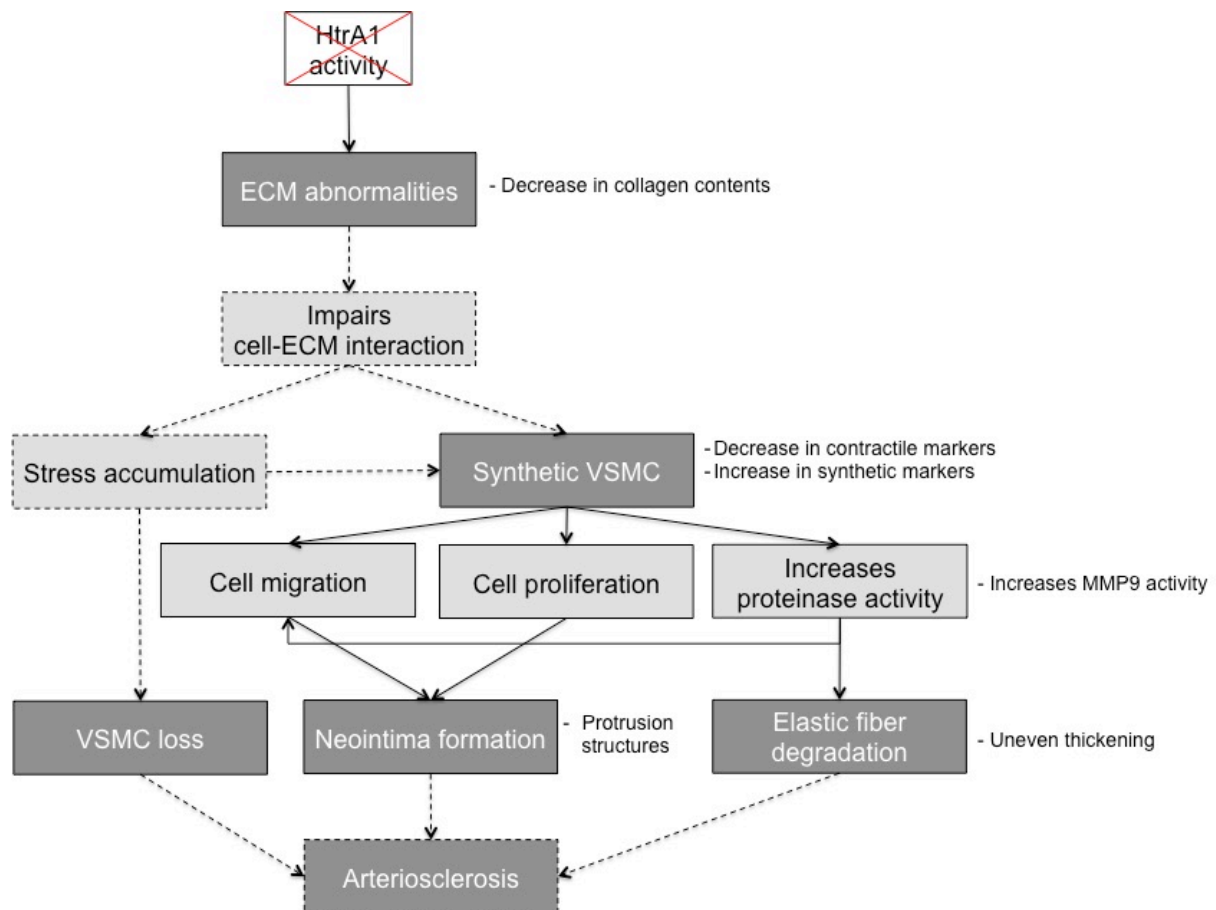
Figure 4.1   **Proposed mechanism of HtrA1 in CARASIL pathogenesis.**   Loss of functional HtrA1 provokes ECM abnormalities and impairs cell-ECM interaction. This, and accumulation of stress, induces phenotypic switching of VSMCs into synthetic phenotype. Stress accumulation overtime eventually caused VSMC degeneration and loss. Synthetic VSMCs contribute to neointima formation. Increases in activities of proteinases (MMP9, etc) cause elastic fiber degradation. VSMC loss, neointima formation, and elastic fiber degradation contribute to the development of arteriosclerosis. Solid-lined box: experimental data, dashed-line box: speculation.

V. ACKNOWLEDGMENTS

VI. REFERENCES

Alexander, M. R. and Owens, G. K. (2012). Epigenetic control of smooth muscle cell differentiation and phenotypic switching in vascular development and disease. *Annu. Rev. Physiol.* 74, 13-40.

Arima, K., Yanagawa, S., Ito, N., and Ikeda, S. (2003). Cerebral arterial pathology of CADASIL and CARASIL (Maeda syndrome). *Neuropathology* 23, 327-334.

Baldi, A., De Luca, A., Morini, M., Battista, T., Felsani, A., Baldi, F., Catricala, C., Amantea,A., Noonan, D. M., Albini, A., Natali, P. G., Lombardi, D., and Paggi, M. G. (2002). The HtrA1 serine protease is down-regulated during human melanoma progression and represses growth of metastatic melanoma cells. *Oncogene* 21, 6684-6688.

Beaufort, N., Scharrer, E., Kremmer, E., Lux, V., Ehrmann, M., Huber, R., Houlden, H., Werring, D., Haffner, C., and Dichgans, M. (2014). Cerebral small vessel disease-related protease HtrA1 processes latent TGF-β binding protein 1 and facilitates TGF-β signaling. *Proc. Natl. Acad. Sci. U.S.A.* 111, 16496-16501.

Bennet, M. R., Sinha, S. and Owens, G.K. (2016). Vascular smooth muscle cells in atherosclerosis. *Circ. Res.* 118, 692-702.

Bianchi, S., Di Palma, C., Gallus, G. N., Taglia, I., Poggiani, A., Rosini, F., Rufa, A., Muresanu, D. F., Cerase, A., Dotti, M. T., *et al*. (2014). Two novel *HTRA1* mutations in a European CARASIL patient. *Neurology* 82, 898-900.

Bowden, M., Di Nezza-Cosse, L., Jobling, T., Salamonsen, L. A., and Nie, G. (2006). Serine proteases HTRA1 and HTRA3 are down-regulated with increasing grades of human endometrial cancer. *Gynecol. Oncol.* 103, 253-260.

Boyle, J. J., Weissberg, P.,L., and Bennet, M. R. (2002). Human macrophage-induced vascular smooth muscle cell apoptosis requires NO enhancement of Fas/Fas-L interactions. *Arterioscler. Thromb. Vasc. Biol.* 22, 1624-1630.

Bunton, T.E., Biery, N.J., Myers, L., Gayraud, B., Ramirez, F., and Dietz, H.C. (2001). Phenotypic alteration of vascular smooth muscle cells precedes elastolysis in a mouse model of Marfan syndrome. *Circ. Res.* 88, 37-43.

Cai, B., Zeng J., Lin, Y., Lin W., Lin, W., and Wang, N. (2015). A frameshift mutation in HTRA1 expands CARASIL syndrome and peripheral small arterial disease to the Chinese population. *Neurol. Sci.* DOI: 10.1007/s10072-015-2121-5.

Campioni, M., Severino, A., Manente, L., Tuduce, I. L., Toldo, S., Caraglia, M., Crispi, S., Ehrmann, M., He, X., Maguire, J., *et al*. (2010). The serine protease HtrA1 specifically interacts and degrades the Tuberous Sclerosis Complex 2 protein. *Mol. Cancer Res.* 8, 1248-1260.

Catalano, V., Mellone, P., d'Avino, A., Shridhar, V., Staccioli, M. P., Graziano, F., Giordani,

P., Rossi, D., Baldelli, A. M., Alessandroni, P., *et al*. (2011). HtrA1, a potential pPredictor of response to cisplatin-based combination chemotherapy in gastric cancer. *Histopathology* 58, 669-678.

Chen, Y., He, Z., Meng, S., Li, H., Yang, H., and Zhang, X. (2013). A novel mutation of the high-temperature requirement A serine peptidase 1 (*HTRA1*) gene in a Chinese family with cerebral autosomal recessive arteriopathy with subcortical infarcts and leukoencephalopathy (CARASIL). *J. Int. Med. Res*. 41, 1445-1455.

Chien, J., Aletti, G., Baldi, A. M., Muretto, P., Keeney, G. L., Kalli, K. R., Staub, J., Ehrmann, M., Cliby, W. A., Lee, Y. K., *et al*. (2006). Serine protease HtrA1 modulates chemotherapy-induced cytotoxicity. *J. Clin. Invest.* 116, 1994 -2004.

Chien, J., Ota, T., Aletti, G., Shridhar, R., Boccelino, M., Quagliuolo, L., Baldi, A., and Shridhar, V. (2009). Serine protease HtrA1 associates with microtubules and inhibits cell migration. *Mol. Cell. Biol.* 29, 4177-4187.

Clausen, T., Kaiser, M., Huber, R., and Ehrmann, M. (2011). HTRA proteases: regulated proteolysis in protein quality control. *Nat. Rev. Mol. Cell Biol.* 12, 152-162.

Clausen, T., Southan, C., and Ehrmann, M. (2002). The HtrA family of proteases: implications for protein composition and cell fate. *Mol. Cell* 10, 433-455.

Crosas-Molist, E., Meirelles, T., Lopez-Luque, J., Serra-Peinado, C., Selva, J., Caja, L., Gorbenko Del Blanco, D., Uriarte, J., Bertran, E., Mendizabal, Y., *et al*. (2015). Vascular smooth muscle cell phenotypic changes in patients with Marfan syndrome. *Arterioscler. Thromb. Vasc. Biol.* 35, 960-972.

Deckert, V., Kretz, B., Habbout, A., Raghay, K., Labbe, J., Abello, N., Desrumaux, C., Gautier, T., Lemaire-Ewing, S., Maquart, G., *et al*. (2013). Development of abdominal aortic aneurysm is decreased in mice with plasma phospholipid transfer protein deficiency. *Am. J. Pathol.* 183, 975-986.

DeWan, A., Liu, M., Hartman, S., Zhang, S. S., Liu, D. T. l., Zhao, C., Tam, P. O. S., Chan, W. M., Lam, D. S. C., Snyder, M., *et al*. (2006). *HTRA1* Promoter Polymorphism in wet age-related macular degeneration. *Science* 314, 989-992.

Emrich, F. C., Okamura, H., Dalal, A.R., Penov, K., Merk, D. R., Raaz, U., Hennigs, J. K., Chin, J. T., Miller, M. O., Pedroza, A. J., *et al*. (2015). Enhanced caspase activity contributes to aortic wall remodelling and early aneurysm development in a murine model of Marfan syndrome. *Arterioscler. Thromb. Vasc. Biol.* 35, 146-154.

Formichi, P., Radi, E., Battisti, C., Di Maio, G., Tarquini, E., Leonini, A., Di Stefano, A., Dotti, M.T., and Federico, A. (2009). Apoptosis in CADASIL: an in vitro study of lymphocytes and fibroblasts from a cohort of Italian patients. *J. Cell. Physiol.* 219, 494-502.

Foucaud-Scheunemann, C. and Poquet, I. (2003). HtrA is a key factor in the response to specific stress conditions in *Lactococcus lactis*. *FEMS Microbiol. Lett.* 224, 53-59.

Francis, P. J., Zhang, H., DeWan, A., Hosh, J., and Klein, M. L. (2008). Joint effects of polymorphisms in the *HTRA1*, *LOC387715/ARMS2*, and *CFH* genes on AMD in a

Caucasian population. *Mol. Vis.* 14, 1395-1400.

Fukutake, T. (2011). Cerebral autosomal recessive arteriopathy with subcortical infarcts and leukoencephalopathy (CARASIL): from discovery to gene identification. *J. Stroke Cerebrovasc. Dis.* 20, 85-93.

Graham, J. R., Chamberland, A., Lin, Q., Li, X. J., Dai, D., Zeng, W., Ryan, M. S., Rivera-Bermudez, M., Flannery, C. R., and Yang, Z. (2013). Serine protease *HTRA1* antagonizes transforming growth factor-β signaling by cleaving its receptors and loss of HTRA1 *in vivo* enhances bone formation. *PLos ONE* 8, e74094. DOI: 10.1371/journal.pone.0074094.

Granata, A., Serrano, F., Bernard, W. G., McNamara, M., Low, L., Sastry, P., and Sinha, S. (2017). An iPSC-derived vascular model of Marfan syndrome identifies key mediators of smooth muscle cell death. *Nat. Gen.* 49, 97-109.

Grau, S., Richards, P. J., Kerr, B., Hughes, C., Caterson, B., Williams, A. S., Junker, U., Jones, S. A., Clausen, T., and Ehrmann, M. (2006). The role of human HtrA1 in arthritic disease. *J. Biol. Chem.* 281, 6124-6129.

Gray, F., Ploivka, M., Viswanathan, A., Baudrimont, M., Bousser, M., and Chabriat, H. (20070. Apoptosis in cerebral autosomal-dominant arteriopathy with subcortical infarcts and leukoencephalopathy. *J. Neuropathol. Exp. Neurol.* 66, 597-607.

Guo, X. and Chen, S. (2012). Transforming growth factor-β and smooth muscle cell differentiation. *World J. Biol. Chem.* 3, 41-52.

Hameedaldeen, A., Liu, J., Batres, A., Graves, G. S., and Graves, D. T. (2014). FOXO1, TGF-β regulation and wound healing. *Int. J. Mol. Sci.* 15, 16257-16269.

Hara K., Shiga A., Fukutake T., Nozaki H., Miyashita A., Yokoseki A., Kawata H., Koyama, A., Arima, K., Takahashi, T., *et al*. (2009). Association of HTRA1 mutations and familial ischemic cerebral small-vessel disease. *N. Engl. J. Med.* 360, 1729-1739.

Hart, M. N., Heistad, D. D., and Brody, M. J. (1980). Effect of chronic hypertension and sympathetic denervation on wall/lumen ratio of cerebral vessels. *Hypertension* 2, 419-423.

Hasan, M. Z., Ikawati, M., Tocharus, J., Kawaichi, M., and Oka, C. (2015). Abnormal development of placenta in HtrA1-deficient mice. *Dev. Biol.* 397, 89-102.

Hayashi, K., Shibata, K., Morita, T., Iwasaki, K., Watanabe, M., and Sobue, K. (2004). Insulin receptor substrate-1/SHP-2 interaction, a phenotype-dependent switching machinery of insulin-like growth factor-I signaling in vascular smooth muscle cells. *J. Biol. Chem.*, 279, 40807-40818.

Hayashi, K., Takahashi, M., Kimura, K., Nishida, W., Saga, H., and Sobue, K. (1999). Changes in the balance of phosphoinositide 3-kinase/protein kinase B (Akt) and the mitogen-activated protein kinases (ERK/p38MAPK) determine a phenotype of visceral and vascular smooth muscle cells. *J. Cell Biol.* 145, 727-740.

He, X, Khurana, A., Maguire, J. L., Chien, J., and Shridhar, V. (2012). HtrA1 sensitizes

Ovarian cancer cells to cisplatin-induced cytotoxicity by targeting XIAP for degradation. *Int. J. Cancer* 130, 1029-1035.

Hildebrand, A., Romarís, M., Rasmussen, L. M., Heinegard, D., Twardzik, D. R., Border, D. A., and Ruoslahti, E. (1994). Interaction of the small interstitial proteoglycans biglycan, decorin and fibromodulin with transforming growth factor β. *Biochem. J.* 302, 527-534.

Hu, S., Carozza, M., Klein, M., Nantermet, P., Luk, D., and Crowl, R. M. (1998). Human HtrA, an evolutionarily conserved serine protease identified as a differentially expressed gene product in osteoarthritic cartilage. *J. Biol. Chem.* 273, 34406-34412.

Ihalainen, S., Soliymani, R., Iivanainen, E., Mykkanen, K., Sainio, A., Poyhonen, M., Elenius, K., Jarvelainen, H., Viitanen, M, Kalimo, H., *et al*. (2006). Proteome analysis of cultivated vascular smooth muscle cells from a CADASIL patient. *Mol. Med.* 13, 305-314.

Jawien, J., Nastalek, P., and Korbut, R. (2004). Mouse models of experimental atherosclerosis. *J. Physiol. Pharmacol.* 55, 503-517.

Jones, A., Kumar, S., Zhang, N., Tong, Z., Yang, J., Watt, C, Anderson, J., Amrita, Fillerup, H., McCloskey, M., *et al*. (2011). Increased expression of multifunctional serine protease, HTRA1, in retinal pigment epithelium induces polypoidal choroidal vasculopathy in mice. *Proc. Natl. Acad. Sci. U.S.A.* 108, 14578-14583.

Joutel, A, Corpechot, C., Ducros, A., Vahedi, K., Chabriat, H., Mouton, P., Alamowitch, S., Domenga, V., Cecillion, M., Marechal, E., *et al*. (1996). *NOTCH3* mutations in CADASIL, a hereditary adult-onset condition causing stroke and dementia. *Nature* 383, 707-710.

Kang, S., Fernandes-Alnemri, T., and Alnemri, E. S. (2013). A novel role for the mitochondrial HTRA2/OMI protease in aging. *Autophagy* 9, 420-421.

Krojer, T., Pangerl, K., Kurt, J., Sawa, J., Stingl, C., Mechtler, K., Huber, R., Ehrmann, M., and Clausen, T. (2008). Interplay of PDZ and protease domain of DegP ensures efficient elimination of misfolded proteins. *Proc. Natl. Acad. Sci. U.S.A.* 105, 7702-7707.

Li, H., Liang, J., Castrillon, D.H., DePinho, R.A, Olson, E.N., and Liu, Z. (2007). FoxO4 regulates tumor necrosis factor alpha-directed smooth muscle cell migration by activating matrix metalloproteinase 9 gene transcription. *Mol. Cell. Biol.* 27, 2676-2786.

Lipinska, B., Fayet, O., Baird, L., and Georgopoulos, C. (1989). Identification, characterization, and mapping of the *Escherichia coli HtrA* gene, whose product is essential for bacterial growth only at elevated temperatures. *J. Bacteriol.* 171, 1574 - 1584.

Lipinska, B., Zylicz, M., and Georgopoulos, C. (1990). The HtrA (DegP) protein, essential for Escherichia coli survival at high temperatures, is an endopeptidase. *J. Bacteriol.* 172, 1791-1797.

Louis, S. F. and Zahradka, P. (2010). Vascular smooth muscle cell motility: from migration to invasion. *Exp. Clin. Cardiol.* 15, e75-e85.

Mack, C. P. (2011). Signaling mechanisms that regulate smooth muscle cell differentiation. *Arterioscler. Thromb. Vasc.* Biol. 31, 1495-1505.

Maeda, S., Nakayama, H., Isaka, K., Aihara, Y., and Nemoto, S. (1976). Familial unusual encephalopathy of Binswanger's type without hypertension. *Folia Psychiatr. Neurol. Jpn.* 30, 165-177.

Majesky, M. W., Dong, X. R., Regan, J. N., and Hoglund, V. J. (2011). Vascular smooth muscle progenitor cells: building and repairing blood vessels. *Circ. Res.* 108, 365-377.

Mao, N., Gu, T., Shi, E., Zhang, G., Yu, L., and Wang, C. (2015). Phenotypic switching of vascular smooth muscle cells in animal model of rat thoracic aortic aneurysm. *Interact. Cardiovasc. Thorac. Surg.* DOI: 10.1093/icvts/ivv074.

Martins, L. M., Morrison, A., Klupsch, K., Fedele, V., Moisoi, N., Teismann, P., Abuin, A., Grau, E., Geppert, M., Livi, G.P., *et al.* (2004). Neuroprotective role of the reaper-related serine protease HtrA2/Omi revealed by targeted deletion in mice. *Mol. Cell. Biol.* 24, 9848-9862.

Massague, J. (2000). How cells read TGF-β signals. *Nat. Rev. Mol. Cell Biol.* 1, 169 – 178.

Massague, J. (2012). TGFβ signalling in context. *Nat. Rev. Mol. Cell Biol.* 13, 616 – 630.

McKee, J. A., Banik, S. S. R., Bayer, M. J., Hamad, N. M., Lawson, J. H., Niklason, L. E., and Counter, C. M. (2003). Human arteries engineered in vitro. *EMBO Rep.* 4, 633-638.

Mendioroz, M., Fernandez-Cadenas, I., Del Rio-Espinola, A., Rovira, A., Sole, E., Fernandez-Figueras, M. T., Garcia-Patos, V., Sastre-Garriga, J., Domingues-Montarani, S., and Alvarez-Sabin, J. (2010). A missense *HTRA1* mutation expands CARASIL syndrome to the Caucasian population. *Neurology* 75, 2033-2035.

Metz, R. P., Patterson, J. L., and Wilson, E. (2012). Vascular smooth muscle cells: isolation, culture, and characterization. In *Cardiovascular Development: Methods and Protocols*, X. Penag and M. Antonyak, eds. (New York: Springer), pp. 169-176.

Mullany, S. A., Moslemi-Kebria, M., Rattan, R., Khurana, A., Clayton, A., Ota, T., Mariani, A., Podratz, K. C., chien, J., and Shridhar, V. (2011). Expression and functional significance of HtrA1 loss in endometrial cancer. *Clin. Cancer Res.* 17, 427-436.

Muratoglu, S.C., Belgrave, S., Hampton, B., Migliorini, M., Coksaygan, T., Chen, L., Mikhailenko, I., and Strickland, D.K. (2013). LRP1 protects the vasculature by regulating levels of connective tssue growth factor and HtrA1. *Arterioscler. Thromb. Vasc. Biol.* 33, 2137-2146.

Murwantoko, Yano, M., Ueta, Y., Murasaki, A., Kanda, H., Oka, C., and Kawaichi, M., (2004). Binding of proteins to the PDZ domain regulates proteolytic activity of HtrA1 serine protease. *Biochem. J.* 381, 895-904.

Nataatmadja, M., West, M., West, J., Summers, K., Walker, P., Nagata, M., and Watanabe, T. (2003). Abnormal extracellular matrix protein transport associated with increased apoptosis of vascular smooth muscle cells in Marfan syndrome and bicuspid aortic valve thoracic aortic aneurysm. *Circulation* 108[suppl II], II-329-II-334.

Newby, A. C. (2006). Matrix metalloproteinases regulate migration, proliferation, and death of vascular smooth muscle cells by degrading matrix and non-matrix substrates. *Cardiovasc. Res.* 69, 614-624.

Nie, G., Hampton, A., Li, Y., Findlay, J. K., and Salamonsen, L. A. (2003a). Identification and cloning of two isoforms of human high-temperature requirement factor A3 (HtrA3), characterization of its genomic structure and comparison of its tissue distribution with HtrA1 and HtrA2. *Biochem. J.* 371, 39-48.

Nie, G., Li, Y., Minoura, H., Batten, L., Ooi, G. T., Findaly, J. K., and Salamonsen, L. A. (2003b). A novel serine protease of the mammalian HtrA family is up-regulated in mouse uterus coinciding with placentation. *Mol. Hum. Reprod.* 9, 279-290.

Nishimoto, Y., Shibata, M., Nihonmatsu, M., Nozaki, H., Shiga, A., Shirata, A., Yamane, K., Kosakai, A., Takahashi, K., Nishizawa, M., Onodera, O., and Suzuki, N. (2011). A novel mutation in the *HTRA1* gene causes CARASIL without alopecia. *Neurology*, 76, 1353-1355.

Oide T., Nakayama H., Yanagawa S., Ito N., Ikeda S., and Arima K. (2008). Extensive loss arterial medial smooth muscle cells and mural extracellular matrix in cerebral autosomal recessive arteriopathy with subcortical infarcts and leukoencephalopathy (CARASIL). *Neuropathology* 28, 132-142.

Oka, C., Tsujimoto, R., Kajikawa, M., Koshiba-Takeuchi, K., Ina, J., Yano, M., Tsuchiya, A., Ueta, Y., Soma, A., Kanda, H., Matsumoto, M., and Kawaichi, M. (2004). HtrA1 serine protease inhibits signaling mediated by Tgfβ family proteins. *Development* 131, 1041-1053.

Owens, G. K. (1995). Regulation of differentiation of vascular smooth muscle cells. *Physiol. Rev.* 75, 487-517.

Owens, G. K., Kumar, M. S., and Wamhoff, B. R. (2004). Molecular Regulation of Vascular Smooth Muscle Cell Differentiation in Development and Disease. *Physiol. Rev.* 84, 767-801.

Pardali, E. and ten Dijke, P. (2012). TGFβ signaling and cardiovascular diseases. *Int. J. Biol. Sci.* 8, 195-213.

Rauter, H., Oeverijnder, M., Doornbosch, D., and Schalkhammer, T. (2003). DegP and related genes as stress-markers for *E.Coli*-viability – ultra-sensitive RT-real-time PCR. *Monatshefte für Chemie* 134, 1489-1498.

Rensen, S. S. M., Doevendans, P. A. F. M., and van Eys, G. J. J. M. (2007). Regulation and characteristics of vascular smooth muscle cell phenotypic diversity. *Neth. Heart J.* 15, 100-108.

Runyon, S. T., Zhang, Y., Appleton, B. A., Sazinsky, S. L., Wu, P., Pan, B., Wiesmann, C.,

Skelton, N. J., and Sidhu, S. S. (2007). Structural and functional analysis of the PDZ domains of human HtrA1 and HtrA3. *Protein Sci.* 16, 2454-2471.

Shaulian, E. and Karin, M. (2001). AP-1 in cell proliferation and survival. *Oncogene* 20, 2390-2400.

Shiga, A., Nozaki, H., Yokoseki, A., Nihonmatsu, M., Kawata, H., Kato, T., Koyama, A., Arima, K., Ikeda, M., Katada, S., *et al*. (2011). Cerebral small-vessel disease protein HTRA1 controls the amount of TGF-β1 via cleavage of proTGF-β1. *Hum. Mol. Genet.* 20, 1800-1810.

Skorko-Glonek, J., Krzewski, K., Lipinska, B., Bertoli, E., and Tanfani, F. (1995). Comparison of the structure of wild-type HtrA heat shock protease and mutant HtrA proteins. *J. Biol. Chem.* 270, 11140-11146.

Skorko-Glonek, J., Zurawa, D., Kuczwara, E., Wozniak, M., Wypych, Z., and Lipinska, B. (1999). The *Escherichia coli* heat shock protease HtrA participates in defense against oxidative stress. *Mol. Gen. Genet.* 262, 342-350.

Spiess, C., Beil, A., and Ehrmann, M. (1999). A temperature-dependent switch from chaperone to protease in a widely conserved heat shock protein. *Cell* 97, 339-347.

Strauch, K. L. and Beckwith, J. (1988). An Escherichia coli mutation preventing degradation of abnormal periplasmic proteins. *Proc. Natl. Acad. Sci. U.S.A.* 85, 1576-1580.

Strauss, K. M., Martins, L. M., Plun-Favreau, H., Marx, F. P., Kautzmann, S., Berg, D., Berg, D., Gasser, T., Wszolek, Z., Muller, T., *et al*. (2005). Loss of function mutations in the gene encoding Omi/HtrA2 in Parkinson's disease. *Hum. Mol. Genet.* 14, 2099-2111.

Supanji, Shimomachi, M., Hasan, M. Z., Kawaichi, M., and Oka, C. (2013). HtrA1 is induced by oxidative stress and enhances cell senescence through p38 MAPK pathway. *Exp. Eye Res.* 112, 79-92.

Suwanabol, P. A., Seedial, S. M., Shi, X., Zhang, F., Yamanouchi, D., Roennerburg, D., Liu, B., and Kent, K. C. (2012). Transforming growth factor-β increases vascular smooth muscle cell proliferation through the Smad3 and extracellular signal-regulated kinase mitogen-activated protein kinases pathways. *J. Vasc. Surg.* 56, 446-454.

Suzuki, Y., Imai, Y., Nakayama, H., Takahashi, K., Takio, K., and Takahashi, R. (2001). A serine protease, HtrA2, is released from the mitochondria and interacts with XIAP, inducing cell death. *Mol. Cell* 8, 613-621.

Tang, Y., Yang, X., Friese, R. E., Vary, C. P. H., and Liaw, L. (2011). Mechanisms of TGF-β-induced differentiation in human vascular smooth muscle cells. *J. Vasc. Res.* 48, 485 – 494.

The Editors of The Encyclopedia of Britanica. (2014). *Artery*. Retrieved from http://global.britannica.com/EBchecked/topic/36874/artery.

Tocharus, J., Tsuchiya, A., Kajikawa, M., Ueta, Y., Oka, C., and Kawaichi, M. (2004). Developmentally regulated expression of mouse HtrA3 and its role as an inhibitor of TGF-β signaling. *Dev. Growth Differ.* 46, 257-274.

Trencia, A., Fiory, F., Maitan, M. A., Vito, P., Barbagallo, A. P., Perfetti, A., Miele, C., Ungaro, P. Oriente, F., Cilenti, L., *et al.* (2004). Omi/HtrA2 promotes cell death by binding and degrading the anti-apoptotic protein ped/pea-15. *J. Biol. Chem.* 279, 46566-46572.

Tsuchiya, A., Yano, M., Tocahrus, J., Kojima, H., Fukumoto, M., Kawaichi, M., and Oka, C. (2005). Expression of mouse HtrA1 serine protease in normal bone and cartilage and its upregulation in joint cartilage damaged by experimental arthritis. *Bone* 37, 323-336.

Vaja, V., Ochodnicky, P., Krenek, P., Klimas, J., Bajuszova, Z., and Kyselovic, J. (2009). Rapid large artery remodeling following the administration and withdrawal of calcium channel blockers in spontaneously hypertensive rats. *Eur. J. Pharmacol.* 619, 85-91.

Verdura, E., Herve, D., Scharrer, E., del Mar Amador, M. M., Guyant-Marechal, L., Philippi, A., Corlobe, A., Bergametti, F., Gazal, S., Prieto-Morin, C., *et al.* (2015). Heterozygous *HTRA1* mutations are associated with autosomal dominant cerebral small vessel disease. *Brain.* DOI: 10.1093/brain/awv155.

Vierkotten, S., Muether, P. S., and Fauser, S. (2011). Overexpression of HTRA1 leads to ultrastructural changes in the elastic layer of Bruch's membrane via cleavage of extracellular matrix components. *PLoS ONE* 6, e22959. DOI: 10.1371/journal.pone.0022959.

von der Thusen, J. H., Borensztajn, K. S., Moimas, S., van Heiningen, S., Teeling, P., van Berkel, T. J. C., and Biessen, E. A. L. (2011). IGF-1 Has Plaque-Stabilizing Effects in Atherosclerosis by Altering Vascular Smooth Muscle Cell Phenotype. *Am. J. Pathol.* 178, 924-934.

Wang, N., Eckert, K. A., Zomorrodi, A. r., Xin, P., Pan, W., Shearer, D. A., Weisz, J., Maranus, C. D., and Clawson, G. A. (2012a). Down-regulation of HtrA1 activates the epithelial-mesenchymal transition and ATM DNA damage response pathways. *PLoS ONE* 7, e39446. DOI:10.1371/journal.pone.0039446.

Wang, X., Li, C., Guo., and Cao, B. (2012b). A novel mutation in the *HTRA1* gene identified in Chinese CARASIL pedigree. *CNS Neurosci. Ther.* 18, 867-869.

Wong, L. S. M., Oeseburg, H., de Boer, R. A., van Gilst, W. H., van Veldhuisen, D. J., and van der Harst, P. (2009). Telomere biology in cardiovascular disease: the TERC-/- mouse as a model for heart failure and ageing. *Cardiovasc. Res.* 81, 244-252.

Xu, Q. (2004). Mouse models of arteriosclerosis from arterial injuries to vascular grafts. *Am. J. Pathol.* 165, 1-9.

Yabluchanskiy, A., Ma, Y., Iyer, R.P., Hall, M.E., and Lindsey, M.L. (2013). Matrix metalloproteinase-9: many shades of function in cardiovascular disease. *Physiology* 28, 391-403.

Yang, Z., Camp, N. J., Sun, H., Tong, Z., Gibbs, D., Cameron, D. J., Chen, H., Zhao, Y., Pearson, E., Li, X., *et al*. (2006). A variant of the *HTRA1* gene increases susceptibility to age-related macular degeneration. *Science* 314, 992-993.

Yokoi, S. and Nakayama, H. (1985). Chronic progressive leukoencephalopathy with systemic arteriosclerosis in young adults. *Clin. Neuropathol.* 4, 165-173.

Zhang, H., Wang, Z., Wu, H., Li, Z., Li, L., Hu, X., Ren, Z., Li, B., and Hu, Z. (2013). Transforming growth factor-β1 induces matrix metalloproteinase-9 expression in rat vascular smooth muscle cells via ROS-dependent ERK–NF-κB pathways. *Mol. Cell Biochem.* 375, 11-21.

Zhang, L., Liu, Y., Song, F., Hu, L., Lu, H., Liu, P., Hao, X., Zhang, W., and Chen, K. (2011). Functional SNP in the microRNA-367 binding site in the 3′UTR of the calcium channel ryanodine receptor gene 3 (RYR3) affects breast cancer risk and calcification. *Proc. Natl. Acad. Sci. U.S.A.* 108, 13653-13658.

Zheng, D. M., Xu, F. f., Gao, Y., Zhang, H., Han, S. C., and Bi, G. R. (2009). A Chinese pedigree of cerebral autosomal recessive arteriopathy with subcortical infarcts and leukoencephalopathy (CARASIL): Clinical and radiological features. *J. Clin. Neurosci.* 16, 847-849.

Zhu, B.H., Ueno, M., Matsushita, T., Fujisawa, H., Seriu, N., Nishikawa, T., Nishimura, Y., and Hosokawa, M. (2001). Effects of aging and blood pressure on the structure of the thoracic aorta in SAM mice: a model of age-associated degenerative vascular changes. *Exp. Gerontol.* 36, 111-124.

Zurawa-Janicka, D., Kobiela, J., Galcynska, N., Stefaniak, T., Lipinska, B., Lachinski, A., Skorko-Glonek, J., Narkiewicz, J., Proczko- Markuszewska, M., and Sledzinski, Z. (2012). Changes in expression of human serine protease HtrA1, HtrA2 and HtrA3 genes in benign and malignant thyroid tumors. *Oncol. Rep.* 28, 1838-1844.

APPENDIX

Appendix 1. Supplementary data of Fig. 3.4

Appendix 1. Supplementary data of Figure 3.4

A. Cross-sectional area

Weeks	WT	Number of sections	Cross-sectional area (µm²)	KO	Number of sections	Cross-sectional area (µm²)	p value (ttest WT vs KO, 95% significance)
16	1	6	320274	1	3	383438	0.245
	2	6	474397	2	6	261751	
	3	3	265475	3	3	524038	
	4	4	322681	4	6	521803	
				5	5	474924	
	average		345707	average		433191	
	SD		89769	SD		111483	
24	1	5	348903	1	6	429686	0.216
	2	8	273507	2	3	491073	
	3	5	255442	3	6	416307	
	4	5	481108	4	4	348340	
	average		339740	average		421352	
	SD		102570	SD		58557	
40	1	8	347543	1	7	520642	0.052
	2	6	320660	2	7	530834	
	3	6	434363	3	8	694095	
	4	8	432385	4	4	493837	
	5	6	359325	5	5	342912	
	average		378855	average		516464	
	SD		51708	SD		124909	
52	1	3	420859	1	3	584344	0.002
	2	3	428193	2	3	537947	
	3	3	414474	3	3	571352	
	4	3	552669	4	3	524113	
	5	3	425435	5	3	497887	
	6	3	448040	6	3	432635	
	7	3	391011	7	3	565226	
	8	3	370702				
	9	3	441105				
	10	3	485086				
	average		437757	average		530501	
	SD		50897	SD		52458	
60	1	5	404552	1	5	644548	0.648
	2	5	484986	2	5	546813	
	3	4	689587	3	5	448199	
	4	5	387732	4	5	424231	
	5	5	586979	5	4	514330	
	6	5	420785	6	5	559135	
	7	5	508064				
	average		497526	average		522876	
	SD		109351	SD		80090	

B. Media thickness

Weeks	WT	Number of sections	Media thickness (µm)	KO	Number of sections	Media thickness (µm)	p value (ttest WT vs KO, 95% significance)
16	1	6	65	1	2	68	0.368
	2	6	69	2	6	51	
	3	3	66	3	1	65	
	4	4	52	4	6	84	
				5	5	85	
	average		63	average		71	
	SD		8	SD		14	
24	1	5	50	1	6	67	0.001
	2	8	47	2	3	69	
	3	5	52	3	6	65	
	4	5	59	4	4	70	
	average		52	average		68	
	SD		5	SD		2	
40	1	8	54	1	7	80	0.415
	2	6	73	2	7	68	
	3	6	66	3	8	71	
	4	8	64	4	4	60	
	5	6	52	5	5	56	
	average		62	average		67	
	SD		9	SD		9	
52	1	3	71	1	3	79	0.903
	2	3	76	2	3	75	
	3	3	70	3	3	67	
	4	3	83	4	3	74	
	5	3	60	5	3	55	
	6	3	56	6	3	54	
	7	3	65	7	3	67	
	8	3	58				
	9	3	69				
	10	3	69				
	average		68	average		67	
	SD		8	SD		10	
60	1	5	71	1	5	97	0.820
	2	5	74	2	5	83	
	3	4	86	3	5	64	
	4	5	73	4	5	60	
	5	5	84	5	4	77	
	6	5	67	6	5	84	
	7	5	77				
	average		76	average		77	
	SD		7	SD		14	

C. Lumen diameter

Weeks	WT	Number of sections	Lumen diameter (µm)	KO	Number of sections	Lumen diameter (µm)	p value (ttest WT vs KO, 95% significance)
16	1	6	488	1	2	548	0.343
	2	6	620	2	6	446	
	3	3	430	3	1	644	
	4	4	523	4	6	617	
				5	5	590	
	average		515	average		569	
	SD		80	SD		77	
24	1	5	554	1	6	614	0.280
	2	8	484	2	3	636	
	3	5	435	3	6	598	
	4	5	659	4	4	536	
	average		533	average		596	
	SD		97	SD		43	
40	1	8	542	1	7	633	0.060
	2	6	483	2	7	673	
	3	6	586	3	8	791	
	4	8	594	4	4	648	
	5	6	544	5	5	522	
	average		550	average		653	
	SD		44	SD		96	
52	1	3	554	1	3	687	0.001
	2	3	591	2	3	659	
	3	3	558	3	3	712	
	4	3	660	4	3	661	
	5	3	590	5	3	669	
	6	3	633	6	3	612	
	7	3	559	7	3	676	
	8	3	545				
	9	3	591				
	10	3	639				
	average		592	average		668	
	SD		40	SD		31	
60	1	5	555	1	5	689	0.303
	2	5	619	2	5	644	
	3	4	720	3	5	617	
	4	5	479	4	5	594	
	5	5	647	5	4	634	
	6	5	569	6	5	661	
	7	5	632				
	average		603	average		640	
	SD		77	SD		33	

Appendix 1. Supplementary data of Figure 3.4

D. Medial VSMC number

Weeks	WT	Number of sections	VSMC number	KO	Number of sections	VSMC number	p value (ttest WT vs KO, 95% significance)	
16	1	6	295	1	2	395	0.412	
	2	6	323	2	6	252		
	3	3	279	3	1	347		
	4	4	260	4	6	296		
				5	5	290		
	average		289	average		316		
	SD		27	SD		56		
24	1	5	269	1	6	303	0.053	
	2	8	223	2	3	301		
	3	5	202	3	6	263		
	4	5	227	4	4	245		
	average		230	average		278		
	SD		28	SD		29		
40	1	8	219	1	7	328	0.024	**p value (ttest KO 40wo vs 52wo 95% significance)**
	2	6	237	2	7	273		0.027
	3	6	246	3	8	274		
	4	8	209	4	4	262		
	5	6	273	5	5	272		
	average		237	average		282		
	SD		25	SD		26		
52	1	3	275	1	3	251	0.623	**p value (ttest KO 52wo vs 60wo 95% significance)**
	2	3	238	2	3	206		0.001
	3	3	248	3	3	214		
	4	3	296	4	3	199		
	5	3	234	5	3	246		
	6	3	215	6	3	268		
	7	3	229	7	3	276		
	8	3	225					
	9	3	240					
	10	3						
	average		244	average		237		
	SD		26	SD		31		
60	1	5	215	1	5	191	0.002	
	2	5	212	2	5	194		
	3	4	310	3	5	159		
	4	5	251	4	5	168		
	5	5	240	5	4	182		
	6	5	226	6	5	181		
	7	5	215					
	average		239	average		179		
	SD		35	SD		13		

Appendix 2. Supplementary data of Fig. 3.5

A. Media thickness

WT	Number of sections	Media thickness (µm)	3KO	Number of sections	Media thickness (µm)	1KO	Number of sections	Media thickness (µm)	DKO	Number of sections	Media thickness (µm)
1	10	32	1	8	27	1	7	33	1	6	30
2	6	34	2	9	38	2	7	32	2	6	36
						3	9	25			
						4	8	25			
						5	8	33			
						6	8	29			
average		33	average		32	average		29	average		33
SD		2	SD		8	SD		4	SD		5

p value (ttest, 95% significance)											
			0.9069								WT vs 3KO
						0.2118					WT vs 1KO
									0.4454		WT vs DKO
						0.2751					3KO vs 1KO
									0.9692		3KO vs DKO

B. Medial VSMC number

Genotype	Mouse	Number of sections	VSMC number	p value (ttest 95% significance)			
WT	1	10	359	**WT vs 3KO**			
	2	6	342				
	average		351		**WT vs 1KO**		
	SD		12	0.024		**3KO vs 1KO**	
3KO	1	8	214				
	2	9	247				
	average		231				**WT vs DKO**
	SD		24		0.012	0.931	
1KO	1	7	239				
	2	7	213				
	3	9	211				
	4	8	181				**1KO vs DKO**
	5	8	250				
	6	8	308				
	average		234				
	SD		44				
DKO	1	6	224			0.0606	0.686
	2	6	273				
	average		249				
	SD		35				

Appendix 3. Supplementary data of Fig. 3.6

A. PCNA immunostaining of 40-week-old wild type and *HtrA1⁻/⁻* mouse aorta

	Mouse	Number of sections	Total cell number (average)	PCNA-positive cells (average)	PCNA-positive cells (%)	p value (ttest WT vs KO, 95% significance)
WT	1	8	219	6	2.82	0.110
	2	6	237	6	2.46	
	3	6	220	6	2.81	
	4	6	246	8	2.06	
	5	8	209	7	3.40	
	6	6	273	2	0.61	
	Average		234	6	2.36	
	SD		23	2	0.96	
KO	1	7	328	23	7.00	
	2	7	273	28	10.25	
	3	8	274	13	4.66	
	4	4	262	6	2.23	
	5	5	272	3	1.28	
	Average		282	15	5.08	
	SD		26	11	3.65	

B. TUNEL staining of 52-week-old wild type and *HtrA1⁻/⁻* mouse aorta

	Mouse	Total cell number	TUNEL-positive cells (average)	TUNEL-positive cells (%)	p value (ttest WT vs KO, 95% significance)
WT	1	220	8	3.64	0.435
	2	199	9	4.52	
	3	227	18	7.93	
	4	236	3	1.06	
	5	222	8	3.60	
	6	217	2	0.92	
	Average	220	8	3.61	
	SD	12	6	2.58	
KO	1	185	5	2.70	
	2	192	4	2.08	
	3	179	7	3.91	
	4	221	10	4.52	
	5	195	3	1.54	
	6	178	2	1.12	
	Average	192	5	2.65	
	SD	16	3	1.34	

Appendix 4. Supplementary data of Fig. 3.9

Rapid proliferation of _HtrA1⁻ᐟ⁻_ VSMCs
Representative data from 1 of 3 batches (batch code #3), passage 7

Wild type (WT)

Incubation time (h)	Treatment	Media A450 nm 1	2	3	average	A450 nm cells 1	2	3	4	corrected 1	2	3	4	average	stdev	fold to 0h 1	2	3	4	average	stdev	p value (ttest WT vs KO, 95% significance)
0	10%FBS	0.161	0.160	0.159	0.160	0.510	0.509	0.526	0.506	0.350	0.349	0.366	0.346	0.353	0.009	0.992	0.989	1.038	0.981	1.00	0.00	
	5% FBS	0.164	0.165	0.162	0.164	0.459	0.443	0.408	0.429	0.295	0.279	0.244	0.265	0.271	0.022	1.089	1.030	0.901	0.979	1.00	0.00	
	0%FBS	0.162	0.163	0.164	0.163	0.329	0.343	0.320	0.281	0.166	0.180	0.157	0.118	0.155	0.021	1.069	1.159	1.011	0.760	1.00	0.00	
24	10%FBS	0.154	0.160	0.165	0.160	0.675	0.696	0.650	0.635	0.515	0.536	0.490	0.475	0.504	0.027	1.461	1.520	1.390	1.348	1.43	0.08	0.3017
	5% FBS	0.156	0.163	0.162	0.160	0.386	0.491	0.300		0.226	0.331	0.140		0.232	0.096	0.832	1.220	0.515		0.86	0.35	0.0205
	0%FBS	0.164	0.166	0.166	0.165	0.270	0.311	0.352		0.105	0.146	0.187		0.146	0.041	0.674	0.938	1.202		0.94	0.26	0.0010
48	10%FBS	0.154	0.157	0.160	0.157	0.766	0.737	0.750	0.733	0.609	0.580	0.593	0.576	0.590	0.015	1.726	1.644	1.681	1.633	1.67	0.04	0.0041
	5% FBS	0.143	0.151	0.174	0.156	0.257		0.495	0.379	0.101		0.339	0.223	0.221	0.119	0.373		1.251	0.823	0.82	0.44	0.0123
	0%FBS	0.156	0.160	0.171	0.162	0.362	0.343	0.339	0.329	0.200	0.181	0.177	0.167	0.181	0.014	1.286	1.164	1.138	1.074	1.17	0.09	0.0000
72	10%FBS	0.148	0.150	0.151	0.150	0.891	0.874	0.961	0.859	0.741	0.724	0.811	0.709	0.747	0.045	2.102	2.053	2.300	2.011	2.12	0.13	0.0184
	5% FBS	0.146	0.151	0.150	0.149		0.860	0.816	0.839		0.711	0.667	0.690	0.689	0.022		2.623	2.460	2.545	2.54	0.08	0.0092
	0%FBS	0.154	0.158	0.161	0.158	0.316	0.287	0.353	0.379	0.158	0.129	0.195	0.221	0.176	0.040	1.020	0.833	1.258	1.426	1.13	0.26	0.0901
96	10%FBS	0.147	0.145	0.148	0.147	1.001	0.990	0.903	0.941	0.854	0.843	0.756	0.794	0.812	0.045	2.422	2.391	2.144	2.252	2.30	0.13	0.0037
	5% FBS	0.138	0.146	0.146	0.143	0.704	0.856	0.958		0.561	0.713	0.815		0.696	0.128	2.068	2.629	3.005		2.57	0.47	0.0042
	0%FBS	0.152	0.158	0.159	0.156		0.336	0.366	0.365		0.180	0.210	0.209	0.199	0.017		1.157	1.351	1.344	1.28	0.11	0.0125

HtrA1⁻ᐟ⁻ (KO)

Incubation time (h)	Treatment	Media A450 nm 1	2	3	average	A450 nm cells 1	2	3	4	corrected 1	2	3	4	average	stdev	fold to 0h 1	2	3	4	average	stdev
0	10%FBS	0.161	0.160	0.159	0.160	0.345	0.347	0.337	0.328	0.185	0.187	0.177	0.168	0.179	0.009	1.032	1.043	0.987	0.937	1.00	0.00
	5% FBS	0.164	0.165	0.162	0.164	0.329	0.264	0.307	0.268	0.165	0.100	0.143	0.104	0.128	0.031	1.288	0.782	1.117	0.813	1.00	0.00
	0%FBS	0.162	0.163	0.164	0.163	0.207	0.221	0.226	0.235	0.044	0.058	0.063	0.072	0.059	0.012	0.743	0.979	1.063	1.215	1.00	0.00
24	10%FBS	0.154	0.160	0.165	0.160	0.473	0.450	0.466	0.378	0.313	0.290	0.306	0.218	0.282	0.044	1.748	1.620	1.709	1.218	1.57	0.24
	5% FBS	0.156	0.163	0.162	0.160	0.370	0.405	0.385	0.323	0.210	0.245	0.225	0.163	0.210	0.035	1.634	1.906	1.751	1.268	1.64	0.27
	0%FBS	0.164	0.166	0.166	0.165	0.296	0.298	0.294	0.274	0.131	0.133	0.129	0.109	0.125	0.011	2.205	2.239	2.172	1.834	2.11	0.19
48	10%FBS	0.154	0.157	0.160	0.157	0.498	0.486	0.480		0.341	0.329	0.323		0.331	0.009	1.902	1.835	1.802		1.85	0.05
	5% FBS	0.143	0.151	0.174	0.156	0.410	0.428	0.390		0.254	0.272	0.234		0.253	0.019	1.979	2.119	1.823		1.97	0.15
	0%FBS	0.156	0.160	0.171	0.162	0.295	0.301	0.288	0.311	0.133	0.139	0.126	0.149	0.136	0.010	2.239	2.340	2.121	2.509	2.30	0.16
72	10%FBS	0.148	0.150	0.151	0.150	0.637	0.601	0.569		0.487	0.451	0.419		0.453	0.034	2.719	2.518	2.339		2.53	0.19
	5% FBS	0.146	0.151	0.150	0.149	0.630	0.549	0.589		0.481	0.400	0.440		0.440	0.041	3.748	3.117	3.429		3.43	0.32
	0%FBS	0.154	0.158	0.161	0.158	0.278	0.258	0.264	0.219	0.120	0.100	0.106	0.061	0.097	0.025	2.031	1.693	1.795	1.035	1.64	0.43
96	10%FBS	0.147	0.145	0.148	0.147	0.639	0.645	0.622		0.492	0.498	0.475		0.489	0.012	2.747	2.780	2.652		2.73	0.07
	5% FBS	0.138	0.146	0.146	0.143	0.696	0.676	0.673		0.553	0.533	0.530		0.538	0.013	4.306	4.151	4.127		4.19	0.10
	0%FBS	0.152	0.158	0.159	0.156	0.258	0.266	0.284		0.102	0.110	0.128		0.113	0.013	1.716	1.851	2.155		1.91	0.22

Appendix 5. Supplementary data of Fig. 3.10

Appendix 5. Supplementary data of Figure 3.10

Rapid migration of *HtrA1^{-/-}* VSMCs
B. Cell migration by a modified Boyden chamber assay
Representative data from batch code #2, passage 12

Sample	Migrated cell number/well			Average	SD	p value (ttest WT vs KO, 95% significance)
	1	2	3			
WT	111	141	233	162	64	0.020
KO	422	851	671	648	215	

Appendix 6. Supplementary data of Fig. 3.11

Production of MMPs by isolated *HtrA1*⁻/⁻ mouse VSMCs

A. Increased MMP9 in the culture media of *HtrA1*⁻/⁻ VSMCs

Sample	pro MMP9 area			Relative band density			Average	SD	p value (ttest WT vs KO, 95% significance)
	#1 (P12)	#2 (P14)	#3 (P14)	#1 (P12)	#2 (P14)	#3 (P14)			
WT	1144	230	534	1.0	1.0	1.0	1.0	-	0.048
KO	5895	2880	10061	5.2	12.5	18.8	12.2	6.9	

B. MMP mRNA expression in WT and *HtrA1*⁻/⁻ VSMCs

Data from batch code #1, passage 10

Sample	*gapdh* concentration				Normalization factor
	1	2	3	Average	
WT	335.6	301.3	267.3	301.4	1.42
KO	209.3	198.9	226.7	211.6	1.00

Sample	*mmp2* concentration		
	1	2	3
WT	306.6	294.3	296.8
KO	254.3	222.8	260.2

Sample	Normalized *mmp2* concentration				Relative mRNA amount			Average	SD	p value (ttest WT vs KO, 95% significance)
	1	2	3	Average	1	2	3			
WT	215.9	207.3	209.0	210.7	1.00	1.00	1.00	1.00	-	0.074
KO	254.3	222.8	260.2	245.8	1.18	1.08	1.37	1.21	0.15	

Sample	*mmp9* concentration		
	1	2	3
WT	56.87	45.50	55.48
KO	279.50	272.60	272.60

Sample	Normalized *mmp9* concentration				Relative mRNA amount			Average	SD	p value (ttest WT vs KO, 95% significance)
	1	2	3	Average	1	2	3			
WT	40.05	32.04	39.07	37.05	1.00	1.00	1.00	1.00	-	0.006
KO	279.50	272.60	272.60	274.90	6.98	8.51	6.98	7.49	0.88	

Appendix 7. Original uncropped gels of Fig. 3.12
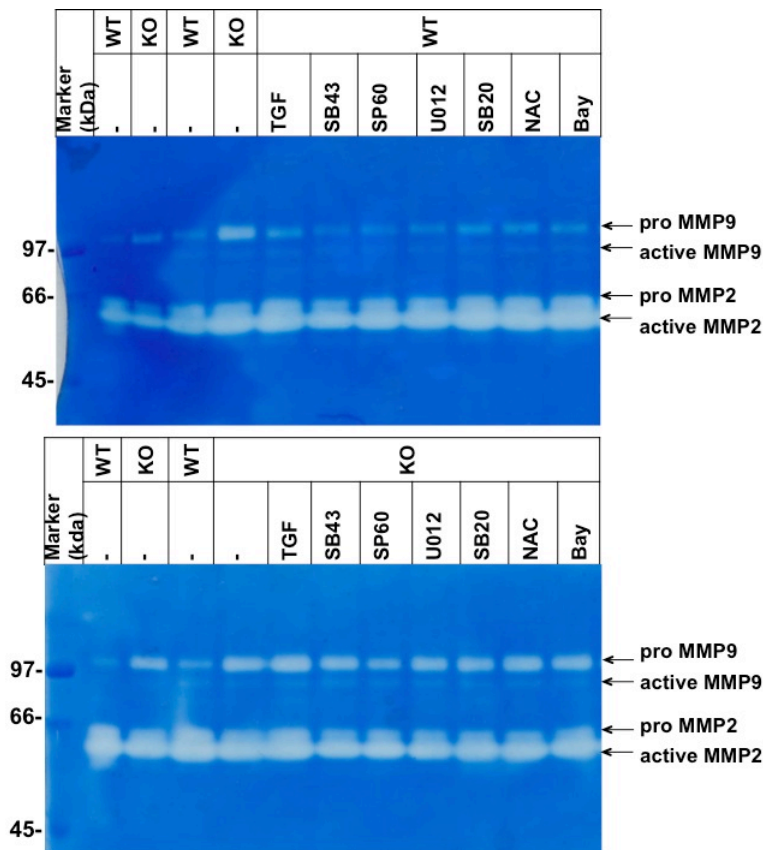
Supplemental Figure 1. Effects of TGF-β1, a radical scavenger, or signaling inhibitors on MMP9 activity of wild type (WT) and *HtrA1*$^{-/-}$ (KO) VSMCs. VSMCs were cultured in medium containing 0.1% FBS and treated for 24 h with various reagents as indicated. The culture supernatant was recovered and applied to a zymography gel as described in Fig. 3.12. The zymography was carried out in two separate gels due to the limitation of wells. The same samples of untreated (-) WT and untreated (-) *HtrA1*$^{-/-}$ were included in both gels (leftmost two lanes) as standards to compensate for any variation in proteolytic activity in the separate gels. TGF=TGFβ1. SB43=SB431542, a TGF-βR1 antagonist. SP60=SP600125, a JNK inhibitor. U012=U0126, a MEK1/2 (ERK1/2 upstream) inhibitor. SB20=SB203580, a p38 MAPK inhibitor. NAC=N- acetylcysteine, a ROS scavenger. Bay=Bay11-7082, a selective NF-κB inhibitor.

Appendix 8. Supplementary data of Fig. 3.14

Effects of PDGF-BB or IGF-1 on VSMC proliferation
Representative data from 1 of 3 batches (batch code #3), passage 7

Wild type (WT)

Incubation time (h)	Treatment	Media A450 1	Media A450 2	Media A450 3	Media average	cells 1	cells 2	cells 3	cells 4	corrected 1	corrected 2	corrected 3	corrected 4	corrected average	stdev	fold to 0h 1	fold to 0h 2	fold to 0h 3	fold to 0h 4	fold average	stdev	p value (ttest WT vs KO, 95% significance)
0	Control (0.5%FBS)	0.158	0.159	0.160	0.159	0.330	0.400	0.372	0.333	0.171	0.241	0.213	0.174	0.200	0.033	0.856	1.207	1.066	0.871	1.00	0.00	
	IGF-1	0.158	0.159	0.160	0.159	0.330	0.400	0.372	0.333	0.171	0.241	0.213	0.174	0.200	0.033	0.856	1.207	1.066	0.871	1.00	0.00	
	PDGF-BB	0.158	0.159	0.160	0.159	0.330	0.400	0.372	0.333	0.171	0.241	0.213	0.174	0.200	0.033	0.856	1.207	1.066	0.871	1.00	0.00	
24	Control (0.5%FBS)	0.154	0.161	0.161	0.159	0.392	0.322	0.374		0.233	0.163	0.215		0.204	0.036	1.168	0.818	1.078		1.02	0.18	0.0591
	IGF-1	0.172	0.172	0.174	0.173	0.413	0.520	0.504	0.524	0.240	0.347	0.331	0.351	0.318	0.052	1.203	1.739	1.659	1.759	1.59	0.26	0.0482
	PDGF-BB	0.168	0.174	0.177	0.173	0.522	0.510	0.463	0.456	0.349	0.337	0.290	0.283	0.315	0.033	1.747	1.687	1.452	1.417	1.58	0.17	0.0207
48	Control (0.5%FBS)	0.148	0.157	0.189	0.165	0.370	0.384	0.402	0.416	0.205	0.219	0.237	0.251	0.228	0.020	1.028	1.098	1.188	1.258	1.14	0.10	0.0300
	IGF-1	0.157	0.168	0.187	0.171	0.510	0.527	0.504	0.510	0.339	0.356	0.333	0.339	0.342	0.010	1.699	1.784	1.669	1.699	1.71	0.05	0.9849
	PDGF-BB	0.159	0.200	0.207	0.189	0.621	0.636	0.614	0.599	0.432	0.447	0.425	0.410	0.429	0.015	2.164	2.239	2.129	2.054	2.15	0.08	0.0577
72	Control (0.5%FBS)	0.149	0.155	0.155	0.153	0.446	0.475	0.511	0.479	0.293	0.322	0.358	0.326	0.325	0.027	1.467	1.612	1.792	1.632	1.63	0.13	0.7599
	IGF-1	0.155	0.161	0.160	0.159	0.609	0.592	0.622	0.575	0.450	0.433	0.463	0.416	0.441	0.020	2.254	2.169	2.320	2.084	2.21	0.10	0.1940
	PDGF-BB	0.149	0.159	0.161	0.156	0.547		0.527	0.546	0.391		0.371	0.390	0.384	0.011	1.956		1.856	1.951	1.92	0.06	0.0001
96	Control (0.5%FBS)	0.144	0.156	0.155	0.152	0.462	0.394	0.421	0.383	0.310	0.242	0.269	0.231	0.263	0.035	1.554	1.213	1.348	1.158	1.32	0.18	0.0099
	IGF-1	0.145	0.157	0.159	0.154	0.441	0.495		0.482	0.287	0.341		0.328	0.319	0.028	1.438	1.709		1.644	1.60	0.14	0.0060
	PDGF-BB	0.138	0.152	0.156	0.149	0.758	0.791		0.674	0.609	0.642		0.525	0.592	0.060	3.050	3.216		2.630	2.97	0.30	0.0105

HtrA1⁻/⁻ (KO)

Incubation time (h)	Treatment	Media A450 1	Media A450 2	Media A450 3	Media average	cells 1	cells 2	cells 3	cells 4	corrected 1	corrected 2	corrected 3	corrected 4	corrected average	stdev	fold to 0h 1	fold to 0h 2	fold to 0h 3	fold to 0h 4	fold average	stdev
0	Control (0.5%FBS)	0.158	0.159	0.160	0.159	0.277	0.266	0.261	0.241	0.118	0.107	0.102	0.082	0.102	0.015	1.154	1.046	0.998	0.802	1.00	0.00
	IGF-1	0.158	0.159	0.160	0.159	0.277	0.266	0.261	0.241	0.118	0.107	0.102	0.082	0.102	0.015	1.154	1.046	0.998	0.802	1.00	0.00
	PDGF-BB	0.158	0.159	0.160	0.159	0.277	0.266	0.261	0.241	0.118	0.107	0.102	0.082	0.102	0.015	1.154	1.046	0.998	0.802	1.00	0.00
24	Control (0.5%FBS)	0.154	0.161	0.161	0.159	0.312	0.296	0.293	0.275	0.153	0.137	0.134	0.116	0.135	0.015	1.500	1.343	1.314	1.138	1.32	0.15
	IGF-1	0.172	0.172	0.174	0.173	0.400	0.393	0.360		0.227	0.220	0.187		0.212	0.021	2.223	2.155	1.832		2.07	0.21
	PDGF-BB	0.168	0.174	0.177	0.173	0.427	0.391	0.375	0.357	0.254	0.218	0.202	0.184	0.215	0.030	2.484	2.132	1.976	1.800	2.10	0.29
48	Control (0.5%FBS)	0.148	0.157	0.189	0.165	0.302	0.306	0.288	0.311	0.137	0.141	0.123	0.146	0.137	0.010	1.343	1.382	1.206	1.431	1.34	0.10
	IGF-1	0.157	0.168	0.187	0.171	0.370	0.344	0.353	0.317	0.199	0.173	0.182	0.146	0.175	0.022	1.949	1.695	1.783	1.431	1.71	0.22
	PDGF-BB	0.159	0.200	0.207	0.189	0.444	0.434	0.405	0.441	0.255	0.245	0.216	0.252	0.242	0.018	2.497	2.399	2.116	2.468	2.37	0.17
72	Control (0.5%FBS)	0.149	0.155	0.155	0.153	0.352	0.335	0.297	0.267	0.199	0.182	0.144	0.114	0.160	0.038	1.946	1.780	1.408	1.115	1.56	0.37
	IGF-1	0.155	0.161	0.160	0.159	0.453	0.460	0.362		0.294	0.301	0.203		0.266	0.055	2.879	2.947	1.989		2.60	0.53
	PDGF-BB	0.149	0.159	0.161	0.156	0.553	0.523	0.514		0.397	0.367	0.358		0.374	0.020	3.879	3.586	3.498		3.65	0.20
96	Control (0.5%FBS)	0.144	0.156	0.155	0.152	0.332	0.325	0.346	0.263	0.180	0.173	0.194		0.183	0.011	1.764	1.695	1.901		1.79	0.10
	IGF-1	0.145	0.157	0.159	0.154	0.459	0.473	0.400	0.330	0.305	0.319	0.246		0.290	0.039	2.986	3.123	2.409		2.84	0.38
	PDGF-BB	0.138	0.152	0.156	0.149	0.551		0.536	0.587	0.402		0.387	0.438	0.409	0.026	3.935		3.788	4.287	4.00	0.26

Appendix 9. Supplementary data of Fig. 3.15

Effects of PDGF-BB or IGF-1 on VSMC migration
B. Cell migration by a modified Boyden chamber assay
Representative data from batch code #2, passage 9

Sample	Treatment	Migrated cell number/well			Average	SD	p value (ttest WT vs KO, 95% significance)
		1	2	3			
WT	Control (0.5%FBS)	9	19	47	25	20	0.259
	IGF-1	13	21	10	15	6	0.253
	PDGF-BB	23	122	23	56	57	0.056
KO	Control (0.5%FBS)	63	95	17	58	39	
	IGF-1	83	367	21	157	184	
	PDGF-BB	765	743	189	566	326	

Appendix 10. Supplementary data of Fig. 3.18

A. Effects of H$_2$O$_2$ on cell viability of WT and *HtrA1$^{-/-}$* mouse VSMCs
Representative data from batch code #1, passage 10

Treatment (in 0.1% FBS)	Wild type (WT)													p value (ttest WT vs KO, 95% significance)
	A450 nm								cell viabilty to control (0 mM)					
	cells				corrected									
	1	2	3	average	1	2	3	average	1	2	3	average	SE	
0 mM H$_2$O$_2$	0.407	0.466	0.405	0.426	0.184	0.243	0.182	0.203	90.64	119.70	89.66	100.00	-	1.0000
0.1 mM H$_2$O$_2$	0.439	0.465	0.439	0.448	0.216	0.242	0.216	0.225	106.40	119.21	106.40	110.67	2.34	0.0026
0.3 mM H$_2$O$_2$	0.373	0.397	0.397	0.389	0.150	0.174	0.174	0.166	73.89	85.71	85.71	81.77	2.16	0.0001
1 mM H$_2$O$_2$	0.280	0.280	0.268	0.276	0.057	0.057	0.045	0.053	28.08	28.08	22.17	26.11	1.08	0.6966
2 mM H$_2$O$_2$	0.283	0.284	0.289	0.285	0.060	0.061	0.066	0.062	29.56	30.05	32.51	30.71	0.50	0.0525
Blanko	0.223	0.223	0.223	0.223										

Treatment (in 0.1% FBS)	*HtrA1$^{-/-}$* (KO)												
	A450 nm								cell viabilty to control (0 mM)				
	cells				corrected								
	1	2	3	average	1	2	3	average	1	2	3	average	SE
0 mM H$_2$O$_2$	0.403	0.436	0.431	0.423	0.183	0.216	0.211	0.203	90.00	106.23	103.77	100.00	-
0.1 mM H$_2$O$_2$	0.367	0.352	0.328	0.349	0.147	0.132	0.108	0.129	72.30	64.92	53.11	63.44	3.06
0.3 mM H$_2$O$_2$	0.240	0.249	0.246	0.245	0.020	0.029	0.026	0.025	9.84	14.26	12.79	12.30	0.71
1 mM H$_2$O$_2$	0.272	0.273	0.269	0.271	0.052	0.053	0.049	0.051	25.57	26.07	24.10	25.25	0.32
2 mM H$_2$O$_2$	0.288	0.287	0.292	0.289	0.068	0.067	0.072	0.069	33.44	32.95	35.41	33.93	0.41
Blanko	0.226	0.215	0.215	0.220									

B. Effects of H$_2$O$_2$ on cell death of WT and *HtrA1$^{-/-}$* mouse VSMCs
Representative data from batch code #1, passage 10

Sample	Well	0.1 mM H2O2					p value (ttest WT vs KO, 95% significance)	
		Cell number			Frequency (%) of			
		Necrosis (red)	Apoptosis (green)	Total (DAPI)	Necrosis	Apoptosis	Necrosis	Apoptosis
WT	1	0	1	56	0.0	1.8	0.155	0.109
	2	1	0	48	2.1	0.0		
	3	1	0	43	2.3	0.0		
	4	2	8	49	4.1	16.3		
	Average				2.1	4.5		
	SE				0.8	4.0		
KO	1	2	7	84	2.4	8.3		
	2	6	9	97	6.2	9.3		
	3	1	8	18	5.6	44.4		
	4	1	10	37	2.7	27.0		
	Average				4.2	22.3		
	SE				1.0	8.6		

Sample	Well	0.3 mM H2O2					p value (ttest WT vs KO, 95% significance)	
		Cell number			Frequency (%) of			
		Necrosis (red)	Apoptosis (green)	Total (DAPI)	Necrosis	Apoptosis	Necrosis	Apoptosis
WT	1	0	4	41	0.0	9.8	0.013	0.002
	2	2	10	43	4.7	23.3		
	3	2	4	60	3.3	6.7		
	Average				2.7	13.2		
	SE				1.4	5.1		
KO	1	7	29	59	11.9	49.2		
	2	5	25	53	9.4	47.2		
	3	5	31	59	8.5	52.5		
	Average				9.9	49.6		
	SE				1.0	1.6		

C. Effects of H$_2$O$_2$ on apoptosis of WT and *HtrA1*$^{-/-}$ mouse VSMCs
Representative data from batch code #1, passage 10

		0.1 mM H$_2$O$_2$			**p value (ttest WT vs KO, 95% significance)**
Sample	**Well**	**Cell number**		**Frequency of apoptosis (%)**	
		Apoptosis (red)	**Total (DAPI)**		
WT	1	0	55	0.0	0.008
	2	0	71	0.0	
	3	0	14	0.0	
	4	0	19	0.0	
	5	0	15	0.0	
	Average			0.0	
	SE			0.0	
KO	1	1	84	1.2	
	2	1	97	1.0	
	3	1	18	5.6	
	4	2	37	5.4	
	5	1	24	4.2	
	Average			3.5	
	SE			1.0	

		0.3 mM H$_2$O$_2$			**p value (ttest WT vs KO, 95% significance)**
Sample	**Well**	**Cell number**		**Frequency of apoptosis (%)**	
		Apoptosis (red)	**Total (DAPI)**		
WT	1	3	50	6.0	0.005
	2	0	52	0.0	
	3	2	32	6.3	
	4	2	35	5.7	
	5	1	49	2.0	
	Average			4.0	
	SE			1.3	
KO	1	28	119	23.5	
	2	16	106	15.1	
	3	19	123	15.4	
	4	9	87	10.3	
	5	20	79	25.3	
	6	7	85	8.2	
	Average			14.9	
	SE			2.9	

Appendix 11. Supplementary data of Fig. 3.21

A. Uneven thickening of aortic media of 40-wo *HtrA1⁻ᐟ⁻* mice
B-C. Calculation of the incidence of uneven thickening and the ratio of thickest-to-thinnest media

		Wild type (WT)						*HtrA1⁻ᐟ⁻* (KO)			
Mouse #	Section #	Length (pixel)		Ratio thickest to thinnest	Section with ratio 2.5 or > (=1, <2.5 =0)	Mouse #	Section #	Length (pixel)		Ratio thickest to thinnest	Section with ratio 2.5 or > (=1, <2.5 =0)
		Thickest	Thinnest					Thickest	Thinnest		
1	1	99.67	43.25	2.30	0	1	1	81.89	34.81	2.35	0
	2	100.88	55.45	1.82	0		2	89.11	23.71	3.76	1
	3	95.03	39.39	2.41	0		3	81.47	28.97	2.81	1
	4	73.28	35.80	2.05	0						
	5	80.75	31.14	2.59	1						
	average			2.24			average			2.97	
	stdev			0.31			stdev			0.72	
2	1	93.46	43.19	2.16	0	2	1	104.52	40.60	2.57	1
	2	78.86	41.80	1.89	0		2	101.81	41.40	2.46	0
	3	82.20	39.24	2.09	0		3	103.17	40.77	2.53	1
	4	75.97	41.79	1.82	0		4	95.61	31.75	3.01	1
	5	73.06	34.13	2.14	0		5	107.40	31.75	3.38	1
	6	65.62	32.62	2.01	0		6	118.66	41.87	2.83	1
	average			2.02			average			2.80	1
	stdev			0.14			stdev			0.35	
3	1	93.65	27.85	3.36	1	3	1	128.24	12.84	9.99	1
	2	90.33	27.42	3.29	1		2	76.45	13.21	5.79	1
	3	86.67	26.27	3.30	1		3	76.89	17.61	4.37	1
	4	90.80	33.44	2.72	1		4	76.62	19.54	3.92	1
	5	103.49	33.67	3.07	1		5	67.19	19.93	3.37	1
	6	97.30	30.05	3.24	1		6	83.01	29.50	2.81	1
	7	86.93	29.89	2.91	1		7	75.34	22.28	3.38	1
	average			3.13			average			4.80	
	stdev			0.24			stdev			2.48	
4	1	56.38	25.68	2.20	0	4	1	157.19	39.41	3.99	1
	2	69.62	25.06	2.78	1		2	136.55	33.47	4.08	1
	3	69.23	32.78	2.11	0		3	133.97	33.09	4.05	1
	4	48.01	28.40	1.69	0		4	117.11	54.61	2.14	0
	average			2.19			5	104.41	37.87	2.76	1
	stdev			0.45			6	101.45	54.37	1.87	0
5	1	63.05	34.45	1.83	0		7	89.64	43.25	2.07	0
	2	71.61	36.79	1.95	0		8	101.69	43.26	2.35	0
	3	63.65	37.88	1.68	0		average			2.91	
	4	61.28	36.55	1.68	0		stdev			0.97	
	5	77.83	34.89	2.23	0	5	1	88.21	48.82	1.81	0
	6	62.57	39.00	1.60	0		2	92.22	35.66	2.59	1
	7	71.13	35.79	1.99	0		3	79.57	35.93	2.21	0
	8	62.66	34.89	1.80	0		4	88.00	51.67	1.70	0
	average			1.84			5	89.13	40.60	2.20	0
	stdev			0.21			6	86.66	45.09	1.92	0
6	1	96.50	46.48	2.08	0		7	73.54	29.54	2.49	0
	2	87.91	35.14	2.50	1						
	3	83.45	46.78	1.78	0						
	4	87.21	42.72	2.04	0						
	5	87.91	45.09	1.95	0						
	average			2.07			average			2.13	
	stdev			0.27			stdev			0.34	
Average of thickness-to-thinnest ratio				2.25		**Average of thickness-to-thinnest ratio**				3.12	
SD				0.45		**SD**				1.00	
Incidence of uneven thickening (section with ratio of 2.5 or >)					10	**Incidence of uneven thickening (section with ratio of 2.5 or >)**					20
Total section number					35	**Total section number**					31
Percentage of uneven thickening					29%	**Percentage of uneven thickening**					65%
p value (ttest of thickest-to-thinnest ratio WT vs KO, 95% significance)											0.084

D. Uneven thickening of aortic media of 52-wo *HtrA1⁻ᐟ⁻* mice
**E-F. Calculation of the incidence of uneven thickening and the ratio of thickest-to-thinnest media**

Wild type (WT)						*HtrA1⁻ᐟ⁻* (KO)					
Mouse #	Section #	Length (pixel) Thickest	Thinnest	Ratio thickest to thinnest	Section with ratio 2.5 or > (=1, <2.5 =0)	Mouse #	Section #	Length (pixel) Thickest	Thinnest	Ratio thickest to thinnest	Section with ratio 2.5 or > (=1, <2.5
1	1	74.23	30.97	2.40	0	1	1	82.88	35.54	2.33	0
	2	64.29	33.93	1.89	0		2	80.72	35.79	2.26	0
	3	68.70	28.39	2.42	0		3	77.58	30.09	2.58	1
	average			2.24			average			2.39	
	stdev			0.30			stdev			0.17	
2	1	52.94	27.51	1.92	0	2	1	66.26	29.05	2.28	0
	2	58.02	38.28	1.52	0		2	66.76	31.37	2.13	0
	3	64.11	30.42	2.11	0		3	75.44	34.98	2.16	0
	average			1.85			average			2.19	
	stdev			0.30			stdev			0.08	
3	1	65.18	29.16	2.24	0	3	1	63.21	21.63	2.92	1
	2	60.90	26.78	2.27	0		2	68.16	23.63	2.88	1
	3	62.34	30.81	2.02	0		3	65.94	18.44	3.58	1
	average			2.18			average			3.13	
	stdev			0.13			stdev			0.39	
4	1	56.79	26.57	2.14	0	4	1	82.48	21.94	3.76	1
	2	55.93	33.06	1.69	0		2	83.22	24.73	3.37	1
	3	52.00	21.40	2.43	0		3	70.79	28.98	2.44	0
	average			2.09			average			3.19	
	stdev			0.37		22.42				0.68	
5	1	89.98	39.17	2.30	0	5	1	75.71	22.42	3.38	1
	2	61.75	23.18	2.66	1		2	82.54	26.91	3.07	1
	3	59.41	34.38	1.73	0		3	48.02	18.54	2.59	1
	average			2.23			average			3.01	
	stdev			0.47			stdev			0.40	
6	1	56.97	17.86	3.19	1	6	1	63.72	17.44	3.65	1
	2	61.45	25.43	2.42	0		2	69.91	18.44	3.79	1
	3	58.82	16.56	3.55	1		3	50.89	20.93	2.43	0
	average			3.05			average			3.29	
	stdev			0.58			stdev			0.75	
7	1	55.14	18.13	3.04	1	7	1	90.29	24.50	3.69	1
	2	47.94	24.50	1.96	0		2	91.58	16.44	5.57	1
	3	46.33	26.10	1.78	0		3	91.16	8.91	10.23	1
	average			2.26			average			6.50	
	stdev			0.68			stdev			3.37	
8	1	54.39	25.03	2.17	0	8	1	98.61	20.32	4.85	1
	2	60.94	28.46	2.14	0		2	80.84	25.26	3.20	1
	3	58.30	23.42	2.49	0		3	81.25	24.53	3.31	1
	average			2.27			average			3.79	
	stdev			0.19			stdev			0.92	
9	1	54.44	22.85	2.38	0						
	2	55.15	25.72	2.14	0						
	3	51.96	25.40	2.05	0						
	average			2.19							
	stdev			0.17							
10	1	77.76	27.67	2.81	1						
	2	66.40	42.70	1.56	0						
	3	58.31	30.58	1.91	0						
	average			2.09							
	stdev			0.31							
Average of thickness-to-thinnest ratio				2.24		**Average of thickness-to-thinnest ratio**				3.44	
SD				0.31		**SD**				1.34	
Incidence of uneven thickening (section with ratio of 2.5 or >)					5	**Incidence of uneven thickening (section with ratio of 2.5 or >)**					17
Total section number					30	**Total section number**					24
Percentage of uneven thickening					17%	**Percentage of uneven thickening**					71%
p value (ttest of thickest-to-thinnest ratio WT vs KO, 95% significance)											0.014

Appendix 12. Elastic fiber degradation in the aortic media of 52-week-old *HtrA1⁻ᐟ⁻* mice
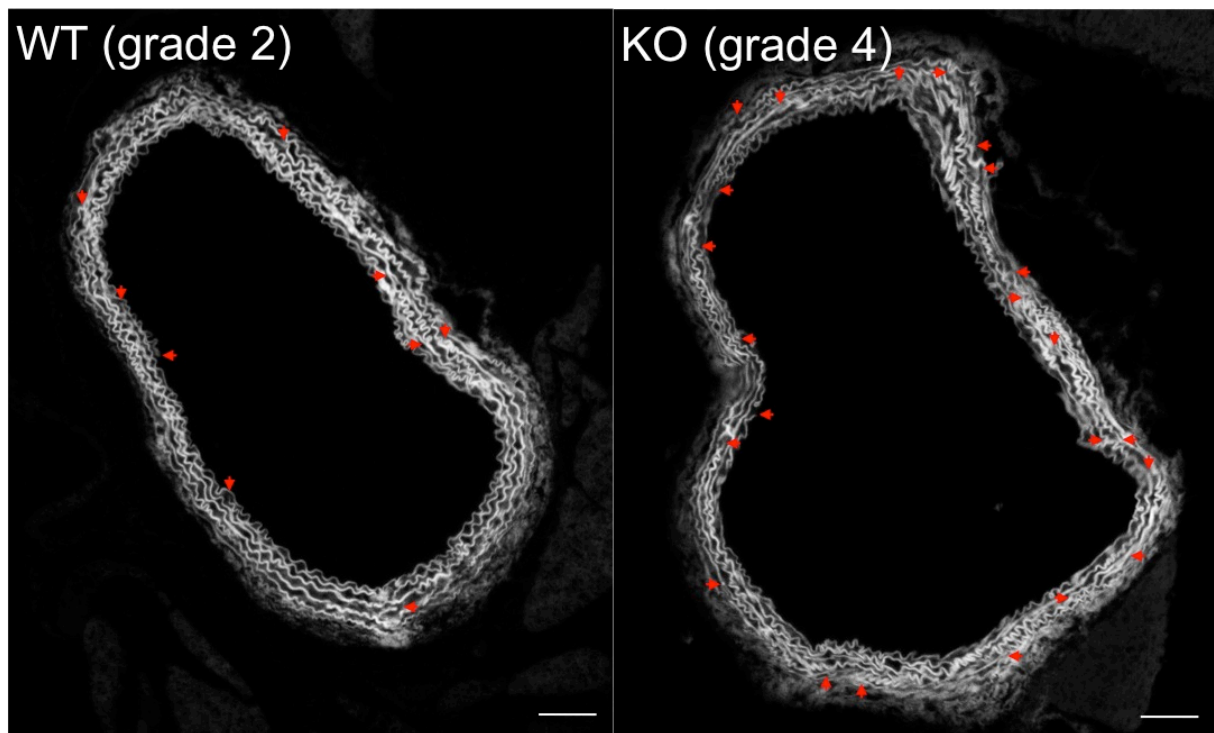
Supplemental Figure 2. Elastic fiber degradation in the aortic media of 52-wo *HtrA1⁻ᐟ⁻* mice. Grading of elastic fiber degradation was carried out using elastic van Gieson-stained sections based on a reported method provided in Materials and Method. Pictures shown are typical images of the wild type (WT) aorta (left) and the *HtrA1⁻ᐟ⁻* (KO) aorta (right). Red arrows indicate damaged elastic fibers. Bar=100 μm.

Appendix 13. Supplementary data of Fig. 3.22

A. Elastic fiber degradation in the aortic media of 40-week-old *HtrA1⁻ᐟ⁻* mice
Sections with the highest thickest-to-thinnest ratio from each mouse (see Appendix 11) were analyzed

Wild Type (WT)

Mouse #	Section #	Incidence of				Total incidence (score)	Grading of elastic fiber degradation				p value WT vs KO
		Intimal protrusion	Discontinue of internal elastic lamina	Branching of elastic fiber	Discontinue of elastic fiber		Grade 1 (score 0-7)	Grade 2 (score 8-15)	Grade 3 (score 16-23)	Grade 4 (score 24 or >)	(nonpar. U-test (Mann-Whitney) 0.084
1	5	0	2	7	2	11		2			
2	1	0	0	4	6	10		2			
3	3	0	0	4	4	8		2			
4	2	0	1	4	2	7	1				
5	5	1	0	4	9	14		2			
6	2	0	0	4	7	11		2			
Grade average								1.8			
SD								0.4			

***HtrA1⁻ᐟ⁻* (KO)**

Mouse #	Section #	Incidence of				Total incidence (score)	Grading of elastic fiber degradation			
		Intimal protrusion	Discontinue of internal elastic lamina	Branching of elastic fiber	Discontinue of elastic fiber		Grade 1 (score 0-7)	Grade 2 (score 8-15)	Grade 3 (score 16-23)	Grade 4 (score 24 or >)
1	2	0	2	9	6	17			3	
2	5	1	2	2	5	10		2		
3	1	1	0	4	3	8		2		
4	2	0	0	12	8	20			3	
5	2	0	0	17	7	24				4
Grade average								2.8		
SD								0.8		

B. Elastic fiber degradation in the aortic media of 52-week-old *HtrA1⁻ᐟ⁻* mice
Sections with the highest thickest-to-thinnest ratio from each mouse (see Appendix 11) were analyzed

Wild Type (WT)

Mouse #	Section #	Incidence of				Total incidence (score)	Grading of elastic fiber degradation				p value WT vs KO
		Intimal protrusion	Discontinue of internal elastic lamina	Branching of elastic fiber	Discontinue of elastic fiber		Grade 1 (score 0-7)	Grade 2 (score 8-15)	Grade 3 (score 16-23)	Grade 4 (score 24 or >)	(nonpar. U-test (Mann-Whitney) 0.02
1	3	0	1	4	5	10		2			
2	3	0	2	3	3	8		2			
3	2	0	1	7	1	9		2			
4	3	0	1	5	7	13		2			
5	2	0	1	7	5	13		2			
6	3	0	1	1	4	6	1				
7	1	0	0	3	5	8		2			
8	3	0	0	4	6	10		2			
9	1	0	1	5	3	9		2			
10	1	0	2	9	3	14		2			
Grade average								1.9			
SD								0.3			

***HtrA1⁻ᐟ⁻* (KO)**

Mouse #	Section #	Incidence of				Total incidence (score)	Grading of elastic fiber degradation			
		Intimal protrusion	Discontinue of internal elastic lamina	Branching of elastic fiber	Discontinue of elastic fiber		Grade 1 (score 0-7)	Grade 2 (score 8-15)	Grade 3 (score 16-23)	Grade 4 (score 24 or >)
1	3	0	2	10	8	20			3	
2	1	0	1	4	8	13		2		
3	3	0	2	4	5	11		2		
4	1	0	4	10	9	23			3	
5	1	0	2	14	8	24				4
6	2	0	3	4	7	14		2		
7	3	1	3	10	12	26				4
8	1	2	3	11	9	25				4
Grade average								3.0		
SD								0.9		